

New Therapeutic Options
for the
Treatment of Lung Cancer by Telomerase Inhibition

Dissertation
zur Erlangung des Grades
des Doktors der Naturwissenschaften
der Naturwissenschaftlich-Technischen Fakultät III
Chemie, Pharmazie, Bio- und Werkstoffwissenschaften
der Universität des Saarlandes

von

Sebastian Tätz

Saarbrücken
2008

Tag des Kolloquiums: 20.02.2009

Dekan: Prof. Dr. Uli Müller

Mitglieder des Prüfungsausschusses:

Vorsitzender: Prof. Dr. Rolf Müller

1. Gutachter: Prof. Dr. Claus-Michael Lehr

2. Gutachter: Prof. Dr. Elias Fattal

Akademische Mitarbeiterin: Dr. Christiane Baldes

Meinen Eltern

Table of Contents

| | |
|--|------------|
| TABLE OF CONTENTS..... | I |
| ABSTRACT | VI |
| KURZZUSAMMENFASSUNG | VII |
| CHAPTER 1: GENERAL INTRODUCTION..... | 1 |
| 1.1 Lung Cancer | 1 |
| 1.2 Telomeres, Telomerase and their Implication in Cancer Development..... | 7 |
| 1.3 Objectives of the studies | 14 |
| CHAPTER 2: BIOPHARMACEUTICAL CHARACTERIZATION OF THE TELOMERASE INHIBITOR BRACO19 | 19 |
| 2.1 Introduction | 21 |
| 2.2 Materials and Methods..... | 23 |
| 2.2.1 Substances and buffers | 23 |
| 2.2.2 Cells and cell culture conditions..... | 23 |
| 2.2.3 Transport studies | 25 |
| 2.2.4 Transport experiments with different inhibitors | 25 |
| 2.2.5 Calculation of apparent permeability coefficient P_{app} | 26 |
| 2.2.6 Determination of uptake into cells and adsorption to filter material..... | 26 |
| 2.2.7 Sample analysis | 26 |
| 2.2.8 IAM chromatography measurements | 27 |
| 2.2.9 HSA binding..... | 28 |
| 2.2.10 MTT cytotoxicity assay | 28 |
| 2.3 Results..... | 29 |
| 2.3.1 Solubility, cytotoxicity, protein binding and IAM chromatography measurements..... | 29 |
| 2.3.2 Transport experiments..... | 29 |
| 2.3.3 Experiments with transport inhibitors and uptake/ adsorption studies..... | 30 |
| 2.4 Discussion | 32 |
| 2.5 Conclusion | 35 |

| | |
|---|-----------|
| CHAPTER 3: DECOMPOSITION OF THE TELOMERE TARGETING AGENT BRACO19 IN PHYSIOLOGICAL MEDIA RESULTS IN PRODUCTS WITH DECREASED INHIBITORY POTENTIAL..... | 37 |
| 3.1 Introduction | 39 |
| 3.2 Materials and Methods..... | 41 |
| 3.2.1 BRACO19 | 41 |
| 3.2.2 Buffers and cell culture medium for stability studies | 41 |
| 3.2.3 HPLC- DAD analysis of BRACO19 and decomposition products | 41 |
| 3.2.4 Decomposition experiments | 42 |
| 3.2.5 Decomposition of BRACO19 for structural analysis of decomposition products by LC/MS and NMR | 43 |
| 3.2.6 LC/MS analysis of decomposition products | 43 |
| 3.2.7 NMR analysis of BRACO 19 and decomposition products..... | 44 |
| 3.2.8 TRAP Assay | 44 |
| 3.3 Results..... | 45 |
| 3.3.1 Stability experiments..... | 45 |
| 3.3.2 LC/MS and NMR analysis | 49 |
| 3.3.3 TRAP Assay | 51 |
| 3.4 Discussion..... | 52 |
| | |
| CHAPTER 4: THE INFLUENCE OF CHITOSAN CONTENT IN CATIONIC CHITOSAN/PLGA NANOPARTICLES ON THE DELIVERY EFFICIENCY OF ANTISENSE 2'-O-METHYL-RNA DIRECTED AGAINST TELOMERASE IN LUNG CANCER CELLS..... | 55 |
| 4.1 Introduction | 57 |
| 4.2 Materials and Methods..... | 59 |
| 4.2.1 Materials | 59 |
| 4.2.2 Nanoparticle preparation | 59 |
| 4.2.3 Purification of nanoparticles | 60 |
| 4.2.4 Characterization of nanoparticle properties | 61 |
| 4.2.5 Formation of 2OMR-Chitosan/PLGA nanoplexes..... | 61 |
| 4.2.6 HPLC analysis of 2'-O-Methyl RNA..... | 62 |
| 4.2.7 Quantification of 5'-FAM-2'-O-Methyl RNA | 62 |
| 4.2.8 Cell cultures | 63 |
| 4.2.9 Assessment of 2OMR association with cells by flow cytometry | 63 |
| 4.2.10 Visualization of cellular uptake by confocal laser scanning microscopy | 64 |

| | |
|---|------------|
| 4.2.11 Cytotoxicity experiments and monolayer integrity | 66 |
| 4.2.12 Telomerase activity measurement (TRAP)..... | 67 |
| 4.2.13 Terminal restriction fragment length determination (TRF) | 68 |
| 4.2.14 Statistical analysis..... | 68 |
| 4.3 Results | 69 |
| 4.3.1 Nanoparticle properties | 69 |
| 4.3.2 Complexation of 2OMR | 71 |
| 4.3.3 Uptake of nanoplexes | 73 |
| 4.3.4 Cytotoxicity and monolayer integrity | 79 |
| 4.3.5 Inhibition of telomerase activity and telomere shortening | 80 |
| 4.4 Discussion | 82 |
| 4.5 Conclusion | 85 |
| | |
| CHAPTER 5: PURIFICATION OF CHITOSAN/PLGA NANOPARTICLES BY SIZE EXCLUSION CHROMATOGRAPHY | 87 |
| 5.1 Introduction | 89 |
| 5.2 Materials and Methods..... | 90 |
| 5.2.1 The size exclusion chromatography system | 90 |
| 5.2.2 Selection of mobile phase | 90 |
| 5.2.3 Particle suspensions | 90 |
| 5.2.4 Evaluation of the separation of particles from polymers | 90 |
| 5.2.5 Quantification of chitosan and PVA in fractions after purification..... | 91 |
| 5.3 Results and Discussion..... | 92 |
| 5.3.1 Selection of the mobile phase..... | 92 |
| 5.3.2 Quantification of chitosan and PVA in different fractions | 95 |
| 5.3.3 Purification of different nanoparticle preparations | 98 |
| 5.3.4 Repeated injection of particle suspensions..... | 99 |
| 5.4 Conclusion | 100 |
| | |
| CHAPTER 6: HYALURONIC ACID- MODIFIED LIPOSOMES FOR THE TARGETED DELIVERY OF SIRNA TO CD44 EXPRESSING LUNG CANCER CELLS | 101 |
| 6.1 Introduction | 103 |
| 6.2 Materials and Methods..... | 105 |
| 6.2.1 Materials | 105 |

Table of Contents

| | | |
|--|---|------------|
| 6.2.2 | siRNAs | 105 |
| 6.2.3 | Radiolabeling of siRNA..... | 105 |
| 6.2.4 | Conjugation of DOPE to hyaluronic acid..... | 106 |
| 6.2.5 | Preparation of liposomes..... | 106 |
| 6.2.6 | Preparation of lipoplexes | 107 |
| 6.2.7 | Characterization of liposomes and lipoplexes | 107 |
| 6.2.8 | Binding efficiencies of lipoplexes | 107 |
| 6.2.9 | Colloidal stability of liposomes and lipoplexes in serum-free cell culture medium | 107 |
| 6.2.10 | Protection of siRNA in lipoplexes in the presence of RNase V1 | 108 |
| 6.2.11 | Stability of siRNA and lipoplexes in the presence of human serum..... | 108 |
| 6.2.12 | Cell cultures and cell culture conditions | 109 |
| 6.2.13 | Western blot analysis for the CD44 receptor | 109 |
| 6.2.14 | Cytotoxicity tests | 110 |
| 6.2.15 | Flow cytometry | 111 |
| 6.2.16 | Determination of telomerase activity by the TRAP-qPCR assay..... | 112 |
| 6.3 | Results..... | 114 |
| 6.3.1 | Properties of liposomes and lipoplexes..... | 114 |
| 6.3.2 | Binding of siRNA | 116 |
| 6.3.3 | Influence of cell culture medium as dispersion medium | 117 |
| 6.3.4 | Protection of siRNA in lipoplexes..... | 118 |
| 6.3.5 | Uptake of lipoplexes..... | 119 |
| 6.3.6 | Cytotoxicity of liposomes and lipoplexes..... | 122 |
| 6.3.7 | Inhibition of telomerase activity | 123 |
| 6.4 | Discussion..... | 125 |
| 6.5 | Conclusion | 128 |
| CHAPTER 7: SUMMARY AND OUTLOOK..... | | 129 |
| CHAPTER 8: ZUSAMMENFASSUNG UND AUSBLICK | | 133 |
| ABBREVIATIONS..... | | 137 |
| REFERENCES..... | | 139 |
| DANKSAGUNGEN ACKNOWLEDGEMENTS..... | | 157 |

| | |
|-----------------------------------|----------------|
| PUBLICATION LIST | 159 |
| Publications | 159 |
| Poster Presentations | 160 |
| Oral Presentations | 161 |
| CURRICULUM VITAE | 163 |

Abstract

The enzyme telomerase plays an important role in cell immortalization and hence cancer development. It can be detected in most kinds of tumors but is not expressed in the majority of healthy cells. Therefore, telomerase inhibition appears to be a promising approach for a specific cancer therapy with reduced side effects.

The work presented here concentrated on the treatment of non-small cell lung cancer by telomerase inhibition and can be divided into three parts:

1. Characterization of the G-quadruplex stabilizing substance BRACO19 under biopharmaceutical and stability aspects. BRACO19 showed a poor permeability across biological barriers and was instable under physiological conditions.
2. Evaluation of cationic chitosan/PLGA nanoparticles as a carrier system for 2'-O-Methyl-RNA antisense oligonucleotides (2OMR), which was directed against the template region of the telomerase specific RNA hTR. The chitosan content in the particles considerably influenced the uptake improvement of 2OMR into cells. Despite a poor complex stability in physiological media a successful inhibition of telomerase activity in lung cancer cells could be achieved.
3. Targeted delivery of anti-telomerase siRNA to CD44-overexpressing lung cancer cells using hyaluronic acid modified DOTAP/DOPE liposomes. These liposomes efficiently bound siRNA, protected it from degradation by nucleases and increased its uptake into CD44-overexpressing lung cancer cells. The modification improved the colloidal stability of lipoplexes in cell culture medium and their cytotoxicity.

Kurzzusammenfassung

Das Enzym Telomerase spielt eine wichtige Rolle bei der Immortalisierung von Zellen und damit auch bei der Entwicklung von Krebserkrankungen. Es wird in einer Vielzahl von Tumoren exprimiert, jedoch nicht in den meisten gesunden Zelltypen. Durch seine Hemmung erhofft man sich eine sehr spezifische und nebenwirkungsarme Krebstherapie.

Die durchgeführten Arbeiten konzentrierten sich auf die Behandlung von nicht-kleinzelligen Lungenkrebs mittels Telomeraseinhibitoren und unterteilen sich in drei Teile:

1. Charakterisierung des G-Quadruplex stabilisierenden Wirkstoffs BRACO19 unter biopharmazeutischen und stabilitätsrelevanten Aspekten. BRACO19 permeierte schlecht über biologische Barrieren und war unter physiologischen Bedingungen instabil.
2. Evaluierung von kationischen Chitosan/PLGA-Nanopartikeln als Trägersystem für ein gegen die Template Region der Telomerase-spezifischen RNA hTR gerichtetes 2'-O-Methyl-RNA Antisense Oligonukelotid. Der Chitosangehalt der Partikel beeinflusste die Aufnahmeverbesserung von 2OMR in Zellen deutlich. Trotz geringer Komplexstabilität in physiologischen Medien konnte das Enzym Telomerase in Lungenkrebszellen effizient gehemmt werden.
3. Targeted Delivery von Anti-Telomerase siRNA mit Hilfe von Hyaluronsäure-modifizierten kationischen DOTAP/DOPE Liposomen in CD44-überexprimierende Lungenkrebszellen. Diese Liposomen konnten effizient die siRNA binden, gegen Abbau durch Nucleasen schützen und steigerten ihre Aufnahme in CD44-überexprimierende Lungenkrebszellen. Weiterhin verbesserte die Modifizierung die kolloidale Stabilität der Lipoplexe in Zellkulturmedium sowie deren Zytotoxizität.

Chapter 1

General Introduction

1.1 Lung Cancer

Together with cancers of the genital and digestive systems, lung cancer is the most prominent type of malignancies in Germany and the United States [1, 2]. In contrast to these other kinds of cancer, it still has a very poor prognosis. It is the leading cause for cancer related deaths and the overall five-year survival rate is only 15 – 20%. Therefore it is considered as one of the most malignant kind of cancers. The reason for this poor prognosis is mostly due to the advanced stage of tumors at the time of discovery. Smoking, both active or passive, is the major cause for the development of lung cancer while other factors like exposure to the radioactive gas radon, carcinogenic substances or fibers like asbestos play a minor role.

Histologically lung cancers are divided into several subtypes. For treatment purposes, the majority of malignancies are roughly classified as small cell lung cancer (SCLC) and non-small cell lung cancer (NSCLC). SCLC accounts for approximately 20% of lung cancers and can be considered a class of its own. The term NSCLC comprises most other types of lung cancer, which are according to the World Health Organization (WHO) [3]:

- squamous cell carcinoma
- adenocarcinoma
- large cell carcinoma
- adenosquamous carcinoma
- sarcomatoid carcinoma
- carcinoid tumors
- salivary gland tumors.

These classes are further subdivided for more specific categorization.

For treatment, an assessment of the progress of the disease is important for the choice of a suitable therapy. This procedure is called “staging”.

Diagnostic methods are x-ray radiography, which has a very low sensitivity, computed tomography (CT), positron emission tomography (PET) or magnetic resonance imaging (MRI). These are noninvasive methods for the detection and localization of malignant lesions. For the correct classification biopsies from the tumors are required. They are obtained by endoscopic methods such as bronchoscopy, mediastinoscopy or thoracoscopy or after surgical intervention.

Patient with SCLC are categorized as having either limited disease (LD) or extensive disease (ED), which depends on the spread of the tumor to distant sites [4]. LD tumors are confined to the ipsilateral hemitorax while ED tumors include malignant pleural or pericardial effusions or hematogenous metastases. Since most SCLC tumors are not resectable and already formed metastases at the time of discovery, chemotherapy and radiotherapy are the treatments of choice for SCLC.

Staging of NSCLC is more complex. For this large group the so-called TNM staging system, which has been developed by the Union International Contre le Cancer (UICC; International Union Against Cancer; <http://www.uicc.org/>) and American Joint Committee on Cancer (AJCC; <http://www.cancerstaging.org/>), is applied to provide a description for the status of the disease. In this system T describes the extent of the primary tumor (T0 – T4), N the involvement of regional lymph nodes (N0 – N3) and M the absence (M0) or presence (M1) of distant metastasis. Using these descriptors, NSCLC is then classified into four stages I – IV, where stages I to III are further subdivided in A and B [5, 6]. Figure 1-1 gives an overview of the staging system and the relevant criteria (adopted from Lababede et al. [7]).

Table 1-1: Percentages of patients diagnosed with non-small cell lung cancer at a certain stage according to the TNM classification system and the average 5-year survival rates [8, 9].

| Diagnosis | | Survival | |
|-----------|---|----------|--------------------------|
| Stage | Patients diagnosed with lung cancer at this stage | Stage | 5-year survival rate |
| I | 25% | I A | 75 – 80% |
| | | I B | 55 – 60% |
| II | 7% | II A | 55 – 60% |
| | | II B | 35 – 45% |
| III | 32% | III A | 30 – 40% (T3, N1, M0) |
| | | | 15% (T1-3, N2, M0) |
| | | III B | 5% |
| IV | 36% | IV | < 1% |

Based on the staging results the appropriate treatment for NSCLC is chosen. The commonly used options are surgery, radiotherapy and chemotherapy. Depending on the disease status they can be used either alone or in combination.

For Patients that were diagnosed as stage I or stage II, surgery is the initial treatment of choice because the disease is still confined to a certain region of the lung. Surgery can be done as:

- segmentectomy or wedge resection, where only parts of a lobe are removed.
- lobectomy, where an entire lobe is removed.
- pneumonectomy, where the entire lung is removed.

Patients that are inoperable because of the tumor localization or their overall poor health and performance status are treated by radiotherapy.

The choice for the correct treatment of patients diagnosed stage III is more difficult because this class is very heterogeneous. At stage III A, if no mediastinal lymph nodes are involved, the treatment is comparable to the one for stage II. If ipsilateral lymph nodes are afflicted a multimodal strategy consisting of surgery and chemotherapy or radiotherapy and chemotherapy is employed. In this case patients might benefit from neoadjuvant chemotherapy prior to the treatment.

Lung cancers at stage III B with contralateral involvement of lymph nodes are considered as being unresectable. Therefore, chemoradiation is the treatment of choice. If the tumor spread can be reduced by this therapy, surgery might follow the initial treatment. Stage III B tumors with malignant pleural effusions are treated as being M1 and hence the same therapeutic conditions as for stage IV tumors apply.

As can be seen from Table 1-1 the prognosis for patients with metastatic tumors (stage IV) is extremely poor. Since patients are considered as being incurable a palliative chemotherapy and/or radiotherapy are applied to relieve pain and other distressing symptoms and improve the patient's quality of life.

After initial therapy an adjuvant chemotherapy or radiotherapy or chemoradiation often continues the treatment to eradicate remaining cancerous cells.

Table 1-2 gives an overview on the drugs that are currently used for chemotherapy. Usually, a platin-based drug is given in combination with another cytostatic agent. New and promising substances are epidermal growth factor receptor tyrosine kinase inhibitors and the angiogenesis inhibitor Bevacizumab, a monoclonal antibody that is directed against the vascular endothelial growth factor.

Table 1-2: Chemotherapeutic agents currently used for the treatment of NSCLC and their mode of action.

| Mechanism | Drugs |
|--|---|
| Platin-based DNA-crosslinker | Cisplatin Carboplatin |
| Mitotic inhibitors | Paclitaxel Docetaxel Vinorelbine Vinblastine |
| Antimetabolites | Gemcitabine Pemetrexed |
| Topoisomerase inhibitors | Etoposide Irinotecan |
| Antitumor antibiotics | Mitomycin C |
| Alkylating agents | Ifosfamide |
| Epidermal growth factor receptor (EGFR) tyrosine kinase inhibitors | Gefitinib Erlotinib |
| Vascular endothelial growth factor (VEGF) inhibitors | Bevacizumab |

All these therapeutic agents are administered systemically resulting in more or less severe unwanted side effects. The most prominent are nausea and vomiting, diarrhea or obstipation, pain, fatigue, reduction of red and white blood cells due to bone marrow depression or hair loss.

To circumvent such problems, regional drug delivery to the lungs via aerosolized chemotherapy has been suggested. This route of administration not only reduces the systemic burden but also avoids hepatic first-pass metabolism and allows the deposition of higher drug levels at the site of interest. Tatsumura et al. reported a high local deposition of 5-Fluorouracil after inhalation and very low systemic drug concentrations while obtaining a good anti-tumor response [10, 11]. Similar results were obtained in other studies with e.g. aerosolized doxorubicine [12], cisplatin [13] or 9-nitro-20(s)-camptothecin [14]. However, inhalative therapy is not yet established as a standard treatment because the effect of high doses of chemotherapeutics administered locally to the lung tissue still has to be evaluated to avoid pulmonary toxicity and drug-induced lung diseases. Therefore, further studies on new anti-cancer agents and drug formulations are needed to help this promising therapeutic approach reach the clinics.

An interesting target for new anti-cancer agents is the enzyme telomerase, which plays an important role in cell immortalization and hence cancer development (see section 1.2). Telomerase has been found to be upregulated in about 85% of lung cancers and its expression correlated with a poor prognosis for NSCLC patients [15-18].

1.2 Telomeres, Telomerase and their Implication in Cancer Development

In 1961 Hayflick and Moorehead demonstrated that human skin fibroblast in culture could only undergo a limited number of about 40 to 50 cell divisions before they entered the state of cellular senescence [19]. Furthermore, in 1965 Hayflick also reported a lower number of divisions for cells in culture derived from older people than for cells from younger people [20]. He suggested that this “countdown for senescence” is initiated at birth. Harley et al. demonstrated in 1990 that the length of chromosomal ends, the telomeres, shortens during aging of human fibroblasts [21]. The connection between telomere shortening and cellular senescence and/or apoptosis was shown after the discovery of the enzyme telomerase [22], a ribonucleoprotein that maintains the chromosomal ends. Ectopic expression of the catalytic subunit of this enzyme resulted in the elongation of telomeres and significantly extended the life span of human primary cells [23, 24].

Telomeres are non-coding guanine-rich repetitive sequences that end in a single-stranded 3'-overhang [25]. Humans telomeres are tandem repeats of the hexameric sequence 5'-(TTAGGG)-3', which is highly conserved in higher eukaryotes [26] (Figure 1-2). Due to their special structure, telomeres protect chromosomal ends from being recognized as damaged DNA. This prevents the initiation of such events like non-homologous end joining or homology directed repair, two mechanisms that strongly compromise the integrity of chromosomal ends. To fulfill their protective function, telomeres form a lasso-like structure, the so-called t-loop [27]. For the t-loop formation the G-rich single strand 3'-overhang invades the double stranded region of telomeres to form base pairs with the C-rich strand, thereby displacing the G-strand (d-loop; Figure 1-2).

Critically short telomeres are identified as damaged DNA most probably because of insufficient protection by shelterin proteins. They are recognized by the two phosphatidylinositol-3-kinase related protein kinases, ATM and ATR. This recognition triggers a molecular mechanism that results in the activation of p53, RB and p21. As a consequence cell cycle progression is inhibited and cells enter the state of senescence or even undergo apoptosis (reviewed by [28, 31]). Telomere erosion alone can also serve as a p53-independent checkpoint for cell proliferation. Cells that continue dividing will face serious chromosomal damages that finally result in cell death. This second checkpoint is termed “crisis” (Figure 1-3).

However, in the absence of functional tumor suppressors and after activation of oncogenes like c-Myc because of the genomic instabilities and rearrangements, cancer cells can escape these cell cycle checkpoints by expressing the enzyme telomerase [31, 33, 34]. Telomerase is a ribonucleoprotein complex that synthesizes new TTAGGG-sequences at the 3'-ends of chromosomes to maintain telomeres at a stable length. It is composed of *human telomerase RNA* (hTR) [35], which contains the template region for the synthesis of new telomeric repeats, and *human telomerase reverse transcriptase* (hTERT), the catalytic subunit of the enzyme (Figure 1-4) [36]. In the active complex two hTR/hTERT units are associated with one dyskerin molecule [37].

Telomerase is normally expressed at high levels during embryonic development but is downregulated after birth in the larger parts of tissues. In the healthy organism telomerase activity is limited to germ lines and certain stem cell compartments, i.e. specialized cells that need to retain their unlimited proliferative capacity [38, 39].

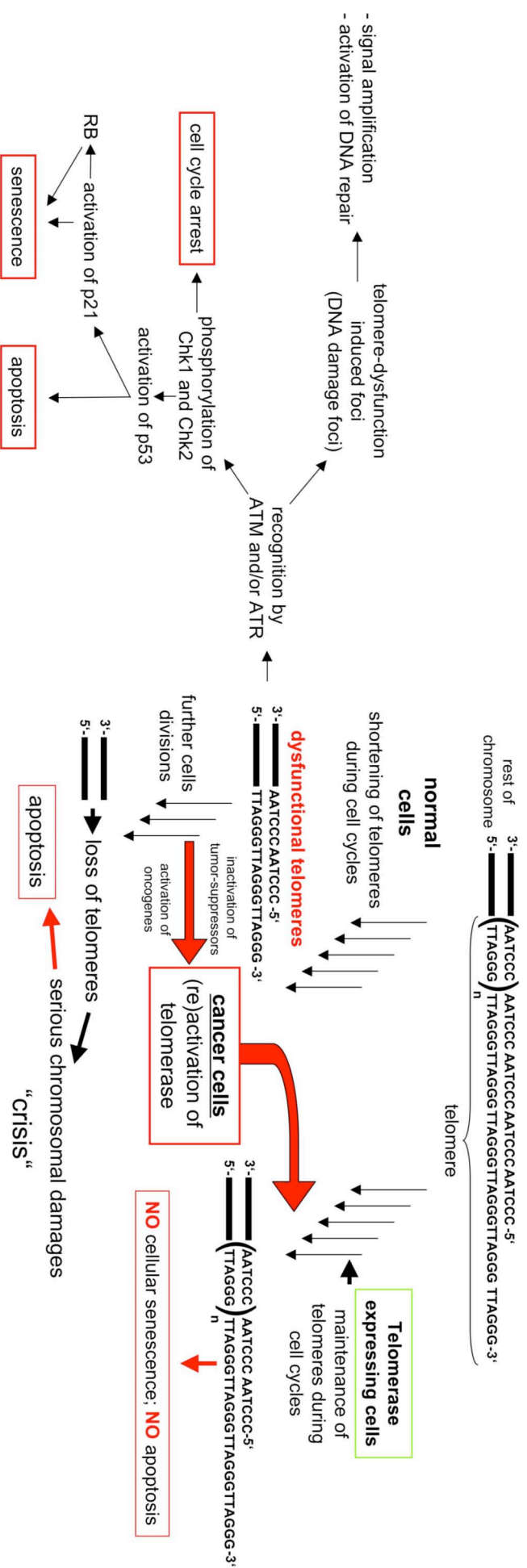


Figure 1-3: Mechanism of cellular senescence and apoptosis and the influence of telomerase expression on cell survival. In normal cells telomeres shorten until they reach a critical length and become dysfunctional. This triggers a mechanism that results in cell cycle arrest, senescence and apoptosis. Cells that do not stop dividing will face serious chromosomal damages due to the loss of telomeres. Few cells like stem cells, germ line cells or fetal cells express the enzyme telomerase and can therefore divide indefinitely. For cancer development the (re)activation of telomerase is a crucial step toward immortality. They normally have very short telomeres that constantly require telomere maintenance by telomerase.

Telomerase has been reported to be active in about 80-90% of cancer cells [40, 41]. Its expression is a crucial step for their limitless replicative potential and evasion from apoptosis, which are two of the six hallmarks of cancer [42]. Those cancer cells that do not express telomerase maintain their telomeres by a homologous recombination-mediated process termed alternative lengthening of telomeres (ALT; reviewed in [43, 44]).

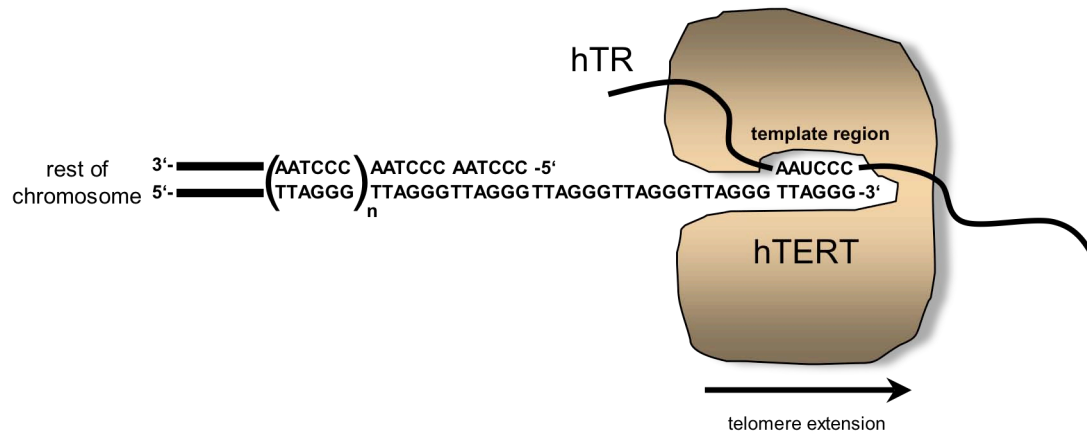


Figure 1-4: Elongation of the 3'-strand overhang by telomerase. hTERT = human telomerase reverse transcriptase (the catalytic subunit); hTR = human telomerase RNA (contains the template region for the synthesis of new TTAGGG-repeats).

Due to its crucial role in carcinogenesis the inhibition of telomerase became quickly an interesting target for the development of new anti-cancer strategies. It could be shown that telomerase inhibition results in telomere shortening and suppression of tumor growth both *in vitro* and *in vivo*.

To date numerous strategies for telomerase inhibition, either directly or indirectly, have been investigated. The direct approaches targeted both the catalytic subunit hTERT and the RNA component hTR. Potent inhibitors of hTERT are the reverse transcriptase inhibitors BIBR 1532 [45] or AZT [46]. hTR could be successfully targeted with chemically modified oligonucleotides that block the template region for the synthesis of new telomeric repeats [47, 48]. The lipid-linked oligonucleotide and telomerase template antagonist GRN163L [49-51] has entered several clinical trials to prove its efficacy either administered alone or in combination with established anti-cancer drugs (www.clinicaltrials.gov).

Another strategy does not focus on telomerase but on its substrates, the telomeres. Here the class of so-called G-quadruplex stabilizing substances has been widely investigated. G-quadruplexes are special structures that can form in guanine-rich DNA sequences like the telomeres. Their stabilization by specially designed molecules prevent telomerase from recognizing the single-strand overhangs. Furthermore, G-quadruplex stabilizers were reported to induce telomere dysfunction due to the displacement of telomere-associated proteins such as the shelterin complex. Therefore, a treatment with this kind of inhibitors results in a faster response as could be expected from telomere erosion alone [52-54].

Vaccination against hTERT as a tumor antigen is another approach currently under investigation in clinical trials. Cancer patients are immunized against short hTERT peptide sequences that can be recognized by cytotoxic T-lymphocytes [55-57].

Other strategies employ adenoviral-mediated gene therapy. The gene constructs contain promoter regions for hTR or hTERT so that transcription of the actual gene sequence will only occur in telomerase expressing cells. This mechanism is currently exploited for suicide gene therapy [58, 59] and oncolytic viral therapy [60].

Concerns were raised that telomere inhibition might lead to severe side effects because other telomerase expressing cells, i.e. germ cells and stem cells, will also be affected by the treatment. However, telomeres from cancer cells are normally considerably shorter than those from other telomerase expressing cells [32]. Since cancer cells divide more rapidly, telomere erosion in tumors should be much faster. Therefore the effect of telomerase inhibition is expected to be much more pronounced in cancer cells than in other cell types.

Another point of criticism in anti-telomerase therapy might be the lag time between the start of the treatment and first effects on cell proliferation. This period strongly depends on the initial telomere length of tumor cells. However, it has been demonstrated that telomerase inhibition enhances the efficacy of other anti-cancer therapies [61-66]. So even if telomerase inhibition alone

cannot be used because of a retarded effect this synergism might be exploited in future therapies.

1.3 Objectives of the studies

This project was done in cooperation with the group of Professor Dr. Ulrich Klotz from the Dr. Margarete Fischer-Bosch Institute for Clinical Pharmacology, Stuttgart, and University of Tübingen and financially supported by the Deutsche Krebshilfe e.V. (Project no.: 10-2035-KI I) and the Robert Bosch Foundation (Stuttgart, Germany).

The work described in Chapter 6 was done in the group of Professor Dr. Elias Fattal, UMR CNRS 8612, Pharmaceutical Faculty of the University Paris Sud 11, Châtenay-Malabry, France, and financially supported by the GALENOS Fellowship in the Framework of the EU Project "Towards a European PhD in Advanced Drug Delivery, Marie Curie Contract MEST-CT-2004-404992.

The aim of the project was the development of new strategies for the treatment of non-small lung cancer by telomerase inhibition with formulations that are suitable for a local application via the inhalative route.

For this purpose different telomerase inhibitors that have been described in the literature were tested. From these studies three substances were selected as potential drug candidates:

- the acridine derivative BRACO19, which belongs to the telomere-targeting G-quadruplex stabilizing substances [67].
- an antisense 2'-O-methyl-RNA (ZOMR) that is complementary to the template region of hTR [48].
- a small interfering RNA (siRNA) that is directed against the mRNA of the catalytic subunit hTERT.

BRACO19 (Figure 1-5) could be regarded as the prototype of a new class of drugs based on 3,6,9-substituted acridine derivatives. Although it has been reported to be a very potent telomerase inhibitor and effective in targeting the telomeres, nothing was known about its biopharmaceutical and physico-chemical properties. Since these information are essential for the development of delivery strategies, the studies with BRACO19 concentrated on a thorough characterization regarding its transport across biological barriers and stability under physiological conditions and a categorization

according to the biopharmaceutical classification system (BCS) as introduced by Amidon et al. [68] (Figure 1-6; Chapter 2 and Chapter 3).

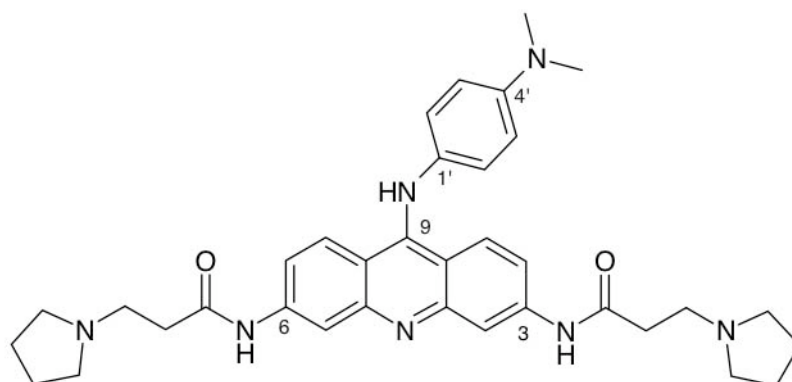


Figure 1-5: Structure of the 3,6,9-substituted acridine derivative BRACO19

| | |
|--|---|
| <p>Class I</p> <p>good solubility</p> <p>good permeability</p> | <p>Class II</p> <p>poor solubility</p> <p>good permeability</p> |
| <p>Class III</p> <p>good solubility</p> <p>poor permeability</p> | <p>Class IV</p> <p>poor solubility</p> <p>poor permeability</p> |

Figure 1-6: The categorization of drug compounds according to the biopharmaceutical classification system. The key factors are the dissolution of the drug in biological fluids and its permeation across biological barriers.

The oligonucleotide-based drugs 2OMR and siRNA are known to be very effective and specific. However, due to their size and negative charge the main obstacle for these molecules is their poor uptake into cells. Furthermore, they are rapidly degraded in the presence of nucleases. Therefore, this kind of drugs requires a suitable carrier system to ensure an efficient and safe uptake.

For 2OMR a delivery system based on cationic chitosan/PLGA nanoparticles was chosen. Chitosan and PLGA (Figure 1-7) are both biocompatible and biodegradable.

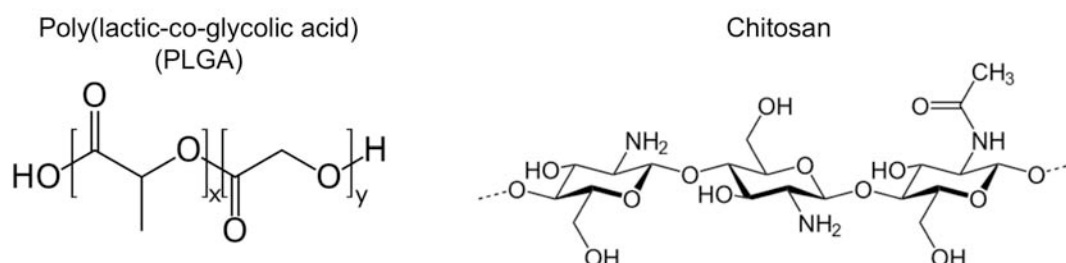


Figure 1-7: Structures of the polyester poly(lactic-co-glycolic acid) (PLGA) and the polysaccharide chitosan which is composed of randomly distributed β-(1-4)-linked D-glucosamine and N-acetyl-D-glucosamine.

Nanoparticles composed of these polymers were previously developed for the delivery of plasmid DNA. In our studies they were evaluated as carriers for the short oligonucleotides 2OMR. The work focused on the influence of chitosan content in the particle formulation on binding and delivery efficiency and the fate of nanoplexes in different cell types as well as the efficacy regarding the inhibition of telomerase activity (Chapter 4 and Chapter 5).

RNA interference (RNAi) is the latest mechanism described for gene silencing. RNAi is mediated via short double stranded RNA sequences with a length of normally 21 base pairs and overhanging 3'-ends [69, 70] termed short inhibitory RNA (siRNA). After its discovery, it became rapidly a powerful tool in molecular biology for studying the downregulation of gene expression. These properties made it also interesting for medical applications.

For the delivery of siRNA a more refined system based on cationic DOTAP/DOPE liposomes was investigated. These liposomes were modified with the endogenous glycosaminoglycan hyaluronic acid (Figure 1-8) for the targeting of cancer cells that overexpress the CD44-receptor.

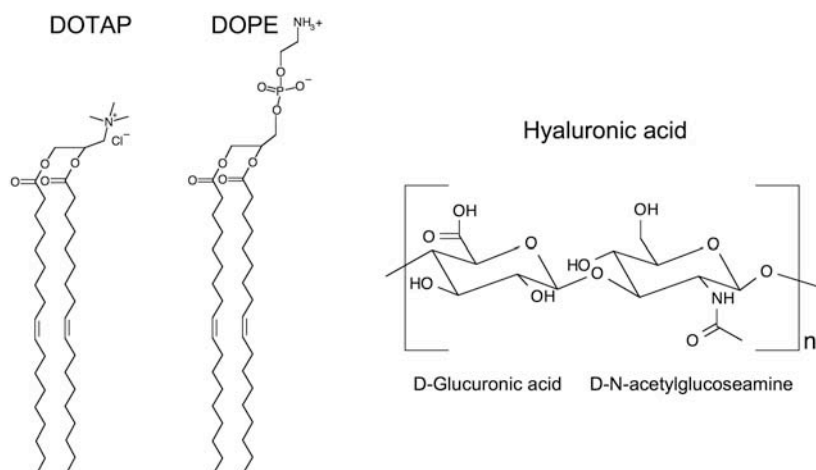


Figure 1-8: Structures of the lipids DOTAP (1,2-dioleoyl-3-trimethylammonium-propane) and DOPE (1,2-Dioleoyl-sn-glycero-3-phosphoethanolamine) and the endogenous polymer hyaluronic acid.

In these studies the influence of the modification on liposome properties was examined in comparison with non-modified liposomes. Special attention was given to the liposome properties, binding and protection of siRNA in the complex, the cytotoxicity of the new system and its efficiency for targeting CD44-expressing lung cancer cells (Chapter 6).

Chapter 2

Biopharmaceutical Characterization of the Telomerase Inhibitor BRACO19

The data presented in this chapter has been published as a short communication in the journal *Pharmaceutical Research*:

Taetz, S., Baldes, C., Mürdter, T. E., Kleideiter, E., Piotrowska, K., Bock, U., Haltner-Ukomadu, E., Mueller, J., Huwer, H., Schaefer, U. F., Klotz, U., Lehr, C.-M.

Biopharmaceutical characterization of the telomerase inhibitor BRACO19. (2006) *Pharm. Res.*, 23(5), 1031-1037.

DOI:

10.1007/s11095-006-0026-y

Weblink:

<http://www.springerlink.com/content/w06750366765q138/>

2.1 Introduction

Telomerase, a ribonucleoprotein enzyme that belongs to the class of reverse transcriptases, plays an important role in the control of proliferation and carcinogenesis by maintaining the length of telomeres. Telomeres are lasso-like structures at the end of chromosomes. They protect them from recombination, nuclease degradation, DNA repair mechanisms and end-to-end fusions. They also act as a kind of “mitotic clock” by constant erosion after each cell cycle. Reaching a critical length is a signal for the cell to stop dividing and enter the state of replicative senescence (M1 stage). Cells that bypass replicative senescence and continue dividing will face serious DNA damages and subsequently cell death due to further telomere shortening (M2 stage or crisis). However, cells expressing high levels of telomerase, like cancer cells, can escape this mechanism by keeping the telomere length above this limit and therefore divide indefinitely [71, 72].

The approach of telomerase inhibition for the treatment of cancer attracted increasing interest in the last years because telomerase is expressed in most types of cancer cells but not in normal cells with the exception of hematopoietic stem cells, germ cells, stem cells of the intestine and the skin.

Non-small cell lung cancer (NSCLC) is the most common form of lung cancer and has a poor prognosis. Misawa *et al.* showed that telomerase inhibition in the NSCLC cell line A549 led to an increase in apoptosis and higher sensitivity to chemotherapeutic agents [64]. Inhibiting telomerase with suitable drugs would ideally affect cancer cells only and spare healthy tissue. Due to such inherent selectivity an inhalative application of telomerase inhibitors might be possible. The drug could be delivered directly to the lung, thereby further reducing unwanted systemic drug effects.

A screening for potential telomerase inhibitors led us to the acridine derivative BRACO19 (9- [4- (N,N- dimethylamino)phenylamino]- 3,6- bis(3- pyrrolidino-propionamido) acridine x 3HCl; Figure 2-1) [73]. This substance inhibits telomerase activity and can lead to telomere dysfunction by G- quadruplex stabilization in telomeres [67, 74].

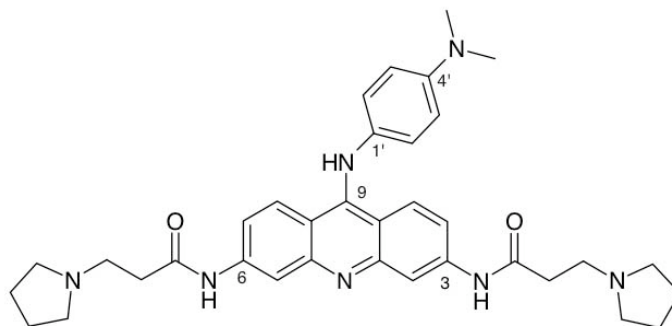


Figure 2-1: The 3,6,9- substituted acridine derivative BRACO19 (9-[4-(N,N-dimethylamino)phenylamino]-3,6-bis(3-pyrrolidinopropionamido) acridine x 3HCl) according to [67].

For the development of a new drug formulation knowledge about biopharmaceutical properties like solubility, cytotoxicity, permeation of the drug across biological barriers (like the lung epithelia) or protein binding are as important as the cytotoxic or pharmacological properties of the drug.

Protein binding and interaction with membrane lipids were tested by two HPLC methods using immobilized human serum albumin (HSA) and immobilized artificial membrane (IAM) chromatography, respectively.

To investigate the permeability of BRACO19 across relevant biological barriers we used the SV40 virus immortalized cell line 16HBE14o⁻ [75, 76] and the adenocarcinoma cell line Calu-3 [77, 78] as models of the bronchial epithelium. The alveolar epithelium was represented by primary human alveolar type II cells which develop type I characteristics when cultivated under appropriate conditions [79, 80]. For comparison we also included the intestinal adenocarcinoma cell line Caco-2, an established model for intestinal drug absorption [81].

2.2 Materials and Methods

2.2.1 Substances and buffers

BRACO19 was synthesized by ENDOTHERM GmbH (Saarbruecken, Germany) according to Harrison *et al.* [82]. Identity was proven by NMR, purity by HPLC. Propranolol- HCl was purchased from Synopharm GmbH & Co. KG (Barsbuettel, Germany), cyclosporin A from Calbiochem® (Merck Bioscience GmbH, Bad Soden, Germany), fluorescein- Na and tetraethylammonium chloride (TEAC) were obtained from Fluka Chemie GmbH (Buchs, Switzerland).

HBSS (Hank's balanced salt solution) buffer was composed of 137.0 mM NaCl, 5.36 mM KCl, 4.26 mM NaHCO₃, 0.18 mM Na₂HPO₄ x 7 H₂O, 0.44 mM KH₂PO₄, 5.55 mM Glucose, 10.0 mM HEPES (N-[2-hydroxyethyl]piperazine-N'-[2-ethanesulfonic acid]), 0.13 mM CaCl₂ x 2 H₂O, 0.05 mM MgCl₂ x 6 H₂O, 0.04 mM MgSO₄ x 7 H₂O. For transport experiments 0.25% BSA (Sigma-Aldrich Chemie GmbH, Taufkirchen, Germany) was added to the HBSS buffer (HBSS/BSA buffer).

Sterile BSS (balanced salt solution) contained 137.0 mM NaCl, 5.0 mM KCl, 0.7 mM Na₂HPO₄ x 7 H₂O, 1.2 mM MgSO₄ x 7 H₂O, 5.5 mM Glucose, 10.0 mM HEPES, 0.18 mM CaCl₂, 100 units/ml penicillin and 100 µg/ml streptomycin. All reagents were of cell culture grade. The pH was adjusted to 7.4 with 1 M NaOH.

2.2.2 Cells and cell culture conditions

Calu-3 cells (HTB- 55, ATCC, Manassas, VA, USA) were cultivated in Minimum Essential Medium (MEM) with Earl's Salts and L- glutamine (PAA Laboratories GmbH, Pasching, Austria) supplemented with 10% FCS, 1% MEM non- essential amino acid (NEAA) solution and 1 mM sodium pyruvate (all from Sigma- Aldrich).

16HBE14o⁻ cells were a gift from Dr. Dieter Gruenert (Department of Medicine, University of Vermont, Burlington, VT, USA). They were grown in MEM with Earl's Salts and L- glutamine (PAA Laboratories GmbH)

supplemented with 10% FCS, 1% NEAA solution and 3 mM glucose (Sigma-Aldrich).

Caco-2 cells (C2BBE1, ATCC) were cultivated in Dulbecco's Modified Eagle Medium (DMEM) with high glucose (4.5 g/ml) and L- glutamine (PAA Laboratories GmbH) supplemented with 10% FCS and 1% NEAA solution.

All cell lines were kept in 5% CO₂ and 90- 98% humidity at 37°C.

For transport studies Calu-3 (passage 27 and 32), 16HBE14o⁻ (passage 2.68) and Caco-2 (passage 83) cells were seeded at a density of 60,000 cells/cm² on Transwell[®] polyester (PET) filter inserts with a growth area of 1.13 cm² and a pore size of 0.4 μm (Transwell[®] Permeable Supports, Corning Inc., NY, USA).

Primary human alveolar epithelial cells (hAEpC) were isolated from non-tumor lung tissue of patients undergoing partial lung resection according to Elbert *et al.* [79] with slight modifications of the enzymatic digestion and cell purification [83]. In brief, the chopped tissue was digested using a combination of 150 mg trypsin type I (Sigma) and 3 mg elastase (Worthington Biochemical Corp., Lakewood, NJ, USA) in 30 ml BSS for 40 min. at 37°C. The AT II cell population was purified by a combination of differential cell attachment, percoll density gradient centrifugation and positive selection of epithelial cells with magnetic beads (human Anti- HEA (Ep-CAM) MicroBeads, Miltenyi Biotec, Bergisch Gladbach, Germany). Cell viability was assessed by trypan blue staining.

The isolated hAEpC were seeded at a density of 600,000 cells/cm² on collagen/ fibronectin coated Transwell[®] polyester filter inserts (Corning Inc.) with a growth area of 0.33 cm². They were grown in SAGM medium (Cambrex BioScience Walkersville Inc., Walkersville, MD, USA) supplemented with 1% FCS, 100 units/ml penicillin and 100 μg/ml streptomycin (Sigma- Aldrich).

The formation of confluent monolayers and tight junctions was verified by measuring the transepithelial electrical resistance (TEER) using an epithelial voltohmmeter (EVOM, World Precision Instruments, Berlin, Germany) with a STX-2 electrode.

For transport experiments, Calu-3 cells were used 14 days post seeding, 16HBE14o⁻ cells and Caco-2 cells were used after 7 and 21 days,

respectively. hAEpC were cultivated for 8 days. TEER values were as reported before or higher for transport experiments [79, 84]: about $1000 \Omega \times \text{cm}^2$ for Calu-3, $800 \Omega \times \text{cm}^2$ for 16HBE14o⁻, $750 \Omega \times \text{cm}^2$ for Caco-2 and $1400 \Omega \times \text{cm}^2$ for hAEpC.

2.2.3 Transport studies

Prior to transport experiments cell culture media were removed and the apical and basolateral compartments were washed twice with HBSS/BSA buffer. Cells were equilibrated for 2- 2.5 hours with this buffer.

After the equilibration period buffer was exchanged with drug solutions of the same buffer in either the apical or basolateral compartment. The volumes for the apical and basolateral side for 16HBE14o⁻, Calu-3 and Caco-2 were 500 μl and 1500 μl , respectively. The volumes for hAEpC were 200 μl for the apical side and 800 μl for the basolateral side.

50 μl samples from the donor compartments were drawn immediately at the beginning and at the end of the transport experiments. 50 μl samples from the acceptor compartments were drawn after 30, 60, 120, 180, 240 and 300 minutes. An equal volume of fresh buffer was returned to the acceptor compartment after each sampling. The filter plates were kept under cell culture conditions and were slightly shaken with an orbital shaker. TEER values were measured after the equilibration period and at the end of transport experiments to verify that the barrier function of the monolayers was not compromised. The drug concentrations in the donor compartments were as follows: 16HBE14o⁻: 20 $\mu\text{g}/\text{ml}$ of propranolol, fluorescein and BRACO19, respectively; Calu-3 and Caco-2: 20 $\mu\text{g}/\text{ml}$ fluorescein, 100 and 200 $\mu\text{g}/\text{ml}$ BRACO19; hAEpC: 100 and 200 $\mu\text{g}/\text{ml}$ BRACO19.

Each experiment was performed fivefold in either direction.

2.2.4 Transport experiments with different inhibitors

Calu-3 cells are known to express the P- glycoprotein (P-gp) efflux system [85] and organic cation transporter proteins (influx/ efflux of organic cations) [84]. Inhibition of BRACO19 transport was studied at a donor concentration of 200 $\mu\text{g}/\text{ml}$ as described in *Transport studies* with the following modifications. For the inhibition of P-gp and other multi drug resistance efflux systems we

added 10 μM cyclosporin A [86] to the HBSS/BSA buffer. For the inhibition of organic cation transporter proteins the buffer was supplemented with 5 mM TEAC [87]. The inhibitors were present in both compartments. Transport experiments were also performed at 4°C to check for other active transport mechanisms as well as at 37°C without inhibitors for comparison. The results were compared to those of the previous experiments with Calu-3 cells.

2.2.5 Calculation of apparent permeability coefficient P_{app}

The apparent permeability coefficient P_{app} was calculated according to :

$$P_{\text{app}} (\text{cm/sec}) = \frac{J}{A \cdot C_0} \quad \text{Equation 2-1}$$

where J is the linear section of the flux ($\mu\text{g/sec}$), A the filter area (cm^2) and C_0 the initial donor concentration ($\mu\text{g/cm}^3$).

2.2.6 Determination of uptake into cells and adsorption to filter material

For adsorption/ uptake studies filters were washed twice with HBSS buffer after the transport experiments and the filter membranes with cells were cut out. Cells were lysed in 1 ml of a 80:20 mixture of methanol:HBSS (v/v) by means of ultrasonication for 30 minutes. For removal of cell fragments the suspensions were first kept at -80°C for 45 minutes and were then centrifuged for 20 minutes at 14,000 rpm and 0°C. An aliquot of the supernatant was used for analysis.

2.2.7 Sample analysis

BRACO19 and propranolol samples were analyzed by reversed phase HPLC using an isocratic Dionex HPLC system consisting of an ASI 100 automated sample injector, UVD 340U diode array detector and P680 pump with Chromeleon® software (version 6.60 SP1 build 1449) (Dionex, Idstein, Germany).

For BRACO19 analysis a Gemini® RP- 18 column (150 x 4.6 mm/ 5 μm / 110 Å) (Phenomenex, Aschaffenburg, Germany) was used. The mobile phase was composed of 80:20 (v/v) methanol:borate buffer pH 10.0 (100 mM). At a

flow rate of 0.6 ml/min the retention time of BRACO19 was 8.9 ± 0.2 minutes. The UV- detector was set at 268 nm.

Propranolol was analyzed with a Lichrospher[®] RP- 18 column (125 x 4 mm/ 5 μ m) (Merck, Darmstadt, Germany). The mobile phase was composed of 45:33:22 (v/v/v) water:methanol:acetonitrile supplemented with 0.033% (v/v) triethylamine and 0.044% (v/v) phosphoric acid. The flow rate was set to 1.2 ml/min and the retention time was 2.9 ± 0.25 minutes. Propranolol was detected at 215 nm.

Injection volumes for both substances were 20 μ l per sample.

Fluorescein was analysed by fluorimetry using a Cytofluor II fluorescence reader with Cytofluor software version 4.2 (PerSeptive Biosystems, Wiesbaden- Norderstedt, Germany). 50 μ l samples were diluted to 200 μ l with 1 mM NaOH in a 96- well plate. The excitation wavelength was set to 485 nm and the emission wavelength to 530 nm.

All unknown samples were calculated against known standards. Standards were in the range of 0.02- 20 μ g/ml. If necessary, samples were diluted 1:10.

2.2.8 IAM chromatography measurements

Immobilized artificial membrane (IAM) chromatography of BRACO19 was performed with a phosphatidylcholine-functionalized column (Regis Technologies). The mobile phase was composed of potassium buffer pH 6.8 and acetonitrile. A Waters HPLC system W2790 and PDA detector W2996 with Millenium³² software (Milford, Massachusetts, USA) was used for analysis. The classification of the drug cellular membrane interaction in terms of permeability was performed by the marker molecules uracil (eluting with the injection peak), atenolol (3.07, 50 %), ketoprofen (5.55, 92 %), carbamazepine (7.64, 70 %) and propranolol (11.55, 90 %). The values in brackets indicate the KIAM values for the compounds and the corresponding fraction absorbed according to the Biopharmaceutical Classification System [88].

2.2.9 HSA binding

HSA binding of BRACO 19 was investigated by using a human serum albumin functionalized column (Thermo Hypersil) according to a method developed by Across Barriers GmbH. The mobile phase was composed of ammonium acetate buffer pH 7.4 and propanol. An isocratic Waters HPLC system W2690 and dual wavelength detector W2487 with Millenium³² software (Milford, Massachusetts, USA) was used for analysis. For the classification of drug binding the following system was established from different literature values: 0- 40% for weak, 40- 50% for weak/ medium, 50- 85% for medium, 85- 95% for medium/ strong and > 95% for strong drug binding to HSA. Substances for calibration were acetaminophen (24% protein binding), carbamazepine (76 %), propranolol (90 %) and naproxen (99 %).

2.2.10 MTT cytotoxicity assay

Cytotoxicity of BRACO19 was tested using the methyl-thiazolyl-tetrazolium (MTT) assay. 16HBE14o⁻, Calu-3 and Caco-2 cells were grown at a density of 60,000 cells/ cm² on 96 well Cellstar[®] tissue culture plates (Greiner bio-one, Frickenhausen, Germany) for 6 days under cell culture conditions (see above) in 200 µl medium with different concentrations of BRACO19. hAEPc were grown under the same conditions but at a density of 30,000 cells/cm². BRACO19 concentrations were in the range of 0- 50 µM. Each concentration was tested in quadruplicate. Cell culture medium with or without BRACO19 was changed every other day. After 6 days the medium was exchanged for 200 µl BRACO19- free medium and 10 µl of 5 mg/ml MTT solution in phosphate buffered saline (PBS) were added to each well. After 3.5 hours incubation the medium was removed and the cells were washed with PBS. 200 µl of 100% isopropanol were added to each well and the plate was left for crystal dissolution on an orbital shaker over night. Absorption was measured at a wavelength of 550 nm with an UV/Vis reader (SLT Spectra, Tecan Deutschland GmbH, Crailsheim, Germany). Viability of cells treated with BRACO19 was related to cells grown in BRACO19- free medium. The IC₅₀ value was determined by non- linear regression using SigmaPlot[®] Version 9 (SPSS Inc., Chicago, Illinois).

2.3 Results

2.3.1 Solubility, cytotoxicity, protein binding and IAM chromatography measurements

BRACO19 (Figure 2-1) showed good and rapid solubility of at least 2 mg/ml in distilled water and physiological buffer solutions in a pH range of 2.8- 7.4. For transport experiments we used a 2 mg/ml stock solution in HBSS/BSA buffer (pH 7.4) which was diluted to the desired concentration before each experiment in the same buffer system.

The IC_{50} values found in the MTT cytotoxicity test were as follows: Calu-3 $13.6 \pm 3.8 \mu\text{M}$, 16HBE14o⁻ $3.6 \pm 1.2 \mu\text{M}$ and hAEpC $6.0 \pm 0.4 \mu\text{M}$. Interestingly, Caco-2 cells were not affected by BRACO19 concentrations up to 50 μM .

BRACO19's binding to human serum albumin was found to be 38% indicating a weak to medium protein binding referring to the reference compounds. By the IAM chromatography measurements BRACO19 was eluted very early from the column together with the injection peak. This points out a low potential for BRACO19 to overcome barriers like phospholipid membranes.

2.3.2 Transport experiments

In the first transport experiment the permeability of BRACO19 was compared with the high permeability marker propranolol and the low permeability marker fluorescein in 16HBE14o⁻ cells. BRACO19 transport was found to be asymmetrical and very low. For the apical to basolateral (AB) direction no transport could be detected at all. In basolateral to apical (BA) direction transport was about tenfold lower than for fluorescein.

The results for Calu-3, Caco-2 and hAEpC were comparable to those found with 16HBE14o⁻ cells. Even after increasing the donor concentrations of BRACO19 to 100 and 200 $\mu\text{g/ml}$ to facilitate detection in the receiver compartment no transport could be detected in AB direction for neither cell line. Also, in BA direction the apparent permeability coefficients were still lower than the permeability of fluorescein. The results of all transport experiments are summarized in Table 2-1.

Table 2-1: Apparent permeability coefficients (P_{app} ; in $\text{cm}/\text{sec} \times 10^7$) of BRACO19 in comparison with propranolol and fluorescein in different cell lines (16HBE14o⁻, Calu-3, Caco-2), primary human alveolar epithelial cells (hAEpC) and cell free filters. n.d. = no substance detectable in acceptor compartment; X = high BRACO19 concentrations led to a collapse of monolayer integrity.

| Substance | initial donor concentration | 16HBE14o ⁻ | | Calu-3 | | Caco-2 | | hAEpC | | filters without cells | |
|-------------|-----------------------------|-----------------------|----------------------|--------------------|--------------------|--------------------|--------------------|-------|--------------------|-----------------------|---------------------|
| | | A → B | B → A | A → B | B → A | A → B | B → A | A → B | B → A | A → B | B → A |
| BRACO19 | 20 $\mu\text{g}/\text{ml}$ | n.d. | 0.98 ± 0.23 | - | - | - | - | - | - | 70.08 ± 10.47 | 94.50 ± 1.85 |
| BRACO19 | 100 $\mu\text{g}/\text{ml}$ | - | - | n.d. | 0.25 ± 0.05 | n.d. | 0.31 ± 0.03 | n.d. | 0.66 ± 0.07 | - | - |
| BRACO19 | 200 $\mu\text{g}/\text{ml}$ | - | - | n.d. | 0.32 ± 0.05 | n.d. | 0.57 ± 0.03 | X | X | - | - |
| Fluorescein | 20 $\mu\text{g}/\text{ml}$ | 4.59 ± 0.66 | 9.59 ± 0.67 | 1.15 ± 0.18 | 1.26 ± 0.14 | 9.46 ± 1.16 | 8.95 ± 1.35 | - | - | - | - |
| Propranolol | 20 $\mu\text{g}/\text{ml}$ | 131.59 ± 7.37 | 106.51 ± 5.97 | - | - | - | - | - | - | - | - |

Transport experiments with cell free filters and BRACO19 solution were performed under analogous conditions to look for the influence of the Transwell[®] system. The P_{app} values were about 100- fold higher than for filters with cells (data not shown), indicating that the permeation through cell free filters is not rate limiting.

TEER values of all cell monolayers remained stable or even increased slightly during transport studies. Only in the experiment with hAEpC and 200 $\mu\text{g}/\text{ml}$ BRACO19 donor concentrations a strong decrease in TEER to about 200 $\Omega \times \text{cm}^2$ could be found. This was accompanied by a comparably strong non- linear increase in BRACO19 concentrations in the respective acceptor compartments.

2.3.3 Experiments with transport inhibitors and uptake/adsorption studies

The results for transport experiments with Calu-3 cells in the presence of different inhibitors are summarized in Table 2-2. They were comparable to those under normal conditions: no transport in AB direction was detected and the P_{app} values for BA transport were within the range of the former experiments. This indicates that efflux/ influx systems or active transport are not involved in the transport of BRACO19.

Table 2-2: P_{app} values (in $\text{cm/sec} \times 10^7$) of BRACO19 (200 $\mu\text{g/ml}$ donor concentration) in Calu-3 cells under normal conditions, in the presence of the P-gp inhibitor cyclosporin A (10 μM), the organic cation transporter protein inhibitor TEAC (5 mM) and at 4°C. n.d. = no substance detectable in acceptor compartment.

| Substance | initial donor concentration | control | | Cyclosporin A | | TEAC | | 4°C | |
|-----------|-----------------------------|---------|--------------------|---------------|--------------------|-------|--------------------|-------|--------------------|
| | | A → B | B → A | A → B | B → A | A → B | B → A | A → B | B → A |
| BRACO19 | 200 $\mu\text{g/ml}$ | n.d. | 0.27 ± 0.03 | n.d. | 0.92 ± 0.10 | n.d. | 0.31 ± 0.03 | n.d. | 0.18 ± 0.04 |

The asymmetry found in the transport experiments could also be observed in the uptake/ adsorption studies (Figure 2-2). Filters that were in direct contact with BRACO19 solution from the basolateral side (BA transport) contained more BRACO19 than those that were in contact with the solution from the apical side (AB transport). An exception was the transport experiment with hAEPc at 200 $\mu\text{g/ml}$ BRACO19 donor concentration where the integrity of the monolayers collapsed. Here the amounts of BRACO19 in filters found for AB transport were similar to those of BA transport. Amounts of BRACO19 found in cell free filters submitted to the same conditions were comparable to those of BA transport.

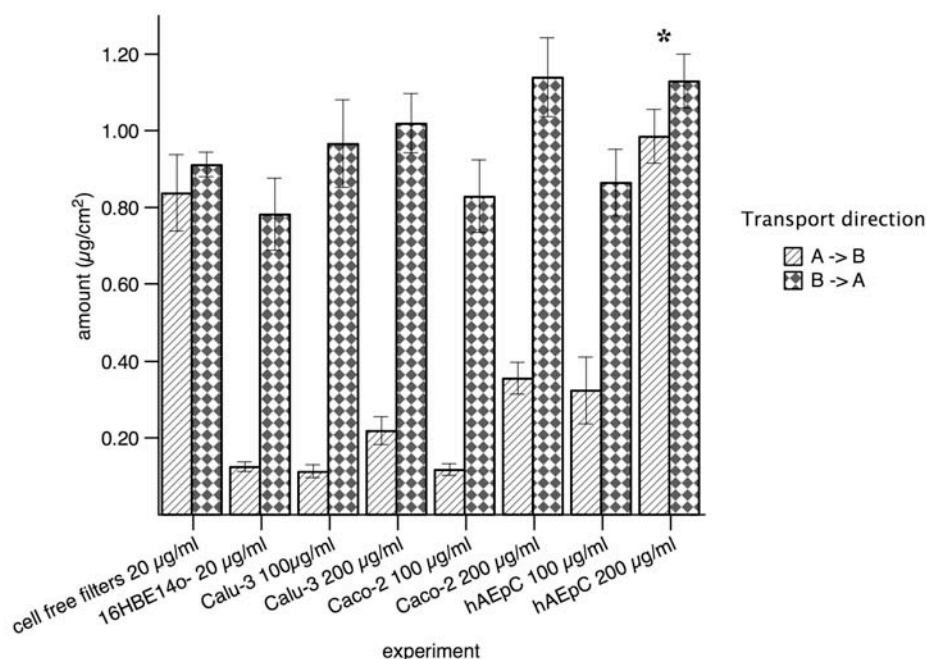


Figure 2-2: Amounts of BRACO19 ($\mu\text{g/cm}^2$) recovered from excised filters. Concentrations refer to initial donor concentration of BRACO19. * = integrity of monolayer compromised by high BRACO19 concentration.

2.4 Discussion

Our studies showed that BRACO19 has a good solubility in aqueous media in the concentrations that were used. The *in vitro* cytotoxicity of BRACO19 for our pulmonary epithelial cells was comparable to values found in literature for other cancerous cell lines derived from other organs (e.g. vulva carcinoma cells, breast cancer cells or uterus carcinoma cells) [67, 74, 89]. In comparison to “classic” anti-cancer drugs, the cytotoxicity of BRACO19 was within the range of cisplatin (10- 25 μM) [90, 91] but lower than for doxorubicin (0.4 - 2.4 μM) [92], paclitaxel (0.7- 1.8 nM) [91] or vincristine (1.9- 3.5 nM) [93]. However, it has to be kept in mind that the strategy of this therapeutic approach is the (re)induction of senescence and apoptosis by telomerase inhibition (i.e. a controlled cell death) and not the simple poisoning of malignant cells. Therefore, a high IC_{50} value is desired.

Protein binding of BRACO19 to HSA was rather weak compared to reference drugs. The results from IAM chromatography measurements suggest that interaction of BRACO19 with membrane lipids is negligible because there is a proportional relationship between the capacity factor k'_{IAM} and the membrane partitioning coefficient K_m [94].

Our transport studies showed that BRACO19 has great problems to overcome biological barriers. The transport experiments with Caco-2 cells, a standard model for intestinal drug absorption, indicate that BRACO19 might not be suitable for oral administration. Burger *et al.* already demonstrated that tumor xenografts in mice did not respond to an oral treatment with BRACO19. Even when BRACO19 was administered intraperitoneally, only early stage tumors were susceptible to the medication but not late stage tumors [74].

Since the results for the intestinal cell line Caco-2 are comparable to those of our bronchial cell lines 16HBE14o⁻ and Calu-3 as well as to the primary alveolar cells hAEpC, we can assume that a topical application, like an inhalative treatment of lung cancer, will face similar problems as the oral route. Although a systemic availability is not needed, BRACO19 has at least to be able to overcome the epithelial (air/ blood) barrier to reach deeper regions of a lung tumor. The transport results are confirmed by

IAM chromatography measurements because the capacity factor k'_{IAM} can be correlated with the apparent permeability coefficient P_{app} [95].

Also, the concentrations used for the transport experiments are not representative for possible therapeutic applications because they were far above the IC_{50} values of our cells ($10 \mu M \approx 7 \mu g/ml$). hAEPc were most sensitive to high BRACO19 concentrations in the transport experiments as could be seen in the strong decrease in TEER at $200 \mu g/ml$ donor concentration. Since the major part of the pulmonary surface belongs to the alveolar region, high drug concentrations would result in unwanted side effects. Lower concentrations, however, would result in even less drug absorption and inefficacy.

The apparent asymmetry in transport can be explained with a relatively strong adsorption to the filter material as has been demonstrated in the experiments with cell free filters (Fig. 2). For transport experiments in BA direction the filters were rapidly saturated with BRACO19 because they were in direct contact with the solution. Hence, transport was not hindered. However, when BRACO19 was applied from the apical side, the small amounts that permeated across the monolayer were completely adsorbed to the filter material. Since the filter was not saturated at the end of the transport experiment no substance could be detected in the basolateral compartment. Differences in adsorptions (Fig. 2) were most likely due to varying amounts of BRACO19 adsorbed to surface mucus and proteins (for AB direction) or entrapped in the intercellular space.

Our observations can be explained by BRACO19's chemical properties. It contains two basic pyrrolidine rings (Fig. 1), which are very likely to be protonated under physiological conditions, i.e. the molecule is positively charged. This results in good water solubility but strongly decreases the interaction with hydrophobic structures like cell membranes. The small amounts that were transported in BA direction most probably took the paracellular route by passive diffusion because no active transport mechanisms or efflux/ influx systems like P-gp or organic cation transporter proteins could be identified. Also the fact that BRACO19 does not interact with membrane phospholipids and that higher amounts were only detectable in

the acceptor compartments and filters after the monolayer integrity collapsed
argue for the paracellular way

2.5 Conclusion

From our results we would suggest that BRACO19 has the typical properties of a class III drug substance according to the Biopharmaceutical Classification System (BCS): a good aqueous solubility and a very poor permeability across biological barriers.

Obviously, BRACO19 is a potent substance with an interesting new mode of action, i.e. telomerase inhibition by G- quadruplex stabilization, but with challenging biopharmaceutical properties. Hence, suitable formulations for the efficient delivery of this compound must be developed first in order to further evaluate this new therapeutic concept.

Chapter 3

Decomposition of the Telomere Targeting Agent BRACO19 in Physiological Media Results in Products with Decreased Inhibitory Potential

The data presented in this chapter has been published as a research article in the journal *International Journal of Pharmaceutics*:

Taetz, S., Murdter, T. E., Zapp, J., Boettcher, S., Baldes, C., Kleideiter, E., Piotrowska, K., Schaefer, U. F., Klotz, U., Lehr, C.-M.

Decomposition of the Telomere-Targeting agent BRACO19 in physiological media results in products with decreased inhibitory potential. (2008) *Int. J. Pharm.*, 357(1-2), 6-14

DOI:

10.1016/j.ijpharm.2008.01.026

Weblink:

http://www.sciencedirect.com/science?_ob=ArticleURL&_udi=B6T7W-4RMNYGY-5&_user=10&_rdoc=1&_fmt=&_orig=search&_sort=d&view=c&_acct=C000050221&_version=1&_urlVersion=0&_userid=10&md5=1bccab3d5f2ceb071d53ea25b525033f

3.1 Introduction

During the last years the concept of telomerase inhibition for the treatment of cancer became an area of intensive research. Telomerase is a reverse transcriptase composed of the catalytic subunit *human telomerase reverse transcriptase* (hTERT) and the template RNA *human telomerase RNA* (hTR). Its substrates, the telomeres, are located at the ends of each chromosome. Telomeres are repetitive TTAGGG/AATCCC sequences that end in a 3'-(TTAGGG)_n single strand overhang. They form a so-called t-loop, a structure stabilized by associated proteins, where the single strand invades the double stranded region. The t-loops prevent the chromosome ends from end-to-end fusions and being recognized as damaged DNA. Due to the end replication problem during DNA duplication telomeres erode at each cell cycle until they approach a certain limit. Reaching this limit is an important signal for a cell to enter the state of cellular senescence. Cells that do not stop dividing will experience severe chromosomal damages leading to cell death (apoptosis). Since most malignant cells express telomerase they are able to maintain their telomeres above this limit and therefore escape these pathways [71, 72, 96]. Various telomerase inhibitors have been developed and successfully tested. They either target hTERT, hTR or the telomeres [97].

Our studies concentrate on the topical treatment of non-small cell lung cancer (NSCLC) via the inhalative route. A search for suitable drug candidates led to the telomere targeting 3,6,9- aminoacridine derivative BRACO19 ((9- [4- (N,N-dimethylamino)phenylamino]- 3,6- bis (3- pyrrolidino-propionamido) acridine; figure 1) which acts by G-quadruplex stabilization [67, 73]. G-quadruplexes are planar G-quartet motifs that can form in guanine-rich DNA sequence like the telomeres. These structures interact with the inhibitor via π - π stacking. Positively charged side chains of the inhibitor interact with the negatively charged phosphate DNA backbone and thereby stabilize the G-quadruplex – inhibitor complex. Due to this mechanism telomeres are not able to form their native structure and hence fail to protect the chromosomes [53, 54].

BRACO19 has shown some promising results in studies in tumor cell cultures and mouse xenografts. It was reported that a treatment with BRACO19 not

only resulted in telomerase inhibition but also in general telomere dysfunction that led to atypical mitosis and consequently to apoptosis [74].

In a previous study we characterized BRACO19 with respect to its biopharmaceutical properties and found it to be a typical class III drug substance with a good aqueous solubility but a very poor permeability across epithelial cell monolayers [98]. During these studies we also found that BRACO19 has stability problems when dissolved in aqueous media at physiological pH.

In the present study we examined the influence of pH, temperature and dissolution media on the stability of BRACO19. We have identified potential decomposition products and evaluated whether they can contribute to the inhibitory action of this drug candidate.

3.2 Materials and Methods

3.2.1 BRACO19

BRACO19 (9- [4- (N,N- dimethylamino)phenylamino]- 3,6- bis (3- pyrrolidino- propionamido) acridine x 3HCl; figure 1) was synthesized by ENDOTHERM GmbH (Saarbruecken, Germany) according to Harrison et al. [82]. Identity and purity were proven by NMR (Table 3-3) and HPLC, respectively, in comparison with the original compound.

3.2.2 Buffers and cell culture medium for stability studies

For stability studies different HBSS (Hank's balanced salt solution) buffers and diluted McIlvain buffer were used.

The basic compositions of HBSS buffers were: 137.0 mM NaCl, 5.36 mM KCl, 4.26 mM NaHCO₃, 0.18 mM Na₂HPO₄ x 7 H₂O, 0.44 mM KH₂PO₄, 5.55 mM Glucose, 0.13 mM CaCl₂ x 2 H₂O, 0.05 mM MgCl₂ x 6 H₂O, 0.04 mM MgSO₄ x 7 H₂O. For the adjustment of the appropriate pH values in HBSS buffers the buffering substances were exchanged as follows: pH 7.4 and 7.0: 10.0 mM HEPES (N-[2-hydroxyethyl]piperazine-N'-[2-ethanesulfonic acid]), pH 6.0: 10.0 mM MES (2-morpholinoethanesulfonic acid), pH 4.0 and 5.0: 10.0 mM sodium acetate. pH values were adjusted with 1 M NaOH or 1 M HCl, respectively.

Diluted McIlvain buffer contained 50 mM citric acid and 1.4 mM Na₂HPO₄. The pH was 2.8. Phosphate buffer was composed of 5 mM KH₂PO₄ and the pH was adjusted with NaOH to pH 7.4.

RPMI cell culture medium was purchased from PAA Laboratories GmbH (Pasching, Austria) and supplemented with 10% FCS (Sigma- Aldrich Chemie GmbH, Taufkirchen, Germany). The pH of the cell culture medium was 7.5.

3.2.3 HPLC- DAD analysis of BRACO19 and decomposition products

BRACO19 was analyzed by reversed phase HPLC using an isocratic Dionex HPLC system consisting of an ASI 100 automated sample injector with adjustable temperature, UVD 340U diode array detector (DAD) and

P680 pump with Chromeleon® software (version 6.60 SP1 build 1449) (Dionex, Idstein, Germany).

We used a Gemini® RP- 18 column/ 150 x 4.6 mm/ 5 µm/ 110 Å (Phenomenex, Aschaffenburg, Germany). The mobile phase was composed of 80:20 (v/v) methanol:borate buffer pH 10.0 (100 mM). At a flow rate of 0.6 ml/min the retention time of BRACO19 was 8.9 ± 0.2 minutes. The wavelength of the detector was set at 268 nm. The detection and quantification limit of BRACO19 were 0.010 µg/ml and 0.025 µg/ml, respectively. Quantification was linear in the range from 0.025 to 12 µg/ml.

3.2.4 Decomposition experiments

All decomposition experiments were performed with the HPLC-DAD system described above in HPLC brown glass vials (hydrolysis grade 1; CS-Chromatography, Langerwehe, Germany). Decomposition experiments over 7 hours were performed at 37° with HBSS buffer of different pH values and diluted McIlvain buffer of pH 2.8. The influence of temperature on BRACO19 decomposition was assessed at 4°C in comparison to the decomposition at 37°C in HBSS buffer pH 7.4. BRACO19 was dissolved at a concentration of 12 µg/ml in each respective buffer. 20 µl samples were drawn every 45 minutes for 7 hours and analyzed by HPLC as described above. Each experiment was done in triplicate.

Long-term decomposition experiments were performed for four days in HBSS buffer pH 7.4, phosphate buffer pH 7.4 and RPMI cell culture medium containing 10% FCS (pH 7.5), respectively. The concentration of BRACO19 was 12 µg/ml and the temperature was set to 37°C. Samples were drawn every 2.54 hours. All experiments were performed in triplicate.

UV spectra of degradation products were recorded with the DAD detector during these long-term experiments.

The decomposition of BRACO19 in different media was described mathematically by assuming first order kinetics. A non-weighted curve fitting was performed using the software Origin (Version 7.5, OriginLab Corp., Northampton, MA, USA) according to the equation:

$$A = A_0 \cdot e^{(-k \cdot t)} \quad \text{Equation 3-1}$$

where A is the amount of BRACO19 (in %) at time point t_i , A_0 the amount at time point $t = 0$, k the rate constant (in h^{-1}) and t the time (in hours).

3.2.5 Decomposition of BRACO19 for structural analysis of decomposition products by LC/MS and NMR

For the analysis of the decomposition products by LC/MS and NMR BRACO19 was dissolved in phosphate buffer pH 7.4 at a concentration of 55 $\mu\text{g/ml}$. The solution was kept at room temperature for 14 days ($\sim 20^\circ\text{C}$). The longer decomposition time was necessary to obtain larger amounts of secondary decomposition products. Decomposition was confirmed by HPLC. LC/MS and NMR analyses were performed with the mixture of decomposition products without isolation and purification of degradation products.

3.2.6 LC/MS analysis of decomposition products

The Surveyor[®]-LC-system consisted of a pump, an autosampler, and a PDA detector. Mass spectrometry was performed on a TSQ[®] Quantum (Thermo Electron Corporation, Dreieich, Germany). The triple quadrupole mass spectrometer was equipped with an electrospray interface (ESI). The system was operated by the standard software Finnigan[™] Xcalibur[®] (Thermo Electron Corporation).

A RP C18 NUCLEODUR[®] 100-5 (125 × 3 mm) column (Macherey-Nagel GmbH, Dueren, Germany) was used as stationary phase. The solvent system consisted of 0.1% formic acid (A) and 0.1% formic acid in methanol (B). Injection volume was 20 μl and flow rate was set to 350 $\mu\text{l/min}$. From 0 to 10 min the percentage of B in the mixture was increased from 20% to 100% and kept at 100% for 3 min. From 13 to 15 min the percentage of B was decreased to the initial 20 %. MS analysis was carried out at a spray voltage of 4200 V, a capillary temperature of 350 $^\circ\text{C}$ and a source CID of 10 V. The polarity of the mass spectrometer was positive and as scan mode a full scan from 100 to 800 m/z was chosen as first scan event.

In a second scan event, the most intense ion determined in scan event one was collided with argon, at a collision gas pressure of 0.9 Pa and a collision energy of 35 V. The resulting fragments were recorded in MS/MS mode.

3.2.7 NMR analysis of BRACO 19 and decomposition products

In NMR analysis the ^1H NMR spectra of (a) the free base of BRACO19 and (b) the decomposition products were compared. For this purpose aqueous solutions of both were lyophilized and redissolved in CD_3OD . The ^1H NMR spectra (500 MHz) of (a) and (b) were recorded at 298K on a Bruker DRX500 spectrometer using the standard pulse program zg30. Chemical shifts are given in parts per million (ppm) on the δ scale referenced to the solvent peak at 3.30 ppm.

3.2.8 TRAP Assay

The TRAP (*Telomeric Repeat Amplification Protocol*) assay was performed according to the instructions of the TRAP_{EZE}[®] Telomerase Detection Kit (Chemicon International, Temecula, CA, USA), a modified version of the TRAP assay originally developed by Kim et al. [40, 99]. 50 ng of a protein extract from lysed A549 lung cancer cells was used per reaction. Decomposition products were obtained from a sample of the solution used for LC/MS and NMR analysis. The absence of intact BRACO19 in the mixture of decomposition products was verified by the HPLC-DAD method described above. The concentrations of BRACO19 and of decomposition products were 2.0, 1.0, 0.5, 0.25, and 0.1 μM . The concentrations refer to the initial BRACO19 concentration. 1 μM BRACO19 and decomposition products, respectively, were added to the control template TSR8. Cell lysis buffer was included as negative control. TRAP products were separated on a 12.5 % non-denaturing polyacrylamide gel. DNA fragments were visualized after SYBR[®] Green I staining (Molecular Probes, Eugene, OR, USA) with the Gel Doc[™] 2000 Gel Documentation System from BioRad (BioRad Laboratories GmbH, Munich, Germany).

3.3 Results

3.3.1 Stability experiments

The stability of BRACO19 in solution was found to be dependent on pH and temperature. As can be seen from Figure 3-1 A at 37°C the stability of BRACO19 increased gradually with decreasing pH of the HBSS buffer. It was least stable at pH 7.4 while at pH 2.8 (Mcllvain buffer) no decomposition occurred. Also, when BRACO19 was dissolved in HBSS buffer pH 7.4 and analyzed at 4°C and 37°C the decomposition at 4°C was considerably slower than at 37°C (Figure 3-1 B). An exchange of the brown glass HPLC vials with clear glass vials or polypropylene vials did not affect the results of the stability assays (data not shown).

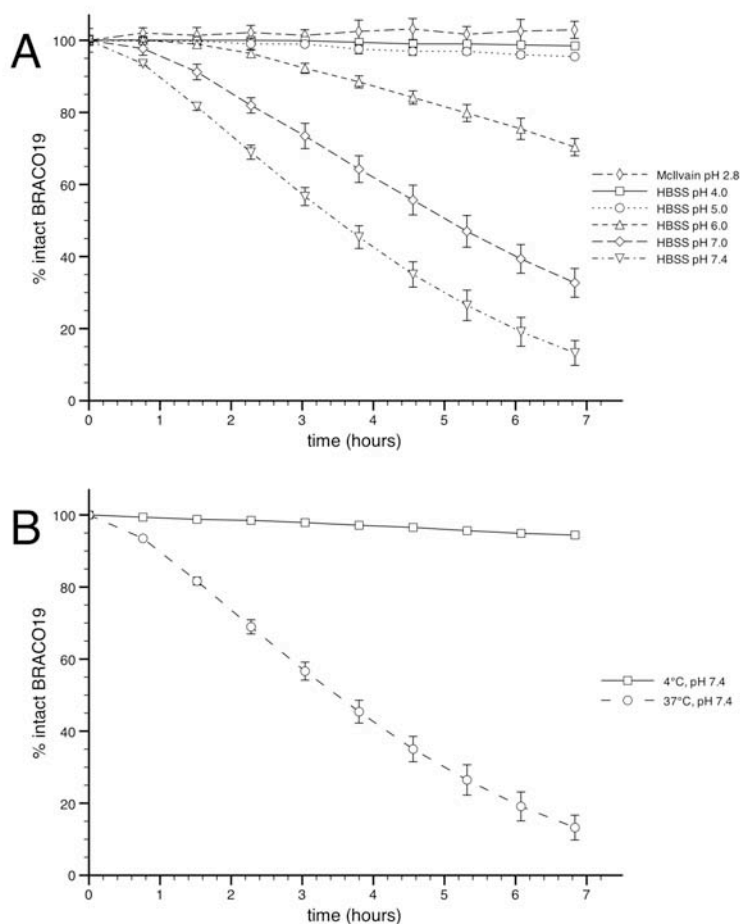


Figure 3-1: (A) Stability of BRACO19 at 37°C in HBSS buffers of different pH values (pH 7.4 – pH 4) and Mcllvain buffer (pH 2.8); (B) Stability of BRACO19 in HBSS buffer pH 7.4 at 4°C and 37°C.

In long-term experiments the type of dissolution medium exerted a less important influence on the stability of BRACO19 than the variation of pH or temperature. As can be seen from Figure 3-2 and Table 3-1 the decomposition was fastest in HBSS buffer pH 7.4. In standard phosphate buffer and RPMI cell culture medium the stability was only slightly better. The half-life in HBSS buffer was about 2.9 hours. In phosphate buffer and RPMI cell culture medium half-lives were about 4 and 4.4 hours, respectively.

Table 3-1: Rate constants, half-lives ($t_{1/2}$) (\pm standard error) and R^2 s of fits for the decomposition of BRACO19 in HBSS buffer, phosphate buffer and RPMI cell culture medium at 37°C.

| Medium | Rate constant (h^{-1}) | $t_{1/2}$ (hours) | R^2 of fit |
|---------------------------------|----------------------------|-------------------|--------------|
| HBSS buffer pH 7.4 | 0.303 ± 0.026 | 2.9 ± 0.17 | 0.986 |
| Phosphate buffer pH 7.4 | 0.174 ± 0.012 | 4.0 ± 0.27 | 0.985 |
| RPMI cell culture medium pH 7.5 | 0.157 ± 0.016 | 4.4 ± 0.45 | 0.967 |

Total decomposition occurred within one day in all solutions at 37°C. Four decomposition products (termed Decomp1 – 4) were identified during these long-term experiments in HBSS buffer and phosphate buffer. Their retention times in the HPLC-DAD system are given in Table 3-2.

Table 3-2: Retention times of BRACO19's decomposition products after decomposition in HBSS buffer pH 7.4 (average \pm standard deviation). For HPLC-DAD parameters see Material and Methods.

| | BRACO19 | Decomp1 | Decomp2 | Decomp3 | Decomp4 |
|----------------------|-----------------|-----------------|-----------------|-----------------|-----------------|
| Retention time (min) | 8.20 ± 0.20 | 6.71 ± 0.02 | 5.16 ± 0.01 | 5.38 ± 0.02 | 4.44 ± 0.02 |

The decomposition products could easily be distinguished by their UV spectra and were the same in HBSS buffer and phosphate buffer (Figure 3-3). In cell culture medium only Decomp2 could be detected under the given conditions (data not shown). As can be seen from Figure 3-4 Decomp1 and Decomp2 appeared first but were also instable. Their decay curves resemble a Bateman-function as seen in pharmacokinetics after oral administration of a drug. Decomp3 and Decomp4 appeared much slower and showed a steady increase over time and might be the decomposition products of Decomp1 and

Decomp2. However, since the exact structures and concentrations of the decomposition products were unknown a calculation of kinetic parameters was not possible.

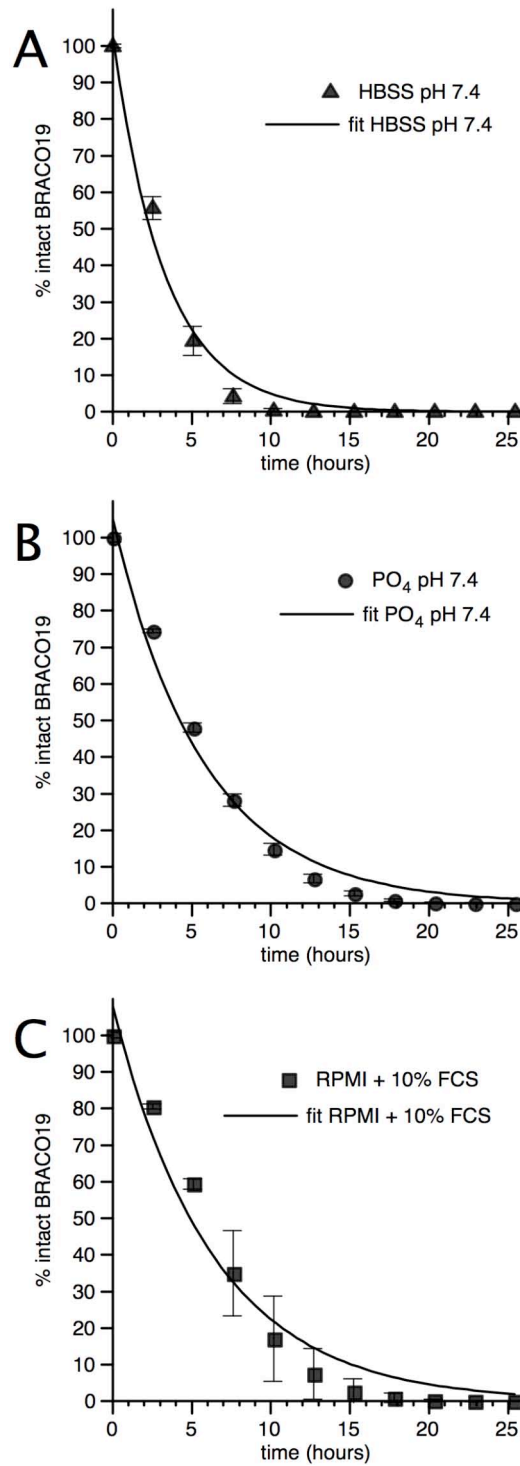


Figure 3-2: Decomposition of BRACO19 in HBSS buffer pH 7.4 (A), phosphate buffer pH 7.4 (B) and RPMI cell culture medium pH 7.5 (C). Curves were fitted according to Equation 3-1 assuming first order kinetics. Fit results are given in Table 3-1.

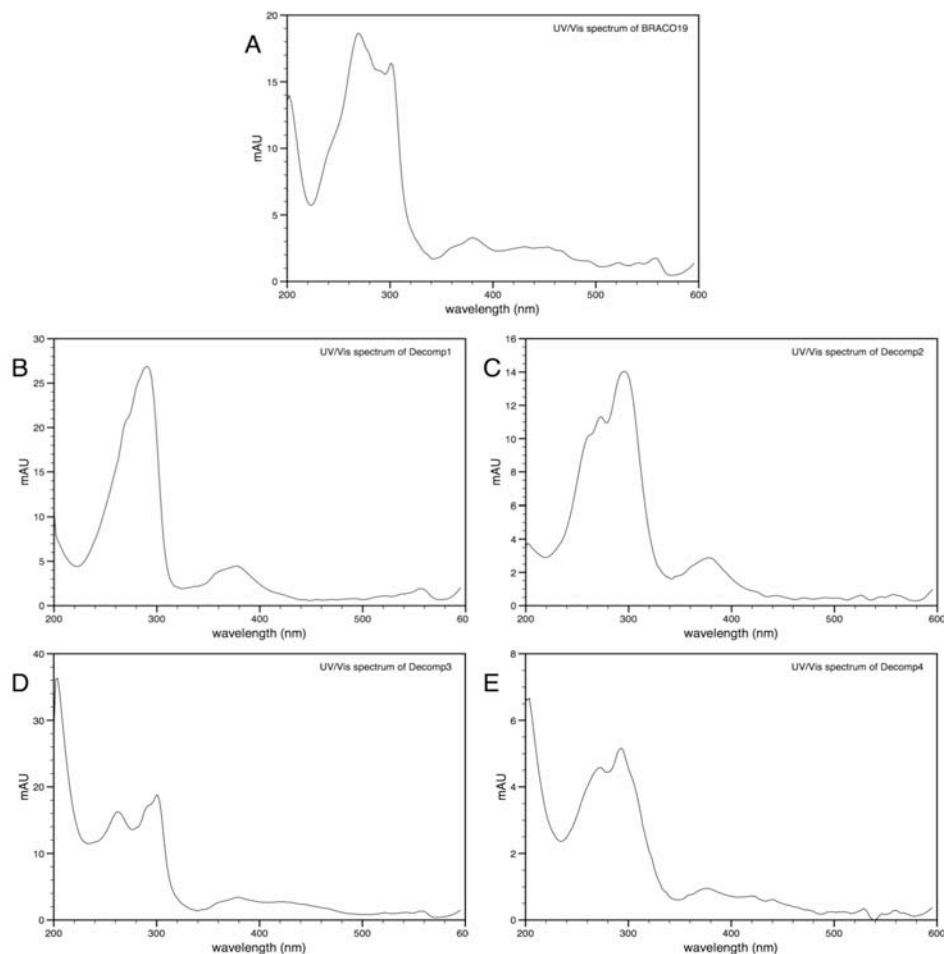


Figure 3-3: UV/Vis spectra of BRACO19 and its decomposition products in the range from 200 to 600 nm. The spectra were obtained during long-term HPLC-DAD analysis with methanol : borate buffer pH 10 (80:20) as mobile phase. A: BRACO19, B: Decomp1, C: Decomp2, D: Decomp3, E: Decomp4. Spectra are corrected for spectra of mobile phase.

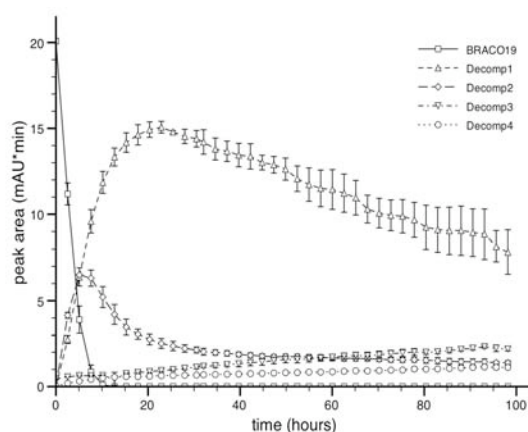


Figure 3-4: Decomposition of BRACO19 at 37°C in HBSS buffer pH 7.4 over 4 days as determined by HPLC-DAD analysis. Decomp1 and Decomp2 are the first decomposition products of BRACO19 while Decomp3 and Decomp4 appear to be the decomposition products of Decomp1 and Decomp2. Each data point represents mean \pm standard deviation of 3 independent measurements.

3.3.2 LC/MS and NMR analysis

The analysis of the decomposition mixture by LC/MS resulted in the discovery of a molecule with a mass (m/z) of 144.2, which corresponds to the mass of the $[M+H]^+$ of 3-pyrrolidino propionic acid (structure **2** in Figure 3-5), i.e. the residue of the amide groups in position 3 and 6 of BRACO19. Thus, hydrolysis of these amides seems to be likely. However, no molecule ions were found that would match the corresponding reaction products (structures **3** and **4** in Figure 3-5). Instead, molecule ions with masses of 567.6, 442.5 and 317.3 were detected. These masses correspond to the $[M+H]^+$ of structures **5**, **6**, and **7**, respectively, indicating a deamination in 4' position, i.e. an exchange of the dimethyl amino group for a hydroxyl group. In MS/MS scans a fragment with the mass of 84.2 was found for structures **2**, **5**, and **6** but not for structure **7**. This fragment matches the structure of N-methyl pyrrolidine and confirms the hypothesis of a hydrolysis of the amide groups.

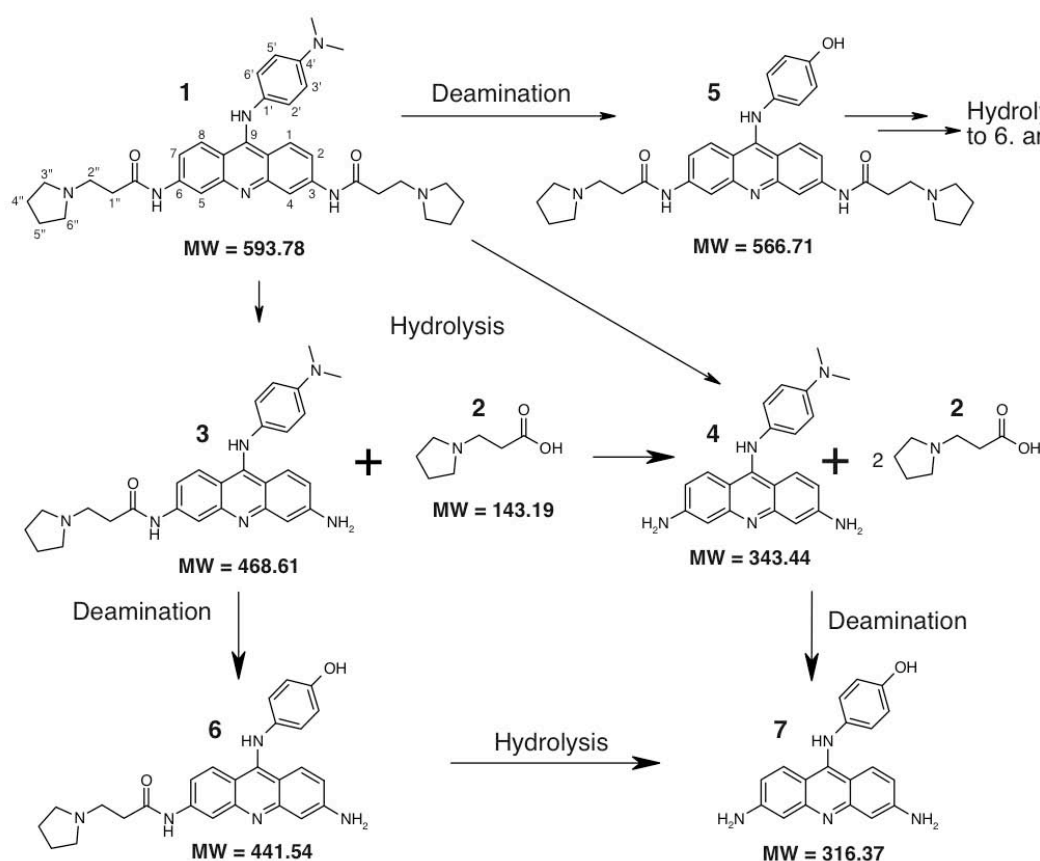


Figure 3-5: The suggested reaction scheme for the decomposition of BRACO19 (**1** = BRACO19). The most important reactions for the decomposition seem to be the hydrolysis of the amide groups in position 3 and 9 and the deamination of the dimethyl amine group in position 4' of the phenyl ring.

The NMR analyses of the decomposition products confirm the findings of LC/MS analysis. The results of the measurements are given in Table 3-3. In the aromatic part of the ^1H NMR spectrum signals of two compounds (i) and (ii) can be found in a ratio of 5 to 1. The data of the major compound (i) are close to those of BRACO19 but lack signals for a dimethyl amino group in the aliphatic part of the spectrum, indicating the presence of a hydroxyl instead of the dimethyl amino group. The data of (i) are in good accordance with structure **5**. Investigation of the NMR spectral data of the minor compound (ii) showed that in contrast to BRACO19 the signals of the outer rings of the acridine system are not identical anymore. The difference of the chemical shifts of both benzene subunits (δ 8.33, 7.99, 7.21 vs. 7.71, 6.69, 6.65) suggests that the molecule has only one 3-pyrrolidino propionic acid group. Correspondingly, the aliphatic part of the ^1H NMR spectrum reveals only signals for one 3-pyrrolidino propionic acid moiety. This together with the fact that the dimethyl amino group is absent leads to structure **6** for compound (ii). The solution must also contain free 3-pyrrolidino propionic acid (structure **2**), since the values for the integrals of the 3-pyrrolidino propionic acid groups are bigger than required for pure compound i and ii.

Table 3-3: ^1H NMR spectral data of compounds BRACO 19, (i) and (ii). Coupling constants are given in parentheses. s = singlet, d = doublet, brs = broad singlet, brd = broad doublet. Signals indicated as *m* were unresolved or overlapped multiplets.

| | BRACO 19 | (i) | (ii) |
|------------------------|---------------------------|---------------------------|---------------------------|
| | δ_{H} (ppm) | δ_{H} (ppm) | δ_{H} (ppm) |
| 1 | 7.91 <i>brd</i> (J = 9) | 7.99 <i>brd</i> (J = 9) | 7.71 <i>brd</i> (J = 9) |
| 2 | 7.20 <i>brd</i> (J = 9) | 7.25 <i>brd</i> | 6.69 <i>brd</i> (J = 9) |
| 4 | 8.09 <i>brs</i> | 8.39 <i>brs</i> | 6.65 <i>brs</i> |
| 5 | 8.09 <i>brs</i> | 8.39 <i>brs</i> | 8.33 <i>brs</i> |
| 7 | 7.20 <i>brd</i> (J = 9) | 7.25 <i>brd</i> (J = 9) | 7.21 <i>brd</i> (J = 9) |
| 8 | 7.91 <i>brd</i> (J = 9) | 7.99 <i>brd</i> (J = 9) | 7.99 <i>brd</i> (J = 9) |
| 2', 6' | 6.80 <i>d</i> (J = 8.5) | 7.13 <i>d</i> (J = 8.5) | 7.13 <i>d</i> (J = 8.5) |
| 3', 5' | 6.90 <i>d</i> (J = 8.5) | 6.89 <i>d</i> (J = 8.5) | 6.89 <i>d</i> (J = 8.5) |
| 1'' | 2.88 <i>m</i> (2H) | 3.07 <i>m</i> | 3.07 <i>m</i> |
| 2'' | 2.64 <i>m</i> (2H) | 2.79 <i>m</i> | 2.79 <i>m</i> |
| 3'', 6'' | 2.66 <i>m</i> (4H) | 2.84 <i>m</i> | 2.84 <i>m</i> |
| 4'', 5'' | 1.84 <i>m</i> (4H) | 1.91 <i>m</i> | 1.91 <i>m</i> |
| NCH₃ | 2.88 <i>s</i> (6H) | ----- | ----- |

3.3.3 TRAP Assay

Decomposed BRACO19 (1 and 2 μM) was still able to reduce the number and intensities of the bands representing the “telomere ladder” (Figure 3-6, D1 - D5). When compared to intact BRACO19 (Figure 3-6, B1 - B5) the decomposition products showed a reduced inhibitory effect. Inhibition of telomerase with BRACO19 at a concentration of 0.25 μM clearly reduced the band intensities of the telomerase products. At 0.5 μM the length of the telomere ladder was considerably shorter. For the decomposition products the same effects were observed at 1 and 2 μM , respectively, demonstrating their reduced inhibitory potential. Both, BRACO19 and the mixture of decomposition products, influenced the amplification of the TSR8 internal standard. For BRACO19 no bands could be found. The decomposition products reduced the band intensities slightly (Figure 3-6 T, TB and TD). The bands in the control Lane (Figure 3-6 C) are most likely due to primer-dimer artifacts. Figure 3-6 is representative for two TRAP assays that were performed with BRACO19 and its decomposition products.

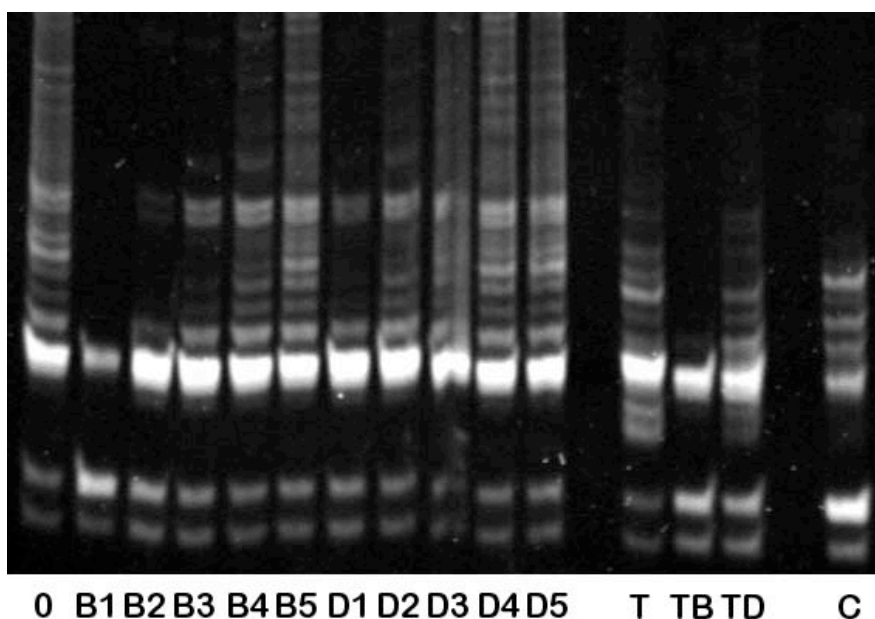


Figure 3-6: The TRAP assay shows the effects of BRACO19 and its decomposition products on telomerase activity. The assay was performed with the same material that has been used for LC/MS and NMR analysis. 0 = positive control; B1 – B5 = BRACO19 2, 1, 0.5, 0.25 and 0.1 μM ; D1 – D5 = mixture of decomposition products 2, 1, 0.5, 0.25 and 0.1 μM (referred to initial BRACO19 concentrations); T = TSR8 internal standard, TB = TSR8 internal standard with 1 μM BRACO19; TD = TSR8 internal standard with 1 μM decomposition products; C = negative control (lysis buffer). This figure is representative for two TRAP assays that were performed with BRACO19 and its decomposition products.

3.4 Discussion

Our experiments demonstrate that the stability of BRACO19 considerably depends on pH and temperature of standard buffers used in biological test systems. At physiological pH BRACO19 decomposed in simple phosphate buffer as well as in more complex cell culture medium. One important mechanism of this decomposition seems to be a hydrolysis of the amide bonds in position 3 and 6 of the acridine part of the molecule as has been shown by LC/MS and NMR analysis. The decomposition is pH dependent and can be approximated by first-order kinetics. The primary decomposition products were also unstable and decomposed further into other products. However, since the exact structures and concentrations of the decomposition products are unknown a determination of kinetic parameters was not feasible. Derivatives of 9-aminoacridine are described to be prone to hydrolysis in position 9 resulting in acridones [100]. In our studies such products could not be found. Instead, a deamination in 4'- position of the phenyl residue seems to be more likely.

BRACO19 has been described as the prototype of a new generation of aminoacridine based anti-cancer drugs that act as telomerase inhibitors by G-quadruplex stabilization in telomeres. A modification of the acridine ring in position 3 and 6 with an aminoalkylamide side chain containing a basic heterocycle (i.e. the pyrrolidine ring in BRACO19) is essential to obtain stable complexes between the quadruplex structures and the drug molecule. The heterocycle is protonated under physiological conditions and thus positively charged. The side chains are directed towards the G-quadruplex grooves where they can interact with the negatively charged phosphate backbones of the DNA [82, 101, 102]. Moore et al. have shown that 9-aminoacridine derivatives without these side chains in position 3 and 6 form only very weak complexes and are not able to inhibit telomerase activity [103]. Our results show that the decomposition, i.e. the hydrolysis of the side chains and the deamination in 4'- position strongly influences the inhibitory effect of BRACO19. In the TRAP assay a significant reduction of telomerase activity only occurs at the highest concentration of decomposition products derived from 2 μ M BRACO19 (Figure 3-6 D1). The interference with the amplification

of the TSR8 standard is not as pronounced as with BRACO19 as can be seen in figure 7 when lines T, TB and TD are compared. TSR8 is an oligonucleotide composed of the TS-primer + 8 telomeric repeats. In the TRAP assay it is normally used as a quantitation control in the absence of telomerase. In a previous study we were able to show that BRACO19 strongly interferes with the amplification of the TSR8 oligonucleotide during PCR [73]. The mechanism for this interference is the formation and stabilization of G-quadruplexes within TSR8, which prevents a proper PCR reaction [104]. The reduced inhibition of the amplification of TSR8 by the decomposition products indicates that the affinity of the decomposition products to G-quadruplex structures is strongly reduced. Whether the remaining inhibitory effect can be attributed to one of the decomposition products alone or to all of them will be the matter of further studies. A reasonable order for inhibitory potential can be established by following the degree of hydrolysis of the pyrrolidino-propionamido groups: structure **5** > structure **6** > structure **7** (Figure 3-5).

The instability of BRACO19 under physiological conditions will cause some problems when the agent is used in biological test systems. Concerning the animal studies that were performed so far [74] it would be interesting to gain more knowledge about the metabolism of BRACO19, i.e. if the effects that have been described are really due to BRACO19 or one of its decomposition products.

In conclusion, G-quadruplex stabilizing substances from the class of alkylamidoacridines like BRACO19 appear to be promising new drug molecules for the treatment of cancer by telomerase inhibition and telomere dysregulation.

However, the results presented in this study show that this class of compounds may face stability problems during the preparation of dosage forms, their storage and after application. This might have serious consequences for the therapeutic success. Any new drug candidate should be submitted to thorough stability investigations prior to in vitro and in vivo tests. We have shown previously that BRACO19 is also a problematic substance from the biopharmaceutical point of view [98]. Since research in this field is

continued and new substances based on the alkylamidoacridine structure are being developed [105] it can be concluded that compounds like BRACO19 will require either further chemical modifications or a suitable formulation and delivery strategy to i) improve their biopharmaceutical properties and ii) reduce stability problems.

Chapter 4

The Influence of Chitosan Content in Cationic Chitosan/PLGA Nanoparticles on the Delivery Efficiency of Antisense 2'-O-Methyl-RNA Directed Against Telomerase in Lung Cancer Cells

The data presented in this chapter has been published as a research article in the journal *European Journal of Pharmaceutics and Biopharmaceutics*:

Taetz, S., Nafee, N., Beisner, J., Piotrowska, K., Baldes, C., Murdter, T. E., Huwer, H., Schneider, M., Schaefer, U. F., Klotz, U., Lehr, C.-M.

The influence of chitosan content in cationic chitosan/PLGA nanoparticles on the delivery efficiency of antisense 2'-O-methyl-RNA directed against telomerase in lung cancer cells. (2008) Eur. J. Pharm. Biopharm., in press

DOI:

10.1016/j.ejpb.2008.07.011

Weblink:

http://www.sciencedirect.com/science?_ob=ArticleURL&_udi=B6T6C-4T2YMWM-1&_user=10&_rdoc=1&_fmt=&_orig=search&_sort=d&view=c&_version=1&urlVersion=0&_userid=10&md5=4748b484e95616d7feb5af7d56b6f479

4.1 Introduction

The treatment of genetic disorders by the administration of exogenous plasmid DNA or the inhibition of gene expression by antisense oligonucleotides or siRNA are promising approaches for the treatment of severe diseases like cancer in the future. However, it is a well-recognized fact that the main obstacle for gene therapy or the therapeutic application of antisense oligonucleotides and siRNA is the lack of a safe and efficient delivery strategy for nucleotide-based drugs *in vivo*.

Our studies focus on the treatment of non-small cell lung cancer by telomerase inhibition. Telomerase is a ribonucleoprotein with reverse transcriptase activity that plays an important role in cell immortalization and cancer development by maintaining chromosomal ends, the telomeres. Telomeres are non-coding, repetitive hexameric (TTAGGG)_n sequences that form lasso-like structures. They are important for chromosomal protection and the control of cell proliferation. In normal cells telomeres shorten during each cell cycle due to the end-replication problem. When they reach a certain limit it is a signal for the cell to stop dividing and enter the state of cellular senescence. Further cell divisions would result in non-functional telomeres and severe chromosomal damages. Cells that express the enzyme telomerase, like most cancer cells, escape this mechanism and can divide indefinitely. Therefore, the reintroduction of the normal cell cycle by telomerase inhibition is an interesting strategy for cancer treatment [71, 72].

A search for suitable telomerase inhibitors resulted in an antisense 2'-O-methyl-RNA (2OMR) [73] directed against the template region of human telomerase RNA (hTR) that has been reported to be a highly potent and sequence-selective inhibitor of human telomerase [48, 106]. Our group previously developed chitosan-coated poly(lactic-co-glycolic acid) (PLGA) nanoparticles based on an emulsion – diffusion – solvent-evaporation method. These nanoparticles proved to be efficient carriers for the delivery of plasmid DNA into A549 lung cancer cells *in vitro* and lungs of mice after intranasal administration *in vivo* [107, 108]. The advantage of these nanoparticles is that their properties with respect to size and surface charge can easily be modified

in a controlled manner by varying the amounts of PLGA, chitosan and PVA during particle preparation [109]. However, although plasmid DNA and antisense oligonucleotides might be regarded to be similar from the chemical point of view their differences in size are likely to influence the properties of complexes formed with nanoparticles and hence their biological efficacy. Therefore, a re-evaluation of these chitosan/PLGA nanoparticles as a carrier system for antisense 2OMR was necessary. The aim of the present study was to evaluate the nanoparticles with regard to binding efficiency, complex stability of nanoplexes in biologically relevant media, their delivery efficacy of the telomerase inhibitor to lung cancer cells and the inhibition of telomerase activity.

4.2 Materials and Methods

4.2.1 Materials

Poly(lactic-co-glycolic acid) (PLGA) 70:30 was purchased from Polysciences Europe GmbH (Eppelheim, Germany), polyvinylalcohol (PVA) Mowiol® 4-88 from Kuraray Specialities Europe GmbH (Frankfurt, Germany), ultrapure chitosan chloride Protasan™ UP CL113 with a molecular weight of 50 - 150 kDa and a degree of deacetylation between 75 and 90% from NovaMatrix (FMC BioPolymer, Drammen, Norway) and ethyl acetate from Fluka Chemie GmbH (Buchs, Switzerland).

Antisense oligonucleotide 2'-O-Methyl-RNA (2OMR) with a phosphorothioate (ps) backbone (5' -2' -O- methyl [C(ps)A(ps)GUUAGGGUU(ps)A(ps)G]-3') directed against human telomerase RNA (hTR), its carboxyfluoresceinamine labeled derivative 5'-FAM-2OMR and a mismatch sequence (5' -2' -O- methyl [C(ps)A(ps)GUUAGAAUU(ps)A(ps)G]-3') were obtained from Biomers.net GmbH (Ulm, Germany).

4.2.2 Nanoparticle preparation

Chitosan-coated PLGA nanoparticles were prepared by an emulsion-diffusion-evaporation technique as described by Kumar *et al.* [107] and Nafee *et al.* [109]. In brief, 5 ml of PLGA dissolved in ethyl acetate (20 mg/ml) were added dropwise to 5 ml of an aqueous chitosan solution containing 2.5% w/v PVA under magnetic stirring. The emulsion was stirred at 1000 rpm for 1 hour. Afterwards, it was homogenized using an UltraTurrax T25 (Janke & Kunkel GmbH & Co-KG, Germany) at 13,500 rpm for 15 minutes. The homogenized emulsion was diluted to a volume of 50 ml under constant stirring with MilliQ-water. Remaining ethyl acetate was evaporated by continuous stirring over night at room temperature. The concentrations of chitosan in the aqueous phase were varied to obtain nanoparticles with different surface charges as has been shown by Nafee *et al.* [109]: 0 mg/ml (pure PLGA nanoparticles; PLGA-NP), 0.5 mg/ml (05CPNP), 1 mg/ml (1CPNP), 3 mg/ml (3CPNP) and 6 mg/ml (6CPNP). The abbreviations in parentheses will be

used throughout the document as reference to the different particle preparations. CPNP stands for chitosan-coated PLGA nanoparticles.

Red fluorescently labeled chitosan/PLGA nanoparticles were prepared as described above but with 2 μM of the lipophilic dye Dil (1,1'-Dioctadecyl-3,3,3',3'-tetramethylindocarbocyanine perchlorate; from Sigma-Aldrich Chemie GmbH, Taufkirchen, Germany) in the organic phase. The chitosan concentration for this preparation in the aqueous phase was 3 mg/ml (DilCPNP).

4.2.3 Purification of nanoparticles

Chitosan/PLGA nanoparticles were purified from excess PVA by preparative size exclusion chromatography (SEC) using an FPLC[®] system from Pharmacia Biotech (now Amersham Biosciences; Uppsala, Sweden) equipped with two P-500 pumps, a LCC-501 Plus controller, a MV-7 injection valve, a 50 ml Superloop, a C 16/70 column with one AC 16 adaptor, an Uvicord SII detector with an interference filter of 206 nm and a FRAC-100 fraction collector. Stationary phase was Sephacryl 1000-SF[®] from GE Healthcare (Munich, Germany) with a dimension of 65 cm in height and 1.6 cm in diameter. Mobile phase was degassed MilliQ-water containing 0.1 mM HCl. The system was operated by the FPLCdirector[™] version 1.3 (Pharmacia Biotech).

Nanoparticles were filtered through non-sterile a 0.2 μm cellulose acetate filter (Chromafil[®] GF/PET-20/25, Macherey-Nagel, Düren, Germany) prior to purification to prevent clogging of the stationary phase. Injection volumes were 5 – 7 ml per run. Flow rate of mobile phase was 1 ml/min under isocratic conditions. Purified particles were collected and concentrated by ultrafiltration using Vivaspin 20[®] (Sartorius, Göttingen, Germany) with a molecular weight cut-off of 300,000 Da at 1000 x g. Afterwards they were sterile filtered (0.2 μm , Minisart[®] sterile cellulose acetate filter, Sartorius). Concentrations of nanoparticles were determined gravimetrically after lyophilization. PVA from pure PLGA nanoparticle suspension was removed by five centrifugation/resuspension (with MilliQ- water) cycles in Vivaspin 20[®] because it was not possible to purify the pure PLGA nanoparticles by the size exclusion method described above. Purified and sterile filtered particle suspensions were stored

at 4°C. For a more detailed description of the purification method see Chapter 5.

4.2.4 Characterization of nanoparticle properties

Particle characteristics were determined directly after preparation, after purification, concentration and filtration and after a storage period of about two months at 4°C. They were characterized with respect to size, polydispersity index (Pdl) and surface charge. Size and Pdl were determined by photon correlation spectroscopy and surface charge by measuring the zeta potential in a ZetaSizer Nano ZS from Malvern Instruments Ltd (Worcestershire, UK). The ZetaSizer was equipped with a 4 mW He-Ne laser. Measurements were performed at 633 nm and a backscattering angle of 173°. Samples were diluted in MilliQ water. All measurements were performed in triplicate at 25°C using the standard settings for water as dispersion medium.

4.2.5 Formation of 2OMR-Chitosan/PLGA nanoplexes

Complexation experiments were performed in MilliQ water, phosphate buffered saline (PBS) pH 7.4 and RPMI cell culture medium (without phenol red; PAA Laboratories GmbH, Pasching, Austria) containing 10% fetal calf serum (FCS; Sigma- Aldrich). For this purpose a fixed amount of 2'-O-Methyl-RNA (2OMR) was mixed and incubated with different amounts of purified chitosan/PLGA nanoparticles. The concentration of oligonucleotides was 4 µM which corresponds to 17.72 µg/ml for non-labeled 2OMR and 19.84 µg/ml for 5'-FAM-2OMR, respectively.

For complex formation 100 µl of a 5-fold concentrated oligonucleotide solution in MilliQ water was mixed with particles at the following weight:weight ratios (concentrations in parentheses refer to the final concentrations of particles in the suspensions): 1:0 (= 100% unbound oligonucleotides), 1:1 (17.72 µg/ml particles), 1:5 (88.6 µg/ml particles), 1:10 (177.2 µg/ml particles), 1:25 (443 µg/ml particles), 1:50 (886 µg/ml particles) and 1:100 (1772 µg/ml particles). The mixtures were vortexed thoroughly and incubated at room temperature for about 10 minutes. Afterwards the volume was made up to 500 µl with MilliQ water, PBS buffer or RPMI cell culture medium (without

phenol red) supplemented with 10% FCS, respectively, vortexed again and incubated at room temperature for another 15 minutes.

After incubation the nanoplex suspensions were centrifuged at about 23,000 x g and 25°C for one hour. Samples from the supernatant were analyzed for unbound oligonucleotide. 2OMR was determined by HPLC analysis. 5'-FAM-2OMR in cell culture medium was quantified by fluorimetry. All experiments were performed in triplicate.

4.2.6 HPLC analysis of 2'-O-Methyl RNA

2'-O-Methyl RNA (2OMR) from complexation experiments was quantified by reversed phase HPLC using an gradient Dionex HPLC system consisting of an ASI 100 automated sample injector, UVD 170S detector and P580 gradient pump with Chromeleon® software (version 6.50 SP5 build 1023) (Dionex, Idstein, Germany).

The column was a Gemini® RP- 18 column (150 x 4.6 mm/ 5 µm/ 110 Å) from Phenomenex (Aschaffenburg, Germany). Mobile phase A was composed of 10 mM triethylammonium acetate buffer pH 7.0, mobile phase B was pure acetonitrile. The gradient was as follows: 0 – 0.3 min: 100% A; 0.3 – 3.3 min: 100% A – 80% A, 20% B; 3.3 – 6.0 min: 80% A, 20% B; 6.0 – 9.0 min: 80% A, 20% B – 100% A; 9.0 – 17.0 min: 100% A. Column temperature was 40°C and the UV detector was set to 260 nm. Injection volume was 50 µl per sample. At a flow rate of 1 ml/min the retention time of 2OMR was 6.47 ± 0.04 minutes. Detection and quantification limits were 0.025 and 0.050 µg/ml, respectively. Standards were in the linear range of 0.05 - 20 µg/ml.

4.2.7 Quantification of 5'-FAM-2'-O-Methyl RNA

5'-FAM labeled 2OMR was quantified by fluorimetry using a Cytofluor II fluorescence reader with Cytofluor software version 4.2 (PerSeptive Biosystems, Wiesbaden- Norderstedt, Germany). 150 µl samples from the supernatant were transferred into a 96- well plate and directly measured. The excitation wavelength was set to 485/20 nm and the emission wavelength to 530/30 nm. Standards were in the linear range of 0.5- 20 µg/ml.

4.2.8 Cell cultures

A549 (CCL-185; ATCC, Manassas, VA, USA) were cultivated in RPMI with L-glutamine (PAA Laboratories GmbH, Pasching, Austria) supplemented with 10% fetal calf serum.

Calu-3 cells (HTB- 55; ATCC) were cultivated in Minimum Essential Medium (MEM) with Earl's Salts and L- glutamine (PAA Laboratories GmbH) supplemented with 10% FCS, 1% MEM non- essential amino acid (NEAA) solution and 1 mM sodium pyruvate (all from Sigma- Aldrich).

Primary human alveolar epithelial cells (hAEpC) were isolated from non-tumor lung tissue of patients undergoing partial lung resection according to Elbert *et al.* [79] with slight modifications of the enzymatic digestion and cell purification [83]. In brief, the chopped tissue was digested using a combination of 150 mg trypsin type I (Sigma) and 3 mg elastase (Worthington Biochemical Corp., Lakewood, NJ, USA) in 30 ml BSS (137.0 mM NaCl, 5.0 mM KCl, 0.7 mM Na₂HPO₄ x 7 H₂O, 1.2 mM MgSO₄ x 7 H₂O, 5.5 mM Glucose, 10.0 mM HEPES, 0.18 mM CaCl₂, 100 units/ml penicillin and 100 µg/ml streptomycin) for 40 minutes at 37°C. The alveolar type II (AT II) cell population was purified by a combination of differential cell attachment, percoll density gradient centrifugation and positive selection of epithelial cells with magnetic beads (human Anti- human epithelial antigen (epithelial cells adhesion molecule; Ep-CAM) MicroBeads, Miltenyi Biotec, Bergisch Gladbach, Germany). Cell viability was assessed by trypan blue staining. They were grown in small airway growth medium (SAGM) (Cambrex BioScience Walkersville Inc., Walkersville, MD, USA) supplemented with 1% FCS, 100 units/ml penicillin and 100 µg/ml streptomycin (Sigma- Aldrich). The use of the human material for isolation of primary cells was reviewed and approved by the Ethics Committee of the State Medical Board of Registration of the Saarland.

All cells were kept in an incubator set to 37°C, 5% CO₂ and 95% humidity.

4.2.9 Assessment of 2OMR association with cells by flow cytometry

The association of 5'-FAM-labeled 2OMR with A549 cells was studied by flow cytometry by measuring the green fluorescence of the oligonucleotides after

incubation with nanoplexes. A549 cells were seeded in 6-well plates at a density of 25,000 cells per well and grown for 3 days. Nanoplexes of 5'-FAM-2OMR and different chitosan/PLGA nanoparticles were prepared at ratios of 1:50 ($\text{weight}_{2\text{OMR}}/\text{weight}_{\text{particles}}$) by incubating the different particle suspensions with oligonucleotides at room temperature for 15 minutes. Afterwards the nanoplex suspensions were diluted with RPMI cell culture medium containing 10% FCS to the desired final concentration of 4 μM 5'-FAM-2OMR. The cells were incubated with these suspensions for 6 hours in the incubator. Subsequently, the incubation medium was exchanged for normal cell culture medium without nanoplexes. Controls were non-treated cells, cells treated with 4 μM 5'-FAM-2OMR alone and cells treated with particle suspensions without 5'-FAM-2OMR. Analysis by flow cytometry was performed the next day with a FACSCalibur flow cytometer from Becton Dickinson (BD) Biosciences (Heidelberg, Germany) using the software CellQuest™ Pro Version 4.02 (BD Biosciences). For this purpose cells were detached by incubation with trypsin/EDTA, washed with PBS and resuspended in sheath fluid (BD Biosciences). Green fluorescence was excited at 488 nm and measured after passing a 530/30 nm band pass filter. The instrument was adjusted with non-treated cells. During each run 20,000 cells were counted. The extent of cell associated 5'-FAM-2OMR was evaluated after gating and selection of a fluorescence threshold referred to non-treated cells. The experiment was performed in triplicate.

4.2.10 Visualization of cellular uptake by confocal laser scanning microscopy

Preparation of cells

Cells were grown in 16 well LabTek chamber slides (Nunc GmbH, Wiesbaden, Germany; growth area: 0.4 cm²). A549 cells were seeded at a density of 2500 cells per well 3 days prior to the experiment. Calu-3 cells were seeded at a density of 20,000 cells per well 6 days prior to the experiment. hAEPc were seeded in collagen/ fibronectin coated wells at a density of 10,000 cells per well 7 days prior to the experiment. All cells were kept under the conditions described above.

For uptake experiments cells were treated with nanoplexes prepared of 5'-FAM-2OMR and 3CPNP at a w/w ratio of 1:50. Nanoplexes were prepared by mixing and incubating 5'-FAM-2OMR solution and 3CPNP suspension for 15 minutes at room temperature. The nanoplex suspension was diluted to 4 μ M 5'-FAM-2OMR with RPMI cell culture medium containing 10% FCS. Cells were incubated with this medium for 6 hours in the incubator. Afterwards the incubation medium was replaced by normal cell culture medium without nanoplexes. If necessary, cell culture medium was exchanged every other day.

Staining of cell membranes and nuclei

Cell membranes were stained with the red fluorescent rhodamine-labeled ricinus communis agglutinin I (Rho-RRCA; excitation maximum 552 nm, emission maximum 577 nm; Vector Laboratories Peterborough, UK). Cells were washed once with PBS and afterwards incubated with 25 μ g/ml of Rho-RRCA in PBS for 15 minutes in the incubator. After two washing steps with PBS the cells were fixed with 4% paraformaldehyde in PBS for 10 minutes at room temperature.

Cell nuclei were stained with TOPRO3 (excitation maximum 642 nm, emission maximum 661 nm; Molecular Probes, Invitrogen GmbH, Karlsruhe, Germany). For this purpose the cells were washed once with PBS. Afterwards they were fixed and permeabilized with ice-cold (-20°C) pure ethanol for 10 minutes at 4°C. After two washing steps with PBS the cells were incubated with 1 μ M TOPRO3 in PBS for 15 minutes at room temperature.

After fixation and staining the cells were washed again twice with PBS and were subsequently mounted in the fluorophor protector FluorSafe[®] reagent (Calbiochem, San Diego, CA, USA) and studied by confocal laser scanning microscopy.

Image acquisition and processing

Confocal laser scanning microscopy was performed with a Bio-Rad 1024 MRC system (BioRad, München, Germany) in combination with an inverted Zeiss Axiovert 100 microscope (Carl Zeiss MicroImaging GmbH, Göttingen, Germany) equipped with a krypton/ argon laser and a 40x oil

immersion objective (NA 1.3). Excitation wavelengths and emission filter sets were dependent on the staining method and are summarized in Table 4-1.

Table 4-1: Excitation wavelengths and filters for confocal microscopy depending on the staining method. (BP = band pass filter; LP = long pass filter)

| staining method | excitation wavelength | emission filter |
|--------------------------|-----------------------|-----------------|
| two colors (dyes) | | |
| green (5'-FAM-2OMR) | 488 nm | 522/35 nm BP |
| red (Rho-RRCA) | 568 nm | 585 nm LP |
| three colors | | |
| green (5'-FAM-2OMR) | 488 nm | 522/35 nm BP |
| red (DiI) | 568 nm | 605/32 nm BP |
| far red (TOPRO3) | 647 nm | 680/32 nm BP |

A step motor was used for the acquisition of 3D images. Images were processed using the software Velocity[®] (Improvision, Tübingen, Germany). XY-images in Figure 4-5 and Figure 4-6 are presented in “extended focus” mode, i.e. an overlay of all images in an image stack merged into one image for better presentation. XZ- and YZ cross sections from the image stacks were used to verify the localization of the green fluorescence of 5'-FAM-2OMR with respect to the stained membrane.

4.2.11 Cytotoxicity experiments and monolayer integrity

Cytotoxicity of 3CPNP was determined by the MTT ((3-(4,5-dimethylthiazol-2-yl)-2,5-diphenyltetrazolium bromide) assay. A549 cells were seeded on 96-well plates at a density of 10,000 cells per well and were allowed to adhere overnight. The next day cells were incubated for 6 hours with 3CPNP and nanoplexes of 2OMR and 3CPNP in cell culture medium at particle concentrations of 443, 886 and 1772 µg/ml. The corresponding nanoplex ratios were 1:25, 1:50 and 1:100 (weight_{2OMR} /weight_{3CPNP} ratios; where 1 = 17.72 µg/ml = 4 µM 2OMR final concentration). Cells treated with cell culture medium and cell culture medium diluted with water (at a volume corresponding to the highest CPNP concentration) were included for comparison. After incubation the medium was exchanged for normal cell culture medium and the cells were grown for three more days. On the third day 10 µl of 10 mg/ml MTT solution in PBS pH 7.4 were added to each well.

After an incubation time of 2 hours under cell culture conditions 90 μ l lysis buffer (15% SDS in a 1:1 mixture of dimethylformamide and water, pH adjusted to 4.5 with 80% acetic acid) were added to each well. Cell lysis was performed at room temperature overnight on an orbital shaker. Absorbance was measured the next day at 560 nm. Each concentration was measured in quadruplicate.

The influence of chitosan/PLGA nanoparticles on the integrity of cell monolayers was assessed by measuring the transepithelial electrical resistance (TEER) using an epithelial voltohmmeter (EVOM, World Precision Instruments, Berlin, Germany) with an STX-2 electrode. Calu-3 cells were grown on 12 mm polyester (PET) Transwell[®] filters (Corning Inc., NY, USA) at a density of 100,000 cells per filter for 3 weeks. Cells were treated with 0.5, 1 and 2 mg/ml of purified 3CPNP in cell culture medium containing 10% FCS. Control cells were treated with cell culture medium only and a 1:1 mixture of cell culture medium with sterile MilliQ water, respectively. The mixture with water was used to check for the influence in changes of osmotic pressure that might occur upon dilution of cell culture medium. Cells were incubated for 6 hours. Afterwards the incubation medium was replaced by normal cell culture medium. TEER values were measured before incubation, after 3 and 6 hours and after 3 days of incubation. Measurements were performed in hexaplicate.

4.2.12 Telomerase activity measurement (TRAP)

Cells (1×10^6) were collected and lysed in 200 μ L ice-cold CHAPS lysis buffer (10 mM Tris-HCl (pH 7.5), 1 mM $MgCl_2$, 1 mM EGTA, 0.1 mM Benzamidine, 5 mM β -mercaptoethanol, 0.5 % CHAPS (3-[(3-cholamidopropyl)dimethylammonio]-1-propanesulfonate), 10 % Glycerol) for 30 min on ice. Lysates were centrifuged at 12,000 g for 20 min at 4°C and the supernatants were snap-frozen and stored at -80°C. Telomerase activity was measured in lysates containing 0.05 μ g protein using a modified protocol of the TRAPeze Telomerase Detection Kit. The manufacturer's protocol was modified as follows: A 6-carboxy-fluorescein (6-FAM) labeled TS primer 5'-AATCCGTCGAGCAGAGTT-3' and CX primer 5'-CCCTTACCCTTACCCTTACCCTAA-3' were used. An internal telomerase assay standard (ITAS) which represents a 150 bp fragment of the

rat myogenin cDNA which is amplified by TS and CX primer was added in the reaction mix. PCR products were separated by fluorescence capillary electrophoresis (ABI PRISM 310 Genetic Analyzer). Fragment sizes were determined using the internal size standard GeneScan-500 ROX and collected data were analyzed with GeneScan Analysis software.

4.2.13 Terminal restriction fragment length determination (TRF)

DNA was isolated from cells using the phenol/chloroform extraction method, digested with 10 U of Hinf I, electrophoresed and transferred to a nylon membrane. The nylon membrane was hybridized with a digoxigenin labeled 5'-(TTAGGG)₇ telomere-specific probe and incubated with anti-DIG-alkaline phosphatase. The immobilized telomere probe was visualized by a chemiluminescent substrate for alkaline phosphatase (CDP-star, Roche). The membrane was exposed to X-ray film (Hyperfilm; Amersham Biosciences) and analyzed using AIDA software (Raytest, Straubenhardt, Germany).

4.2.14 Statistical analysis

One-Way-ANOVA was used for statistical analysis using the software SigmaStat[®] version 3.01 from SPSS Inc. (Chicago, Illinois, USA). Results were regarded to be statistically different when $P < 0.05$.

4.3 Results

4.3.1 Nanoparticle properties

The physico-chemical characteristics of the different nanoparticles in terms of size, polydispersity and zeta potential were determined directly after the preparation, after purification by size exclusion chromatography and after a storage period of about two months at 4°C.

As can be seen from Figure 4-1 A particle sizes were in the range of 135 nm (PLGA-NP) to 175 nm (6CPNP). The increase in size correlated with the amount of chitosan. The purification procedure and storage did not affect the mean particle size for all preparations. In all cases the nanoparticles showed monomodal distribution. However, there was an increase in polydispersity indices (PDIs; Figure 4-1 B) after purification and storage except for 05CPNP. After preparation PDIs were in the range of 0.060 (PLGA-NP) to 0.160 (6CPNP). After purification they were in the range of 0.070 (05CPNP) to 0.240 (6CPNP) indicating a change in the size distribution because of the purification procedure. This observation is most probably due to a degglomeration of small particle agglomerates. A comparison of the size distribution curves before and after purification revealed that the fraction of smaller particles increased slightly after purification, giving rise to a broadening of the size distribution curves and hence an increase in PDI (data not shown). PDIs decreased again during storage to values below 0.190 (6CPNP). All zeta potentials (ZPs) were positive for preparations containing chitosan while those for PLGA-NP were negative (Figure 4-1 C). There was a good correlation between chitosan content and increase in zeta potentials after purification. For 05CPNP, 1CPNP and 3CPNP the ZPs remained stable during storage. For 6CPNP there was a drop in ZP from about 42 mV to 30 mV and PLGA-NP showed an increase from about -19 mV to -8 mV.

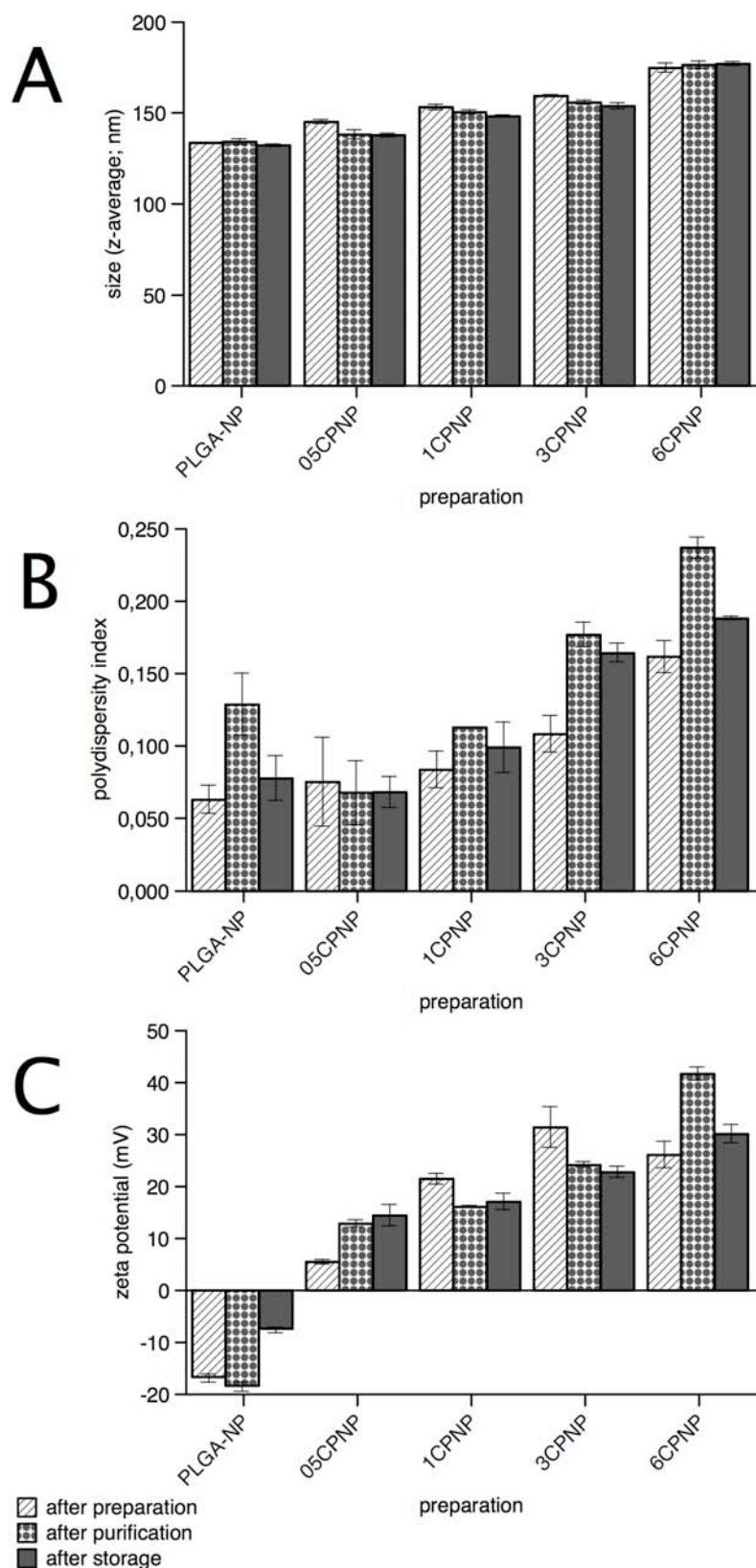


Figure 4-1: Properties of different chitosan/PLGA nanoparticles: after preparation (striped bars), after purification (bars with grey circles) and after storage for two months at 4°C (grey bars); A = size (nm), B = polydispersity index, C = zeta potential (mV). Measurements were performed in triplicate. Data represents mean values ± SD.

4.3.2 Complexation of 2OMR

To examine complexation efficiencies and nanoplex stabilities nanoplexes at different 2OMR : nanoparticle w/w ratios were preformed in water and subsequently diluted with either water, PBS or RPMI cell culture medium + 10% FCS. The amounts of unbound 2OMR were determined from the supernatant after removal of nanoplexes by centrifugation.

In MilliQ water the amount of unbound 2OMR decreased with increasing amounts of nanoparticles (Figure 4-2 A). Up to a $\text{weight}_{2\text{OMR}}/\text{weight}_{\text{particles}}$ ratio of 1:25 there was a good correlation between the chitosan content and the binding: particles prepared with higher amount of chitosan bound 2OMR better than particles with lower amounts of chitosan. At higher concentrations of nanoparticles the binding efficiency was between 80 – 100% for all preparations. As expected, there was no binding of oligonucleotides to negatively charged PLGA nanoparticles. For all preparations the pH values decrease gradually with increasing particle concentrations from about pH 5.3 to pH 3.2 (see insert Figure 4-2 A).

In PBS the stabilities of preformed nanoplexes proved to be very weak. As can be seen from Figure 4-2 B there was practically no binding of 2OMR after dilution and incubation of the nanoplexes with PBS for all preparations. pH values remained in the neutral range (pH 7.0 – 7.4) with increasing amounts of chitosan-coated particles.

A similar result was found in RPMI cell culture medium containing 10% FCS (Figure 4-2 C). Only at the highest particle concentrations about 10 to 20% of 2OMR were still bound to the particles. For all preparations pH values remained in the neutral range of 7.4 to 7.7.

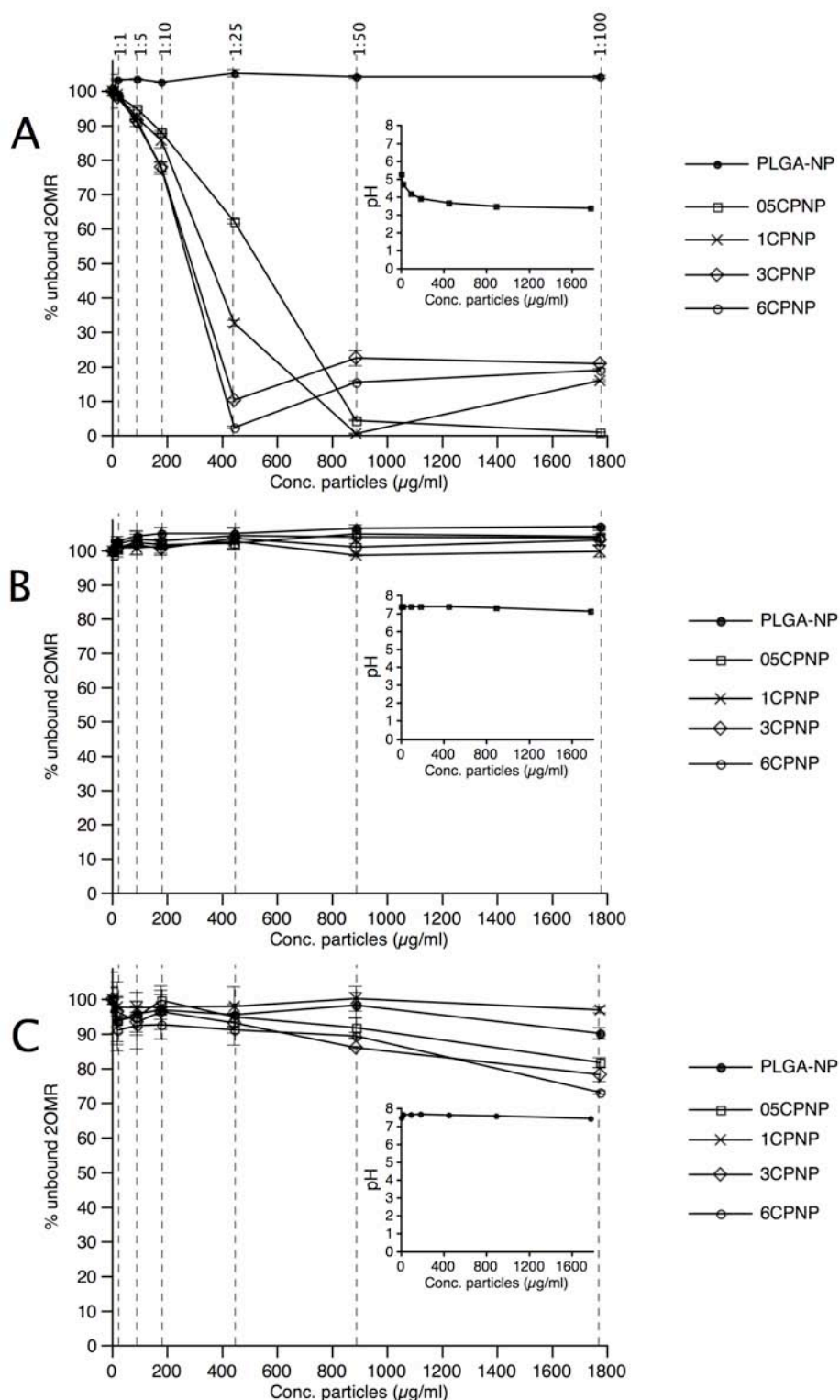


Figure 4-2: Binding efficiencies and complex stabilities of nanoplexes between 2OMR and chitosan/PLGA nanoparticles. Nanoplexes were preformed in MilliQ water and then diluted with: MilliQ water (A), PBS pH 7.4 (B) and RPMI cell culture medium + 10% FCS (C). The figure shows the percentages of unbound 2OMR recovered from the supernatant after centrifugation referred to the initial amounts. $w_{2OMR}/w_{particles}$ ratios are given on top of the figure and indicated by vertical dashed lines. Inserts: pH profiles for different particle concentrations in respective suspension medium. All experiments were performed in triplicate. Data represents mean values \pm SD.

4.3.3 Uptake of nanoplexes

Cell-associated levels of FAM-labeled 2OMR after incubation with different nanoplex preparations were studied by flow cytometry. Confocal laser scanning microscopy (CLSM) was used to visualize the uptake of nanoplexes (w_{2OMR}/w_{NP} ratio 1:50) and nanoparticles into A549, Calu-3 and hAEPc.

Flow cytometry (Figure 4-3) showed an increase in green fluorescence, i.e. cell-associated 5'-FAM-2OMR levels, which was dependent on the formulation. While the incubation of A549 cells with nanoplexes of PLGA-NP did not increase the green fluorescence intensities, there was a shift to higher values with the chitosan-modified PLGA nanoparticles. Best results were obtained for 3CPNP and 6CPNP with about 88% and 83%, respectively. (Figure 4-3). An incubation of cells with plain nanoparticles (i.e. not complexed with 2OMR) showed no interference with this experiment (data not shown).

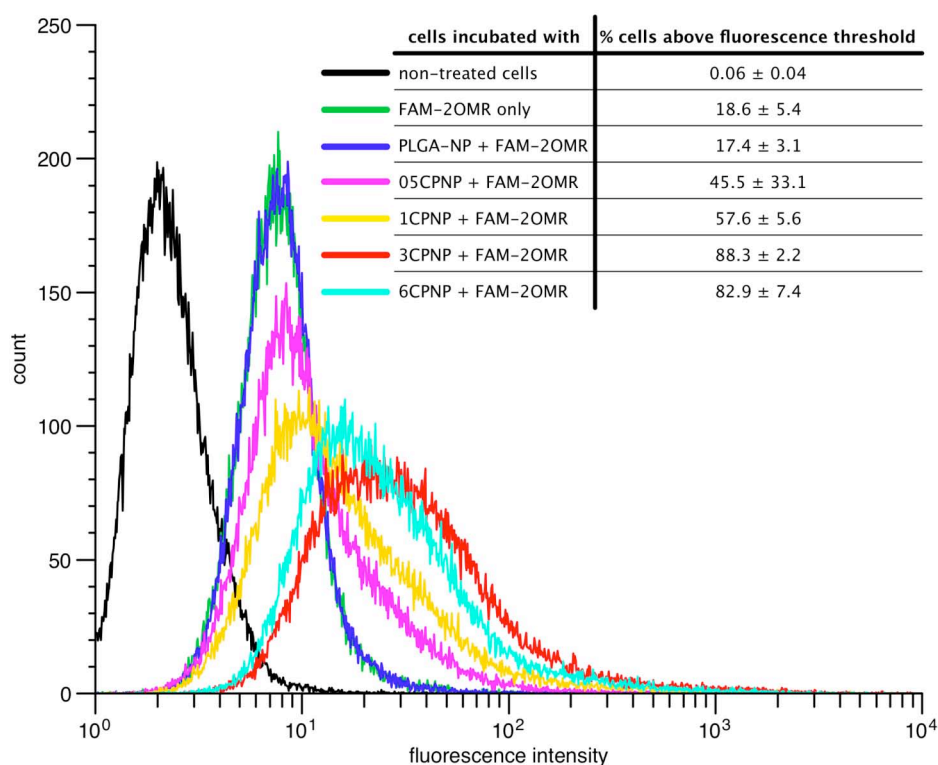


Figure 4-3: Histogram from flow cytometry with A549 cells treated with nanoplexes of FAM-labeled 2OMR and different particle preparations at a $w_{2OMR}/w_{particles}$ ratio of 1:50. The green fluorescence of cells was measured 24 hours after incubation with nanoplexes. The results in the table were obtained after gating and selection of a fluorescence threshold. 20000 cells were counted per sample. Values are presented as mean values ± SD (n = 3).

The characterization of the nanoplexes with respect to size and surface charge at the 1:50 ratio (Figure 4-4) demonstrated that nanoplexes prepared with PLGA-NP and 05CPNP were negatively charged. Their sizes were comparable to nanoparticles without 2OMR. 1CPNP exhibited a surface charge around zero mV and the increase in size indicates an agglomeration of the nanoplexes due to the loss of electrostatic repulsion. The sizes of nanoplexes with 3CPNP and 6CPNP were again comparable to the nanoparticles without 2OMR. Both formulations possessed positive surface charges > 10 mV. Since the formulation with 6CPNP did not further increase the cell-associated fluorescence, further experiments were performed with 3CPNP only.

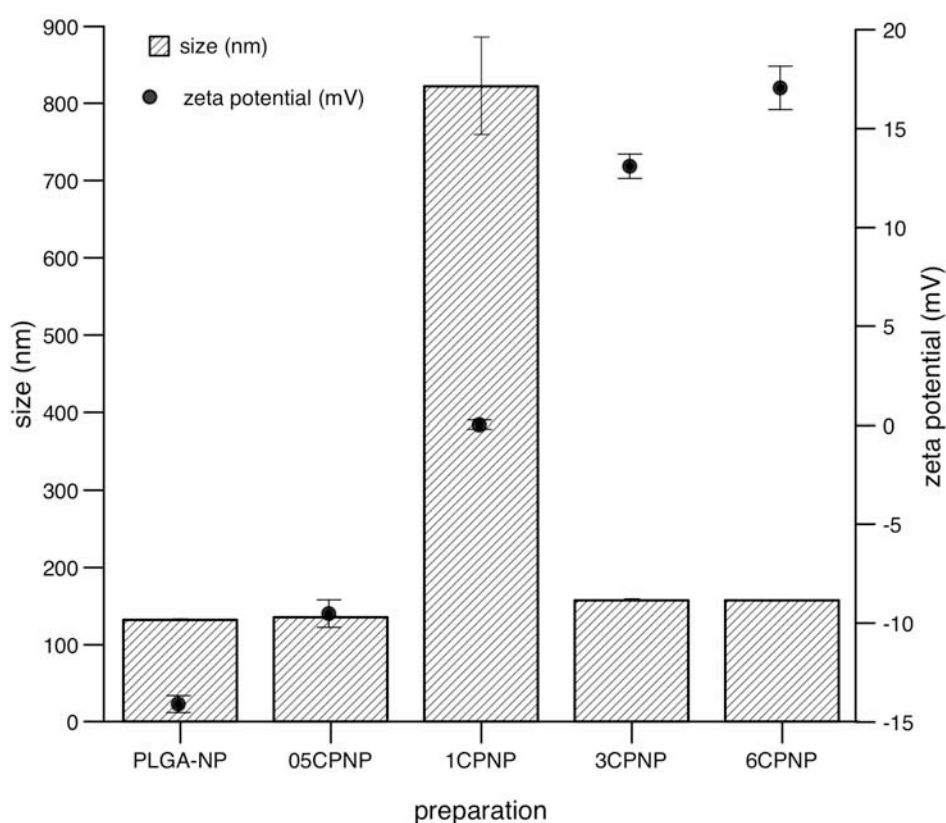


Figure 4-4: Properties of nanoplexes at a ratio of 1:50 that were used for flow cytometry experiments measured in MilliQ water. Bars: size (z-average; nm); dots: zeta potential (mV). All measurements were performed in triplicate. Data represents mean values \pm SD.

CLSM demonstrated that the increase of fluorescence intensities 24 hours after incubation as observed in the flow cytometry experiments is due to an uptake and not only an adsorption of nanoplexes to the cell surface (Figure 4-5). As can be seen in Figure 4-5 A2 – A4 the treatment of A549 cells with nanoplexes of 5'-FAM-2OMR and 3CPNP resulted in a strong green fluorescence compared to cells incubated with 5'-FAM-2OMR alone (Figure 4-5 A1). Interestingly, the uptake of nanoplexes into A549 cells appeared to be a very slow process. After 6 hours of incubation the green fluorescence was still colocalized with the red fluorescence of the cell membranes (Figure 4-5 A2). An uptake into the cells was observed 24 hours post incubation as can be seen in Figure 4-5 A3. The green fluorescence appeared mostly point-shaped indicating an entrapment of the nanoplexes in intracellular vesicles. A comparable result was obtained 48 hours after incubation (Figure 4-5 A4).

The uptake of nanoplexes into A549 cells was compared to the uptake into Calu-3 cells and non-cancerous hAEPc. In contrast to A549 cells Calu-3 cells also showed an uptake of 5'-FAM-2OMR alone. The green fluorescence intensity and distribution was comparable to cells treated with nanoplexes. Also, there was no adsorption to the cell membrane. The green fluorescence could be observed inside the cells directly after 6 hours of incubation (Figure 4-5 B1 and B2). Comparable to A549 cells the green fluorescence could be observed for at least 48 hours (Figure 4-5 B3 and B4). In case of non-cancerous hAEPc a colocalization of nanoplexes with the cell membrane was observed but optical sections of these rather thin cells (< 1 μm) at least suggested that the nanoplexes were not internalized. The nanoplexes showed a patch-like pattern and were permanently colocalized with the cell membranes for 48 hours (Figure 4-5 C1-C4).

Nanoplexes prepared of Dil-stained 3CPNP and 5'-FAM-2OMR (Figure 4-6) allowed to demonstrate that 2OMR uptake in A549 cells occurred as a complex with the nanoparticles although the complex stability in cell culture medium was very weak (compare Figure 4-2 C). As can be seen in Figure 4-6 the green fluorescence of the oligonucleotides and the red fluorescence of the nanoparticles are colocalized after incubation resulting in a yellowish/orange

color. A similar result was obtained 1 and 2 days after incubation indicating a slow release of FAM-2OMR from complexes. However, in comparison to the red fluorescence the green fluorescence seemed to decrease over time. After 5 days red cloudy structures could be found around the cell nuclei (white arrows in Figure 4-6). This observation is most probably due to the degradation of the nanoparticles and the release of Dil into the cytoplasm.

Next page:

Figure 4-5: Confocal images of A549 (A1-A4), Calu-3 (B1-B4) and hAEpC (C1-C4) presented in extended focus mode. Yellow lines indicate the positions of XZ- and YZ-cross sections through image stacks. The location of apical and basolateral sides are given in A1. Bars = 50 μ m. A1, B1, C1: cells after 6 hours of incubation with 4 μ M of FAM-2OMR only; A2, B2, C2: cells after 6 hours of incubation with nanoplexes of FAM-2OMR and 3CPNP ($w_{2OMR}/w_{particles}$ ratio: 1:50); A3, B3, C3: cells 24 hours after incubation; A4, B4, C4: cells 48 hours after incubation. Green fluorescence = FAM-labeled 2OMR; red fluorescence: cell membranes counterstained with Rho-RRCA. FAM-2OMR alone is not taken up into A549 cells and hAEpC (A1 and C1) but into Calu-3 cells (B1). A549: after 6 hours of incubation nanoplexes of FAM-2OMR and 3CPNP are colocalized with the cell membrane (A2) but can be found inside the cells after 24 and 48 hours (A3 and A4). Calu-3: nanoplexes are directly taken up after 6 hours of incubation (B2). hAEpC: The green fluorescence is colocalized with the cell membrane for 48 hours (C2-C4).

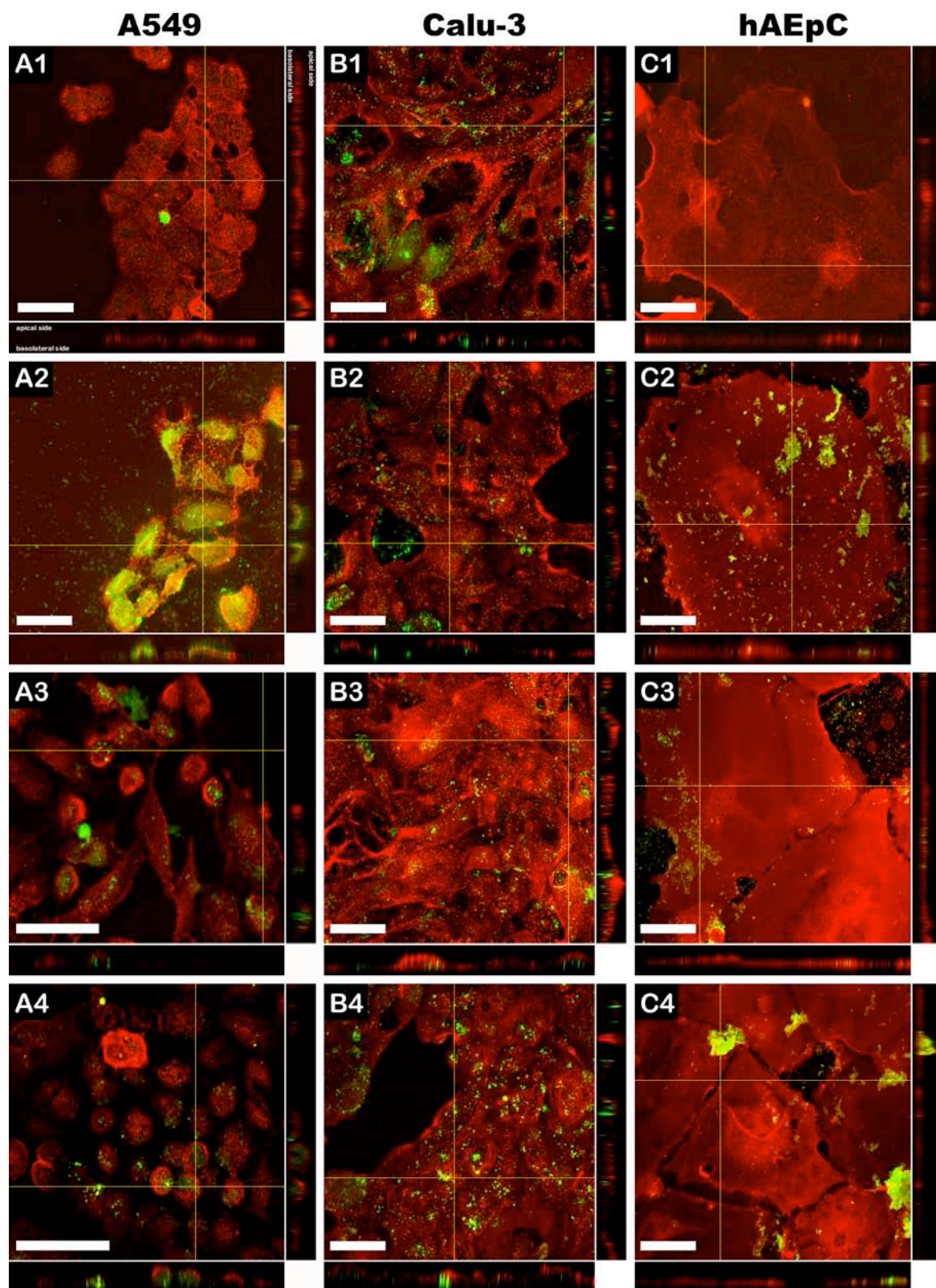


Figure 4-5

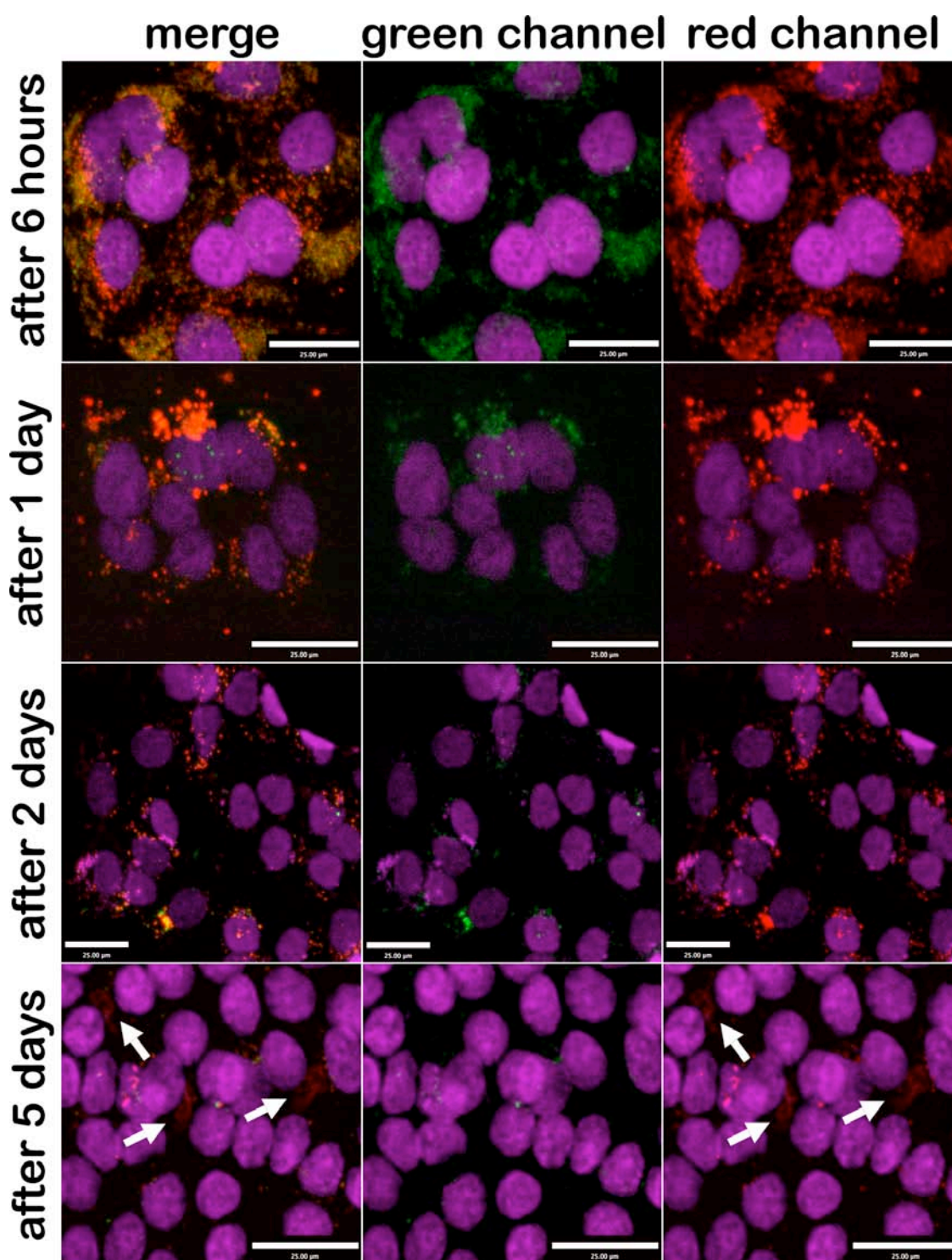


Figure 4-6: The uptake of 2OMR in A549 cells is mediated via nanoplexes. The green fluorescence of FAM-2OMR is colocalized with the red fluorescence from Dil-stained 3CPNP. Colocalization can be observed for at least two days by the yellowish/orange color in the left column (“merge”). Middle column and right column: fluorescence of FAM-2OMR (green) and Dil-3CPNP (red), respectively. After five days red cloudy structures (white arrows) indicate the degradation of nanoparticles and release of Dil into the cytoplasm. Purple = cell nuclei counterstained with TOPRO-3. Bars = 25 µm

4.3.4 Cytotoxicity and monolayer integrity

The MTT cytotoxicity assay showed that cell survival after a treatment with different concentrations of 3CPNP and nanoplexes of 3CPNP and 2OMR, respectively, is reduced to 70%- 80% of control independent of nanoparticle concentration (Figure 4-7). However, a treatment of cells with a mixture of cell culture medium and water also led to a reduced cell survival (about 90% of control).

Furthermore, the treatment with nanoparticles did not show an effect on monolayer integrity of Calu-3 cells. When grown on Transwell® filters Calu-3 cells typically form tight monolayers with transepithelial electrical resistance (TEER) values between 1300 and 1500 $\Omega \times \text{cm}^2$ [110]. TEER for cells incubated with nanoparticles was comparable to controls during the incubation period and 72 hours after treatment (data not shown).

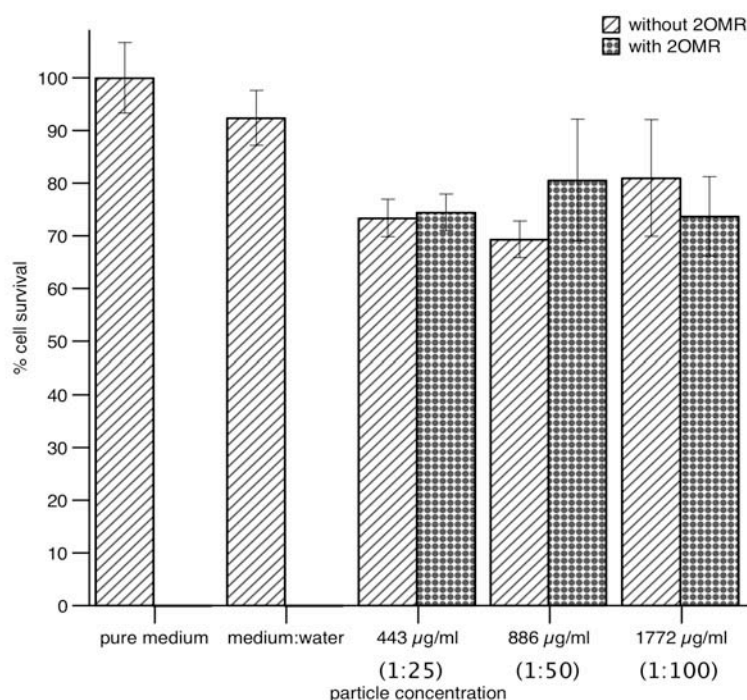


Figure 4-7: MTT assay with purified 3CPNP: A549 cells show a reduced survival in the presence of nanoparticles and nanoplexes. Cells were treated with nanoplexes of the $W_{2OMR}/W_{particles}$ ratios 1:25 (= 443 $\mu\text{g}/\text{ml}$ nanoparticles), 1:50 (= 886 $\mu\text{g}/\text{ml}$ nanoparticles) and 1:100 (=1772 $\mu\text{g}/\text{ml}$ nanoparticles). Cells treated only with plain nanoparticles in the corresponding concentrations were used as controls. Each concentration was measured in quadruplicate. Data represents mean values \pm SD.

4.3.5 Inhibition of telomerase activity and telomere shortening

The treatment of A549 cells with nanoplexes of either purified (Figure 4-8 A) or non-purified (Figure 4-8 B) 3CPNP and 2OMR resulted in comparable reductions of telomerase activity for both batches.

The strongest inhibitory effect was observed after treatment with nanoplexes at a $w_{2OMR}/w_{particles}$ ratio of 1:100 resulting in about 60% inhibition of telomerase activity. However, at this ratio the mismatch control, which contains two mismatches relative to the template sequence [48], also showed a considerable telomerase inhibition. This observation is most probably due to non-specific effects. Best results were obtained with non-purified particles at the 1:50 ratio. Here a statistically significant difference between normal 2OMR and the mismatch sequence has been found ($P < 0.05$). Telomerase activity was decreased by about 50% with normal 2OMR while mismatch 2OMR showed only a slight effect. Such a statistically significant difference between normal and mismatch 2OMR could not be found for purified particles. The telomerase inhibition by nanoplexes prepared with non-purified nanoparticles was as efficient as using the lipid-based transfection reagents DOTAP and MegaFectinTM, which was described recently by our group [111].

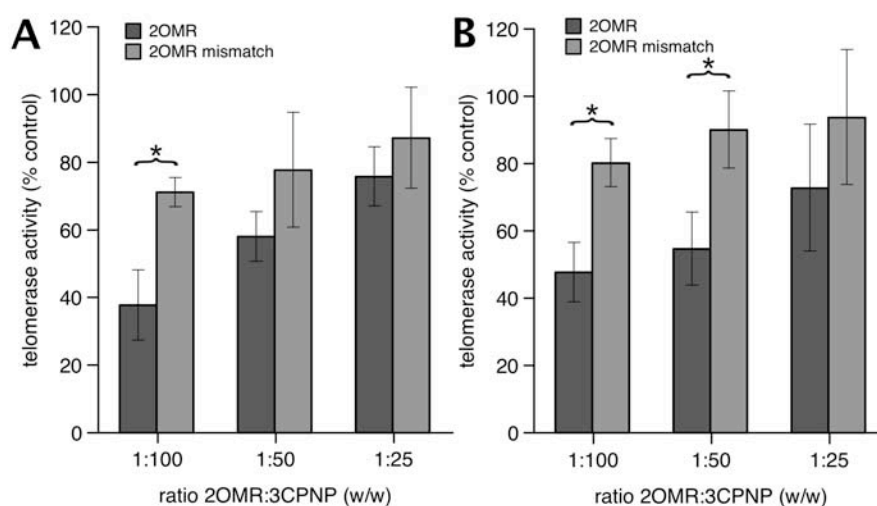


Figure 4-8: Reduction of telomerase activities in A549 cells 72 hours after incubation with 2OMR:3CPNP nanoplexes at different w/w ratios in comparison to a 2OMR mismatch control. Telomerase activities were normalized to non-treated cells. A: nanoplexes were formed with purified 3CPNP nanoparticles; B: nanoplexes were formed with non-purified 3CPNP nanoparticles. Data represent mean values \pm SD of at least 3 independent experiments. * = statistically significant difference between normal 2OMR and mismatch control ($P < 0.05$, One-Way ANOVA).

Reduction of telomere length was examined after repetitive treatments (twice weekly) of A549 cells over 35 days in comparison with the lipid-based transfection reagents DOTAP and MegaFectinTM. As can be seen in Figure 4-9, 3CPNP were as effective as the two commercial transfection reagents. Reduction in telomere length was significant for all three preparations compared to control ($P < 0.05$; One-Way-ANOVA) but there was no significant difference between the transfection reagents.

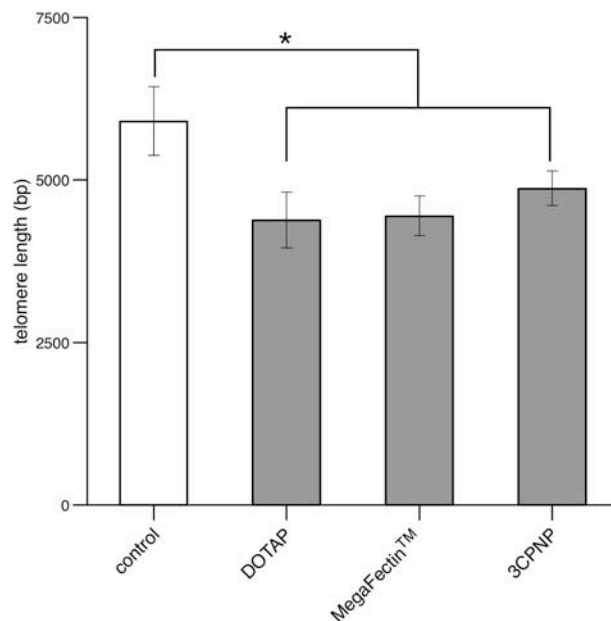


Figure 4-9: Telomere length in A549 cells after repeated treatment with 2OMR:3CPNP nanoplexes over 35 days in comparison to cells treated with the commercially available transfection reagents DOTAP and MegaFectinTM. 3CPNP are as efficient as DOTAP and MegaFectinTM. * = all treated cells were statistically significant different from control (One-way-ANOVA; $P < 0.05$). There was no statistical significant difference between the lipid-based transfection reagents and 3CPNP.

4.4 Discussion

Our results show that changing the amounts of chitosan in the preparation procedure can easily vary particle properties. These variations significantly influence their efficiency for the delivery of antisense 2OMR to lung cancer cells.

The particles proved to be stable after purification and storage over two months and they showed a high binding of 2OMR and complex stability in water. However, dilution in buffered media strongly reduced complex formation. In our previous study, suspensions of CPNP either as particles alone or in complex with 2OMR proved to be stable in NaCl solution, PBS pH 7.4 and HBSS buffer pH 7.4 with regard to their colloidal properties. However, they showed a strong reduction in their surface charge when diluted in buffered media, which is due to the neutralization of the protonated primary amine groups of chitosan [109]. This charge neutralization results in a reduced ability to bind the negatively charged 2OMR as could be demonstrated by our binding/complexation experiments. Chitosan is a weak base. The type that was used for these experiments has a pK_a value of about 6.5 [112]. Complexes diluted in pure MilliQ water were stable because pH values were below this pK_a resulting in protonation of most of the amino groups. In contrast, due to the neutralization of the positive charges, complex stability was strongly reduced and dissociation occurred when the preformed complexes were diluted in buffered media like PBS and cell culture medium with pH values ≥ 7 .

From these results one could expect that nanoplexes in cell culture medium are unstable and do not improve the uptake of 2OMR into cells. But this was not the case. As we could demonstrate in the following experiments with A549 cells, uptake was significantly increased for nanoplexes prepared with 3CPNP and 6CPNP and telomerase activity was successfully inhibited (Figures 4-3, 4-5, 4-6, 4-8 and 4-9).

From the nanoplex characterizations it could be argued that the uptake correlated with the particle surface charge (Figure 4-4) as described by Lorenz *et al.* [113]. However, the characterization was performed in water while the uptake experiments were performed in cell culture medium

containing 10% fetal calf serum. Beside the neutralization of the surface charge in cell culture medium it is known that serum proteins adsorb to cationic nanoparticles [114, 115], which significantly influences the surface charge. The fact that there was no difference in uptake improvement between nanoplexes prepared with 3CPNP and 6CPNP indicates that the uptake cannot only be attributed to the surface charge but also must be related to the chitosan density on the particle surface. That the uptake of FAM-2OMR into A549 is really mediated via nanoplexes could clearly be demonstrated by confocal microscopy (Figure 4-5 and Figure 4-6), which shows that there is no complete dissociation of complexes in cell culture medium and that the nanoplexes are still able to interact with the cell surface. Whether these non-dissociated complexes corresponds to the about 15% of bound 2OMR (Figure 4-2 C; 1:50 ratio 3CPNP) will be the subject of future studies. Fang *et al.* have shown with liposomes composed of DPPC that even at pH 7.4 an adhesion between chitosan and the phospholipid membrane occurs [116]. Löhbach *et al.* demonstrated that the adhesion of chitosan-coated carboxypolystyrene nanoparticles dispersed in PBS to endothelial cells is higher in the presence of FCS than without proteins [117]. Therefore, besides remaining ionic forces other factors like hydrogen bonds or even the combination of chitosan and proteins on the particle surfaces might play an important role in the nanoplex – cell surface interaction.

Huang *et al.* reported that the uptake of FITC-labeled chitosan nanoparticles into A549 cells is a saturable process dependent on adsorption of particles to the cell membrane and subsequent clathrin-mediated endocytosis [118, 119]. This mechanism corresponded well to the observations in our experiments. The uptake of FAM-2OMR alone was very poor but the adsorption of nanoplexes to the cell surface significantly enhanced its internalization. The results from flow cytometry suggest that a certain chitosan density on the particle surface is required to achieve optimal adsorption. This level was reached in 3CPNP because 6CPNP with their higher chitosan content did not further increase the nanoplex uptake (Figure 4-4). The differences in chitosan content were shown by zeta potential measurements in this (Figure 4-1 and

Figure 4-2 B) and our previous study [109] where 6CPNP exhibit a higher zeta potential than 3CPNP.

However, nanoplexes also adsorbed on hAEpCs, but no clear internalization was observed over two days. HAEPc are primary isolated human alveolar type (AT) II cells that acquire characteristics of AT I cells after a certain time under the given cell culture conditions [80]. Since AT I cells are reported to be deficient in clathrin-mediated endocytosis [120] this might explain the lack of nanoplex internalization by these cells. In contrast, Calu-3 expressing both clathrin and caveolin [121] showed even an uptake of FAM-2OMR alone. However, a closer investigation of the exact uptake mechanism was not done. The data from the MTT toxicity test demonstrates that the nanoparticles have only a slight cytotoxicity as they reduce the A549 cell growth about 20 - 30% (Figure 4-7). The nanoparticles did not influence the integrity of Calu-3 monolayers, and hence their barrier function, since TEER values did not differ from controls. Grenha et al. reported a comparable result for chitosan nanoparticles in respirable powder formulations [122].

Furthermore, we were able to show that a treatment of A549 cells with these nanoplexes results in an inhibition of telomerase activity and telomere shortening. The comparison of our chitosan/PLGA nanoparticles with established transfection reagents was encouraging for further studies since the results were comparable to DOTAP or MegaFectin™. However, the purification of CPNP does not seem to be necessary with regard to their biological effect because telomerase inhibition was not significantly different for either purified or non-purified particles. Regarding the specificity of 2OMR in comparison with the mismatch sequence, nanoplexes prepared with non-purified particles appeared to be even more effective than those prepared with purified particles. For this study purification was done to assure that the observed effects in binding and uptake experiments can only be attributed to the nanoparticles and not to remaining polymers in the suspensions. Since the presence of these polymers does not seem to influence the biological activity future studies concerning the long-term efficacy of nanoplexes will be performed with non-purified particles.

4.5 Conclusion

Nanoplexes formed between cationic chitosan-coated PLGA nanoparticles and antisense 2'-O-methyl-RNA were efficiently taken up by human alveolar (A549) and bronchial (Calu-3) epithelial cancer cell lines, while cellular uptake was not obvious for non-cancerous human alveolar epithelial cells in primary culture. In thus transfected cells, a significant inhibition of telomerase activity and shortening of telomeres could be observed. Transfection proved to be dependent on the chitosan content of the nanoplexes, allowing to optimize the formulation for such application. The resulting nanoplexes were well tolerated by the cells and appeared to be equally efficient as some commercially available lipid-based transfection reagents.

Chapter 5
**Purification of chitosan/PLGA nanoparticles by size
exclusion chromatography**

5.1 Introduction

The development of a suitable purification method for chitosan/PLGA nanoparticles was necessary to verify that the results described in Chapter 4 could only be attributed to the particles and not to remaining free polymers in the suspensions. However, the purification method that was available at that time was based on repeated ultrafiltration-resuspension steps of nanoparticle suspension using the Centriscart[®] system from Sartorius (Figure 5-1). This method required centrifugation after each resuspension, which increased the risk for particle agglomeration. Another point was that only small volumes of 2 ml maximum could be purified in one tube, which proved to be very time consuming and laborious for the purification of larger volumes.

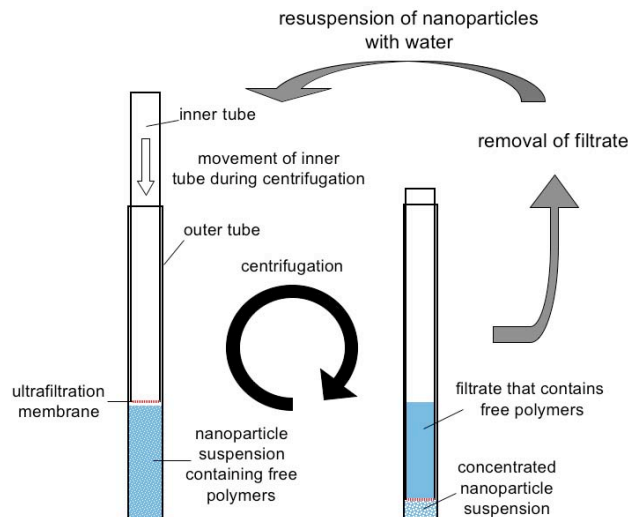


Figure 5-1: Principle of the nanoparticle purification with Centriscart[®] ultrafiltration tubes. The choice of the membrane pore size allowed the separation of free polymers from nanoparticles by ultrafiltration during the centrifugation step. Suspensions were submitted to several ultrafiltration-resuspension steps for complete removal of free polymers.

Since the experiments described in Chapter 4 and long-term cell culture experiments required higher amounts of purified nanoparticles, another purification strategy was needed. We developed a method based on size exclusion chromatography that allowed the semi-automatic processing of volumes up to 50 ml, i.e. the volume of one particle preparation.

This chapter describes the development of this purification method including factors that are important for a successful separation of nanoparticles from free polymers.

5.2 Materials and Methods

5.2.1 The size exclusion chromatography system

Size exclusion chromatography (SEC) was done using a FPLC[®] system from Pharmacia Biotech (now Amersham Biosciences; Uppsala, Sweden) equipped with two P-500 pumps, a LCC-501 Plus controller, a MV-7 injection valve, a 50 ml Superloop, a C 16/70 column with one AC 16 adaptor, an Uvicord SII detector with an interference filter of 206 nm and a FRAC-100 fraction collector. Stationary phase was Sephacryl S-1000 SF[®] from GE Healthcare (Munich, Germany) with a dimension of 65 cm in height and 1.6 cm in diameter. The system was operated by the FPLCdirector[™] software version 1.3 (Pharmacia Biotech). Flow rate of mobile phase was 1 ml/min under isocratic conditions.

5.2.2 Selection of mobile phase

Three different mobile phases were tested: pure MilliQ water, 0.9% sodium chloride (NaCl) solution and 0.1 mM hydrochloric acid (HCl), which was prepared by dilution of 1 M HCl in MilliQ water.

5.2.3 Particle suspensions

Different chitoan/PLGA nanoparticles were prepared as described in Chapter 4 under 4.2.2. Most parts of the method development described here were performed with chitosan/PLGA nanoparticles prepared with 3 mg/ml chitosan (3CPNP). All particle suspensions were filtered through a 0.2 µm cellulose acetate filter (Chromafil[®] GF/PET-20/25, Macherey-Nagel, Dueren, Germany) prior to injection.

5.2.4 Evaluation of the separation of particles from polymers

To demonstrate the different retention times of particles, chitosan and PVA, 1.5 ml of each sample were injected into the SEC system. Particle suspension was 3CPNP. The concentrations for chitosan and PVA solutions were 3 mg/ml and 25 mg/ml, respectively. Mobile phases were either MilliQ water or 0.1 mM HCl.

5.2.5 Quantification of chitosan and PVA in fractions after purification

For the evaluation of the purification method 5 ml of a filtered chitosan/PLGA nanoparticle suspension was injected into the size exclusion chromatography system. Mobile phases were MilliQ water and 0.1 mM HCl. The flow rate was 1 ml/min. 10 ml fractions of the eluate were collected continually over 150 minutes. Afterwards, each fraction was submitted to ultrafiltration in Vivaspins 20[®] at 1000 x g. 8 ml of filtrate from each fraction were lyophilized and the dried polymers were redissolved in 4 ml MilliQ water. For comparison 5 ml of non-purified particle suspension was diluted to 10 ml with MilliQ water and also submitted to ultrafiltration.

Chitosan was quantified by mixing 0.25 ml of polymer solution with 0.25 ml 4 M Na-acetate buffer pH 5.5 and 0.5 ml of an acetic ninhydrin reagent (2 g ninhydrin, 0.08 g SnCl₂ x 2 H₂O, 50 ml 2- methoxy ethanol, 25 ml 4 M Na-acetate buffer pH 5.5, 25 ml water) [123]. The mixture was incubated at 100°C for 20 minutes on a boiling water bath. After cooling down to room temperature 200 µl samples were transferred to a 96 well plate and absorptions were measured at 550 nm with an UV/Vis reader (SLT Spectra, Tecan Deutschland GmbH, Crailsheim, Germany). Standards were in the range from 0.01 – 0.4 mg/ml chitosan.

The concentrations of PVA were determined by mixing 100 µl of sample with 480 µl water, 300 µl 3.8% (w/v) boric acid solution and 120 µl 0.05 M I₂/KI solution. The mixtures were incubated in a closed container over night at room temperature. Absorptions were measured at 650 nm using a Lambda 25 UV/Vis spectrophotometer from PerkinElmer (Wiesbaden, Germany). Standards were in the range of 0.025 – 0.25 mg/ml. If necessary, samples were diluted to fit the range of calibration. Every sample was measured in triplicate.

5.3 Results and Discussion

5.3.1 Selection of the mobile phase

Good results for the SEC of chitosan/PLGA nanoparticles were obtained with water and 0.1 mM HCl as mobile phase (Figure 5-2). Sharp and symmetric peaks appeared after about 50 minutes, which approximately corresponds to the dead volume of the stationary phase. The peak with water as mobile phase was wider than for 0.1 mM HCl. The isotonic sodium chloride solution proved to be unsuitable for SEC of chitosan/PLGA nanoparticles. At 50 minutes no peak appeared. Only after about 90 minutes a low and asymmetric peak was found. Initially the sodium chloride solution was favored as mobile phase because it was intended to compensate for changes in osmotic pressure in uptake experiments after mixing cell culture medium with nanoplexes.

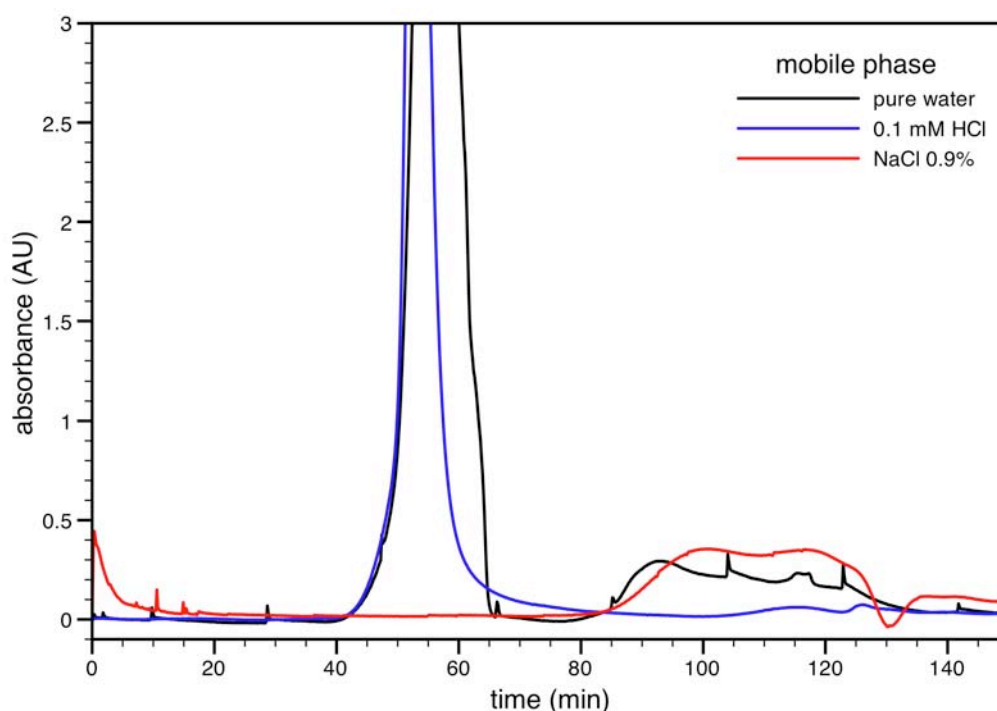


Figure 5-2: Comparison of SEC chromatograms with different mobile phases: pure MilliQ water (black), 0.1 mM HCl (blue) and 0.9% NaCl solution (red). Particles were 3CPNP.

Comparing the retention times for solutions of PVA and chitosan with water and 0.1 mM HCl there was no difference for the two mobile phases (Figure 5-3 A and B). The PVA peak was well separated from the particle peak with a maximum at about 120 minutes. Chitosan showed a broad flat peak between 55 and 110 minutes and partly co-eluted with particles.

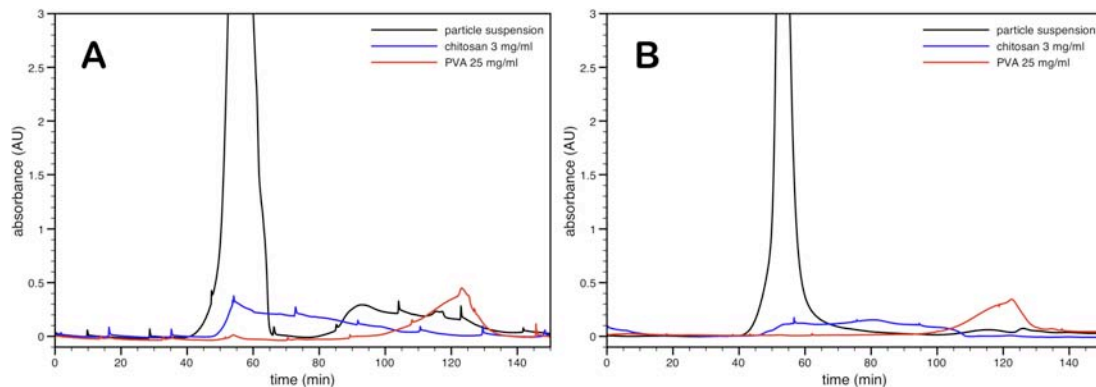


Figure 5-3: Chromatograms of particles and polymer solutions with MilliQ water (A) and 0.1 mM HCl (B) as mobile phase. PVA is well separated from the particle peaks while chitosan partly coelutes with particles. Retention times are comparable for both mobile phases.

From the data shown so far there seems to be no great difference between water and 0.1 mM HCl as a suitable mobile phase. However, the reason why 0.1 mM HCl was finally chosen for the purification of nanoparticle suspensions (see previous chapter) was the influence of the mobile phase on the purification efficiency of the low-chitosan preparation 05CPNP. Figure 5-4 A and B show the chromatograms from purifications of 7 ml 05CPNP suspensions with water and 0.1 mM HCl, respectively, as mobile phases. It can clearly be seen that the performance of water was very poor. The particle peak that was observed for 3CPNP between 40 and 60 minutes retention time is almost non-existent. In contrast, when 0.1 mM HCl was used a sharp peak was found.

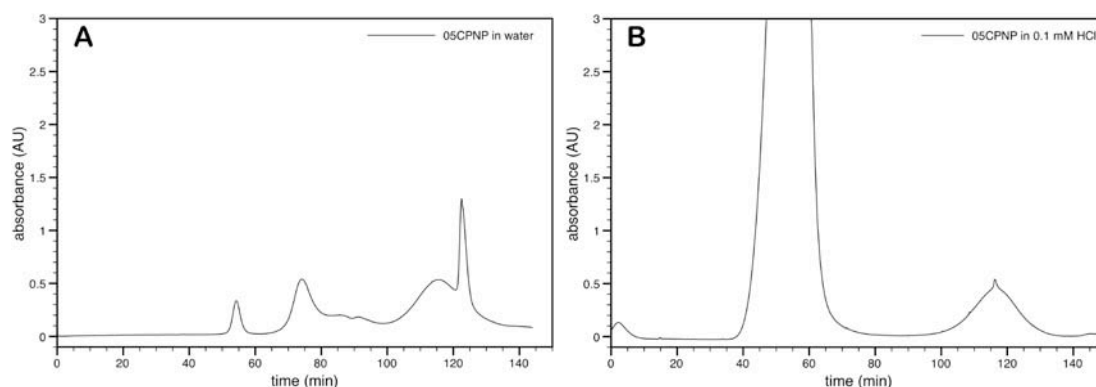


Figure 5-4: Chromatograms of 05CPNP eluted with MilliQ water (A) and 0.1 mM HCl (B). When MilliQ water was used as mobile phase only a very small particle peak was visible.

Interestingly, neither of the two mobile phases could be used for the purification of plain negatively charged PLGA nanoparticles. An experiment with a small column filled with Sephacryl 1000-SF (ca. 16 cm length x 1 cm diameter), which was used for quick evaluations of new experimental parameters, showed that no peak occurred for PLGA nanoparticles under both conditions, while 05CPNP could be eluted satisfactorily with 0.1 mM HCl (Figure 5-6).

These results strongly suggest that particle charge strongly influences elution and retention. Negatively charged PLGA nanoparticles seem to interact with the stationary phase and their strong retention might therefore not only be due to the principle of size exclusion while the positive charge of chitosan coated particles seems to prevent this interaction. Sephacryl S-1000 SF is a hydrophilic matrix composed of allyl dextran cross-linked with N,N'-methylene bisacrylamide (Figure 5-5). The hydroxyl groups of the dextran can form hydrogen bonds with the negatively charged carboxyl groups of the PLGA polymer. Since no elution of PLGA nanoparticles occurred under both neutral (water) and acidic (0.1 mM HCl) conditions, where most of the negative charges should be neutralized, a positive surface charge seems to be necessary for an early elution. As has been demonstrated with 05CPNP an acidification of the mobile phase results in a much better elution of particles.

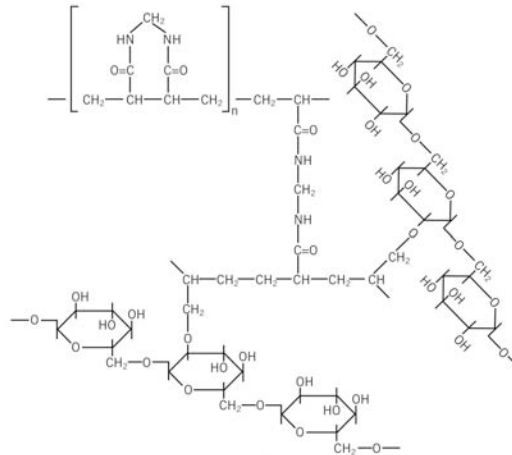


Figure 5-5: Structure of Sephacryl S-1000 SF (according to the manufacturer).

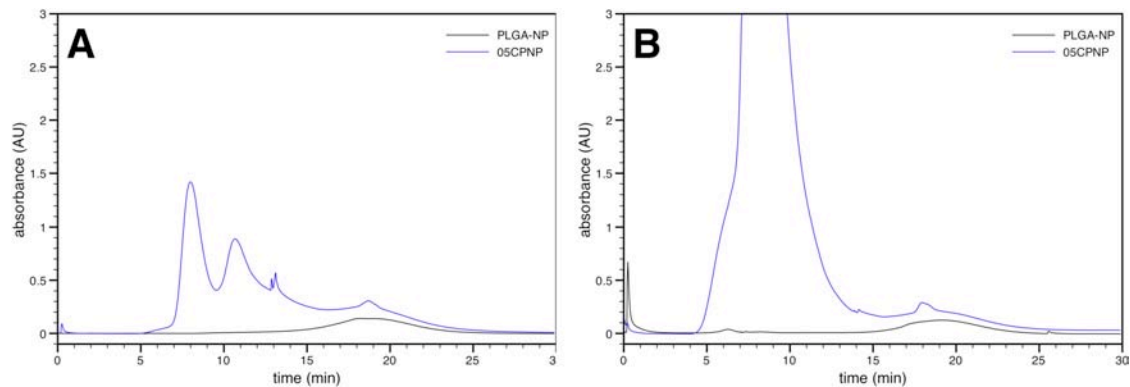


Figure 5-6: Comparison of chromatograms of PLGA nanoparticles and 05CPNP obtained with a short column filled with Sephacryl 1000-SF (16 cm length x 1 cm diameter). A: no particle peaks were obtained when MilliQ water was used as mobile phase; B: the use of 0.1 mM HCl as mobile phase resulted in a sharp peak for 05CPNP but not for PLGA nanoparticles.

5.3.2 Quantification of chitosan and PVA in different fractions

The quantification of chitosan and PVA in fractions that were continuously collected during the purification procedure of 3CPNP with either water or 0.1 mM HCl as mobile phase showed that chitosan must be almost quantitatively associated with the particles (Figure 5-7 A and B). No fraction from either mobile phase contained amounts of chitosan that were significantly different from a basal level that was measured for all fractions. Messai et al. have shown that chitosan efficiently adsorbs to the particle surface of pre-formed PLGA nanoparticles [124] and that it is also partly incorporated into particles prepared by the emulsification-diffusion-solvent

evaporation method employed here [125]. We were able to demonstrate in a previous study by zeta potential measurements that the surface of 3CPNP is not saturated with chitosan [109]. Hence, it is very likely that the larger fraction of chitosan is associated with the particles and that the amount of potentially unbound chitosan is below the detection limit of the assay that was used for these experiments.

In contrast, high amounts of PVA were found in fractions that were collected between retention times of 90 to 130 minutes (Figure 5-7). This result is in good agreement with the retention times found for PVA injected alone into the SEC system and detected by UV absorbance (Figure 5-3).

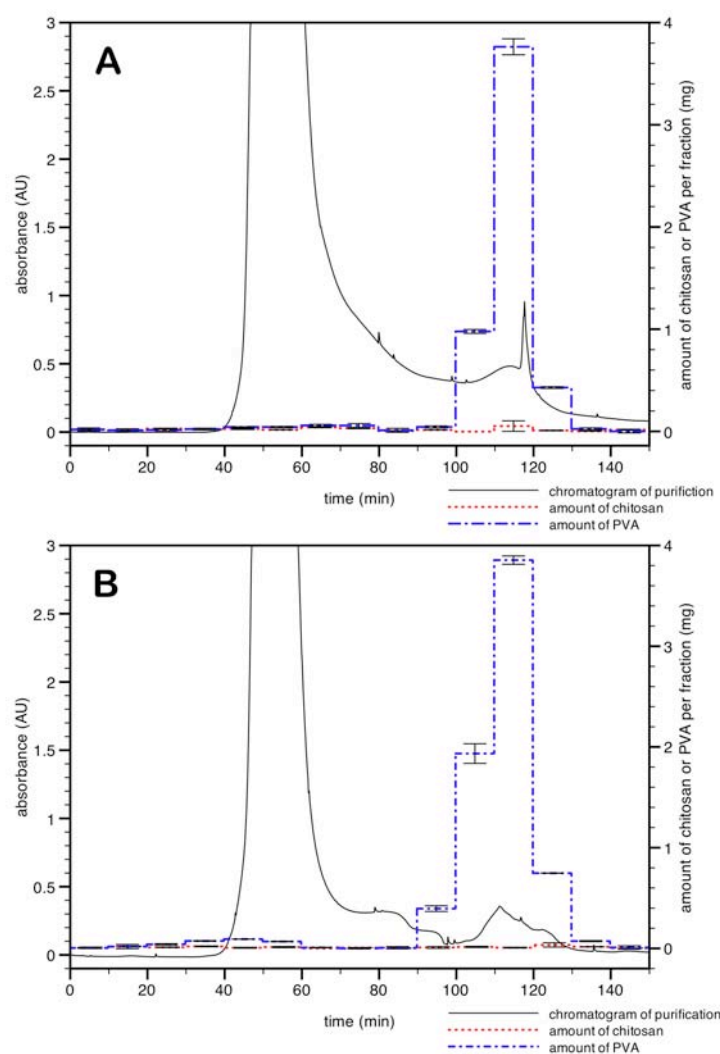


Figure 5-7: Quantification of chitosan and PVA from a 3CPNP particle suspension in fractions that were continually collected during the SEC run. A: water as mobile phase; B: 0.1 mM HCl as mobile phase. Chitosan (red dots) was below the quantification limit in all fractions. The increase in PVA in fractions 9 - 13 (= 90 – 130 minutes retention time) corresponded well to the peaks at 110 minutes and the chromatograms of PVA in Figure 5-3.

Calculating the total amount of PVA from all fractions showed that the purification with 0.1 mM HCl as mobile phase was the most efficient with about 7.5 mg compared to about 5.5 mg when water was used. Interestingly, the amount of PVA obtained from non-purified 3CPNP after a simple ultrafiltration was below 2 mg. Comparing these results with the expected amount of 12.5 mg showed that there must also be a high degree of association/ integration of PVA with/ into nanoparticles. The fact that the amounts of recovered PVA from purified particles are higher than for non-purified strongly indicates that PVA adsorbs to the surface and cannot be removed by a simple centrifugation step. During the purification procedure this adsorbed PVA is then washed off the surface because of the steady flow of mobile phase. The differences in PVA recovery with water and 0.1 mM HCl, respectively, as mobile phase are most probably due to the change in degree of protonation and conformation of surface polymers.

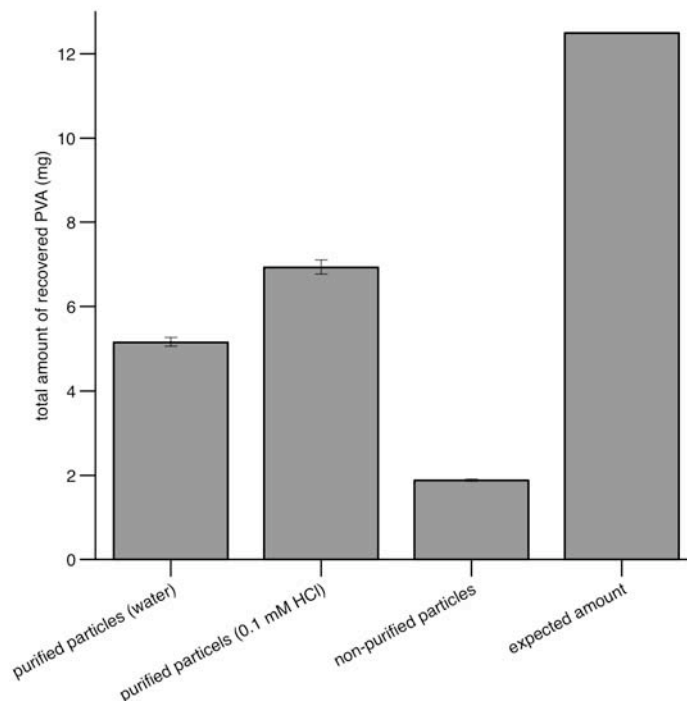


Figure 5-8: Comparison of PVA recovered from purified particles (with water and 0.1 mM HCl as mobile phase, respectively), non-purified particles after direct ultrafiltration and the amount expected in 5 ml particle suspension.

5.3.3 Purification of different nanoparticle preparations

The purification method was employed for all chitosan/PLGA nanoparticle preparations that were used for the experiments described in Chapter 4. As can be seen in Figure 5-9 the particle peaks broadened with increasing chitosan concentrations, which is most probably due to a more heterogeneous size distribution at higher chitosan contents (compare PDIs in Figure 4-1). Also, 3CPNP and 6CPNP showed a stronger tailing than 05CPNP and 1CPNP. Whether this tailing is due to subfractions of nanoparticles or unbound polymers, especially chitosan, could not be clarified during these studies. Regarding the results from the quantification experiments for free polymers (see above) the presence of unbound chitosan appears unlikely. Also, particle collection during the purifications was automatically initiated when peaks exceeded an absorbance value higher than 1.5 and stopped when absorbance dropped below this threshold again. So even if the tailing can be attributed to free chitosan, the amounts of the polymer within the particle fraction of 3CPNP and 6CPNP should be negligible concerning their influence on the results described in Chapter 4.

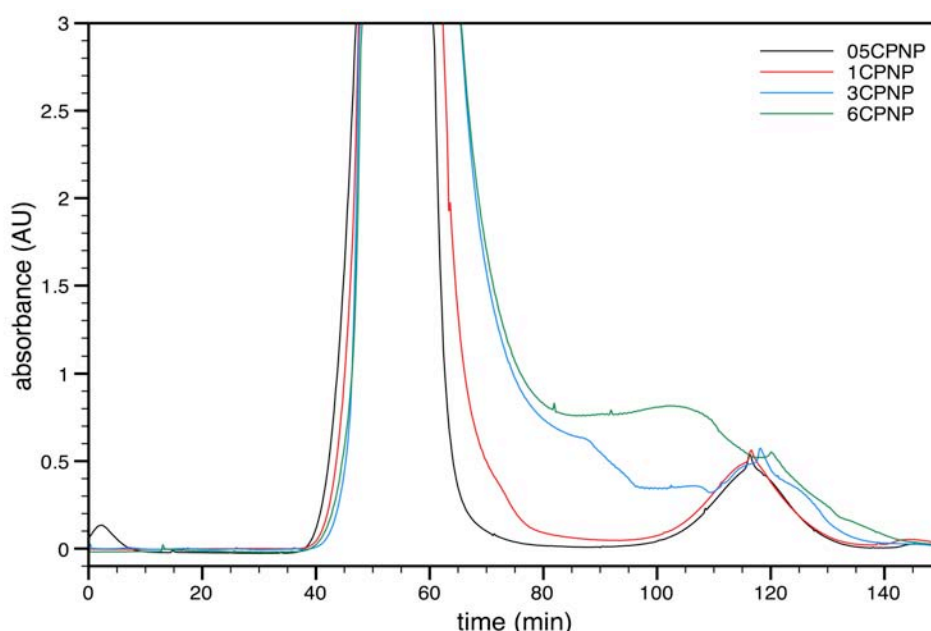


Figure 5-9: Comparison of chromatograms from different particle preparations after purification with 0.1 mM HCl as mobile phase. Peaks broaden with increasing chitosan content in particle suspensions. 05CPNP, 1CPNP, 3CPNP and 6CPNP = chitosan/PLGA nanoparticles prepared with 0.5, 1, 3 and 6 mg/ml chitosan, respectively.

5.3.4 Repeated injection of particle suspensions

Figure 5-10 shows the chromatogram from three successive injections of 3CPNP during a purification run. It can clearly be seen that the peaks appear in a reproducible way. This shows that an additional washing or re-equilibration of the column is not necessary after a purification step.

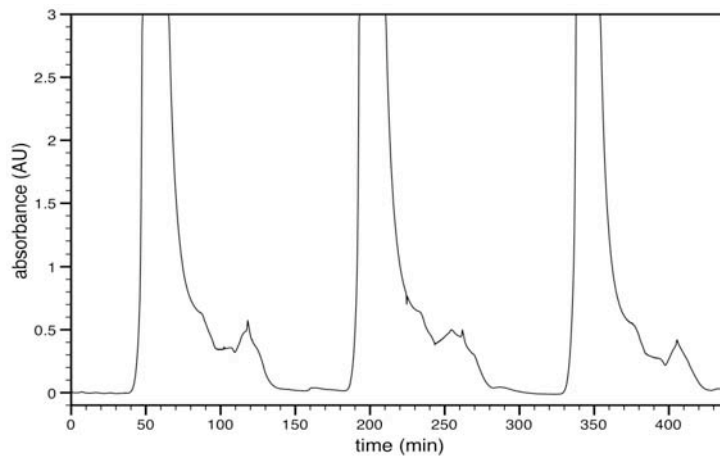


Figure 5-10: Successive injections for the purification of a larger volume of 3CPNP suspension. The peaks appear in a reproducible way.

5.4 Conclusion

We were able to demonstrate that preparative size exclusion chromatography can be used as an efficient method for the purification of chitosan/PLGA nanoparticles from excess PVA in particle suspensions. The advantage of this method is that it can handle larger volumes up to 50 ml in a semi-automated purification procedure. Interventions of the operator are limited to the filtration of particle suspensions prior to and their concentration after purification. However, as could be demonstrated with pure PLGA nanoparticles, this method is limited to the purification of cationic chitosan-coated PLGA nanoparticles.

Chapter 6

Hyaluronic Acid- Modified Liposomes for the Targeted Delivery of siRNA to CD44 Expressing Lung Cancer Cells

The data presented in this chapter has been accepted for publication as a research article in the journal *Oligonucleotides*:

Taetz, S., Bochot, A., Surace, C., Arpicco, S., Schaefer, U.F., Marsaud, V., Kerdine-Roemer, S., Lehr, C.-M., Fattal, E.

Hyaluronic acid- modified DOTAP/DOPE liposomes for the targeted delivery of anti-telomerase siRNA to CD44 expressing lung cancer cells. (2009) *Oligonucleotides*, accepted

Journal ISSN: 1545-4576

Journal Online ISSN: 1557-8526

Weblink: <http://www.liebertpub.com/products/product.aspx?pid=121>

6.1 Introduction

Since its discovery, the mechanism of RNA interference via small interfering RNA (siRNA) developed rapidly into a powerful tool in molecular biology for studying the downregulation of gene expression. Due to their high efficiency and selectivity siRNA became rapidly interesting for medical applications like the treatment of severe diseases such as cancer. However, siRNA faces the same obstacles for a successful application as other nucleotide-based therapeutics like plasmid DNA or antisense oligonucleotides, i.e. a poor uptake and stability in serum and the lack of selectivity for the target tissue [126-128]. Therefore, different carrier systems based on cationic liposomes or nanoparticles coupled with tumor-recognizing ligands (e.g. transferrin-coupled DOTAP/cholesterol liposomes [129], PEGylated polyethyleneimine nanoparticles conjugated with an RGD peptide [130] or a PEGylated liposome-polycation-DNA complex modified with anisamide [131]) were developed.

Our study concentrated on cationic hyaluronic acid (HA)-modified 1,2-dioleoyl-sn-glycero-3-phosphoethanolamine (DOPE) / 1,2-dioleoyl-3-trimethylammonium-propane (DOTAP) liposomes as carriers for the targeted delivery of a siRNA directed against the enzyme telomerase to lung cancer cells that over-express the HA binding receptor CD44. The discovery that many cancer types over-express this receptor led to the development of HA-drug conjugates [132, 133] and HA-modified drug carrier systems [133-139] that were able to target these cancer cells very specifically *in vitro* and *in vivo*. HA is an endogenous polymer of repeating disaccharide units of D-glucuronic acid and D-N-acetylglucosamine with a wide range of molecular weights. It is widely distributed in the mammalian body where it fulfills important mechanical or structural functions [140]. However, by interaction with its principal cell surface receptor CD44, a transmembrane glycoprotein that exists in different isoforms, it also plays an important role on cell – cell / cell – matrix interaction, cell adhesion and migration and signal transduction from the extracellular to the intracellular compartment [141-143].

Among the carrier systems mentioned above HA-modified liposomes were reported to be very efficient in the delivery of anti-cancer drugs like doxorubicin or mitomycin C [134, 138, 139]. In mouse tumor models these liposomes showed a much higher efficacy compared to non-modified liposomes and also a longer systemic circulation time, which was attributed to a “hydrophilic coat effect” of the hyaluronic acid. In terms of cytotoxicity, CD44-expressing cells were much more sensitive to the cytotoxic drugs encapsulated in HA-modified liposomes while toxicity for CD44 deficient cells was unchanged.

The target of the siRNA used in this study was a mRNA coding for the catalytic subunit of human telomerase hTERT (*human telomerase reverse transcriptase*). Telomerase plays an important role in cell immortalization and hence cancer development. Many types of cancer over-express this enzyme, which is inactive in normal somatic cells. Therefore, telomerase is believed to be a suitable target for the specific treatment of cancers that overexpress this enzyme [97].

The aim of our study was to prepare and characterize cationic HA-modified DOTAP/DOPE liposomes using a conjugate of HA and DOPE that has been successfully employed by Surace et al. [144] for the targeted delivery of plasmid DNA to CD44 expressing breast cancer cell lines. We investigated the influence of the modification with regard to the colloidal properties of the liposomes and lipoplexes, siRNA binding and protection, cytotoxicity, uptake into CD44 expressing and non-expressing cancer cells and the efficiency in telomerase inhibition in comparison with non-modified liposomes and the commercially available transfection reagent Lipofectamine 2000.

6.2 Materials and Methods

6.2.1 Materials

1,2-Dioleoyl-3-trimethylammonium-propane (DOTAP) chloride salt was obtained from Avanti Polar Lipids (Alabaster, AL, USA), 1,2-Dioleoyl-sn-glycero-3-phosphoethanolamine (DOPE) and 1-ethyl-3-[3-dimethyl]amiopropyl]carbodiimide hydrochloride (EDAC) from Sigma-Aldrich (Saint-Quentin Fallavier, France), Lipofectamine 2000 (LF 2000) from Invitrogen (Eragny sur Oise, France), high molecular weight hyaluronic acid (HA; 1,500,000 Da) from Fluka (Sigma Aldrich Chemie, Buchs, Switzerland).

6.2.2 siRNAs

SiRNA was obtained as single strands from Eurogentec (Seraing, Belgium). It was directed against a region between nucleotides 1523 and 1543 of the mRNA encoding for human telomerase reverse transcriptase (hTERT-mRNA; referred to transcript variant 1 of hTERT-mRNA; NCBI Entrez Nucleotide databank accession number: NM_198253). The sequence of the sense strand was 5'-GGAACACCAAGAAGUUCAUtt-3' and the sequence of the antisense strand was 5'-AUGAACUUCUUGGUGUUCctg-3', where tt and tg are deoxynucleotides, respectively (anti-hTERT siRNA). Annealing of single strands was achieved according to the manufacturer's recommendation in an annealing buffer containing 100 mM potassium acetate, 30 mM HEPES-KOH pH 7.4 and 2 mM magnesium acetate. A fluorescently labeled version of this siRNA was modified with 6-FAM at the 5'-ends. A nonsense siRNA was used as negative control.

6.2.3 Radiolabeling of siRNA

Radiolabeling of siRNA was performed by labeling the 5'-end of the sense strand with γ -³³P-ATP (111 TBq/mmol; Perkin-Elmer Life Science, Mechelen, Belgium) catalyzed by T4 polynucleotide kinase (New England Biolabs, Frankfurt am Main, Germany) according to the manufacturer's protocol. Labeled sense strand was purified by gel filtration using Bio-Gel P-6 Bio-Spin columns (Bio-Rad, Mitry Mory, France). Purity was proven by autoradiography

after gel electrophoresis of a sample on a 15% denaturing 7 M urea polyacrylamide gel. The labeled sense strand was annealed with the antisense strand as described above.

6.2.4 Conjugation of DOPE to hyaluronic acid

The conjugate of HA with DOPE was synthesized as reported by Surace et al. [144] based on a modified reaction described by Yerushalmi et al. [145]. In brief, 14 mg HA were dissolved in 5 ml water and preactivated for 2 hours at 37°C by incubation with 6 mg EDAC at pH 4 which was adjusted by titration with 0.1 N HCl. Afterwards, DOPE suspension (360 µg) was added to the HA solution and pH was adjusted to 8.6 with 0.1 M borate buffer. The reaction was proceeded for 24 hours at 37°C. The conjugate was purified by ultrafiltration using a membrane with a molecular weight cut off of 100,000 Da (Amicon Ultrafiltration, Millipore, Billerica, MA, USA), lyophilized and stored at -25°C until further use.

6.2.5 Preparation of liposomes

DOTAP/DOPE liposomes were prepared by the ethanol injection method [146, 147]. DOTAP and DOPE were dissolved separately in chloroform of analytical grade (Carlo Erba Reagents, Val de Reuil, France). The solutions were mixed at the required amounts at a molar ratio of 1:1 and chloroform was evaporated under vacuum. Lipid films were stored under nitrogen at -20 °C. For liposome preparation the lipid films were redissolved in absolute ethanol (analytical grade; Carlo Erba Reagents) at a concentration of 10 mg/ml. For liposome preparation 50 µl of ethanolic lipid solution were rapidly injected into 1 ml filtered (0.22 µm) MilliQ water (Millipore, Guyancourt, France) under stirring with a magnetic bar to obtain a final lipid concentration of 500 µg/ml. HA-modified liposomes were prepared by diluting an aqueous stock solution of the HA-DOPE conjugate (1 mg/ml) to different concentrations in filtered MilliQ water before injection. The content of HA-DOPE conjugate is expressed in percent as $w_{\text{HA-DOPE}}/w_{\text{total lipids}} \times 100$. For the removal of ethanol liposome suspensions were dialyzed against MilliQ water over night in Spectra/Por CE dialysis tubes with a molecular weight cut-off of 100,000 (Spectrum Laboratories, Inc., Rancho Dominguez, CA, USA).

6.2.6 Preparation of lipoplexes

Lipoplexes were prepared at different +/- ratios by rapidly injecting different volumes of 500 µg/ml liposome suspension in 2.5 µM siRNA solution. Suspensions were mixed thoroughly by pipetting up and down and incubated for 15 minutes at room temperature. Afterwards they were diluted with the respective medium to a final siRNA concentration of 100 nM.

6.2.7 Characterization of liposomes and lipoplexes

Liposomes and lipoplexes were characterized with regard to their size, size distribution and surface charge by dynamic light scattering and zeta potential measurement using a ZetaSizer Nano ZS (Malvern Instruments, Worcestershire, United Kingdom). Measurements were performed with 50 µg/ml total lipids in filtered MilliQ water at 25°C using the standard settings of the instrument. Results are expressed as z-average (size), polydispersity index (PDI; size distribution) and zeta potential values (surface charge). All measurements were at least performed in triplicate.

6.2.8 Binding efficiencies of lipoplexes

Lipoplexes were prepared with radiolabeled siRNA at different +/- ratios as described above. The final siRNA concentration was 100 nM. Suspensions were submitted to ultracentrifugation using an Optima[®] LE-80K ultracentrifuge equipped with a type 50.4 Ti rotor (both Beckman-Coulter, Villepinte, France) at an average centrifugal force of 130,000 x g at 4°C under vacuum for 1 hour. Binding efficiencies were determined by comparing the specific radioactivities of samples from the supernatant with samples taken before the centrifugation step. Experiments were performed in triplicate in MilliQ water and serum-free RPMI 1640 with GlutaMAX[™] cell culture medium (Gibco, Paisley, UK).

6.2.9 Colloidal stability of liposomes and lipoplexes in serum-free cell culture medium

Lipoplexes of non-modified and 15% HA-DOPE at charge ratios of +/- 2:1 and +/- 8:1 were prepared as described above and diluted to 50 µg/ml total lipids with serum-free RPMI cell culture medium. Suspensions with liposomes only

were prepared accordingly but without siRNA. Changes in size were measured with the ZetaSizer Nano ZS (Malvern Instruments) at 25°C for two hours. The accuracy of measurements was verified by mixing each suspension thoroughly after each measurement to avoid false results that might be due to a quick sedimentation of agglomerates. All experiments were performed in triplicate.

6.2.10 Protection of siRNA in lipoplexes in the presence of RNase V1

Lipoplexes of non-modified and 15% HA-DOPE liposomes at +/- ratios of 2:1 and 8:1 were prepared as described above with radiolabeled siRNA. Suspensions were diluted to 100 nM siRNA with RNase V1 (Ambion Applies Biosystems, Courtaboeuf, France) containing reaction buffer to a final ratio of 0.1 U RNase V1 per 100 ng siRNA. Samples were incubated at 37°C for 30 minutes. Afterwards RNase V1 activity was inhibited and lipoplexes were lysed using a mixture of 10% (w/v) sodium dodecylsulfate (SDS) and 5% (v/v) Triton X-100. All samples were kept on ice. After centrifugation at 10,000 x g and 4°C for 5 minutes samples from the supernatant were run on a 12% non-denaturing polyacrylamide gel. The radiolabeled siRNA was visualized after gel drying by autoradiography. To verify that no degradation occurs during sample processing after incubation a post-incubation degradation control was included in the experiment: RNase V1 and siRNA were incubated separately and mixed only after addition of the SDS/Triton X-100 mixture to the RNase V1 solution.

6.2.11 Stability of siRNA and lipoplexes in the presence of human serum

Lipoplexes of non-modified and 15% HA-DOPE liposomes at +/- ratios of 2:1 and 8:1 were prepared as described above with radiolabeled siRNA. Suspensions were diluted to 100 nM siRNA with RPMI cell culture medium (Gibco) containing different concentrations of human serum (Sigma, St. Quentin Fallavier, France) and incubated for 30 minutes at 37°C. Afterwards samples were run on a 12% non-denaturing polyacrylamide gel

without further lysis of lipoplexes. The radiolabeled siRNA was visualized after gel drying by autoradiography.

6.2.12 Cell cultures and cell culture conditions

The human lung cancer cell lines A549 and Calu-3 were obtained from American Type Culture Collection (ATCC-nos.: CCL-185 and HTB-55, respectively; Manassas, VA, USA). A549 cells were grown in RPMI 1640 with GlutaMAX™ cell culture medium (Gibco) supplemented with 10% fetal calf serum (Lonza, Verviers, Belgium) and 100 U penicillin/ 100 U streptomycin (Lonza). Calu-3 cells were grown in RPMI 1640 with GlutaMAX™ cell culture medium (Gibco) supplemented with 10% fetal calf serum (Lonza), 1 mM sodium pyruvate (Sigma) and 100 U penicillin/ 100 U streptomycin (Lonza). Cells were grown on 80 cm² polystyrene cell culture flasks in an incubator at 37°C, 5% CO₂ and 90% humidity. Media were changed every other day and cells were subcultured once a week.

6.2.13 Western blot analysis for the CD44 receptor

Cells were washed with cold PBS and detached from the culture flask bottom by scrapping. Lysis was done after pelleting with a lysis buffer containing 1% Triton X-100, 50 mM Tris pH7.4, 150 mM sodium chloride, 1% deoxycholic acid, 0.1% sodium dodecylsulfate (SDS) and protease inhibitor cocktail (Complete Mini®, Roche, Mannheim, Germany). Protein concentrations were determined with the Bio-Rad Protein Assay (Bio-Rad Laboratories Inc., Marnes-la-Coquette, France). Protein samples were separated on a 8% denaturing SDS polyacrylamide gel and electroblotted to a Immobilo-P transfer membrane (Millipore). After blocking with 2% (w/v) bovine serum albumin (BSA) in 0.1% (v/v) Tween 20/PBS CD44 was detected by incubating the membrane with a 1:20 dilution of the monoclonal antibody Hermes I in 2% BSA/Tween 20/PBS (rat IgG2a; Department of Pathology, Stanford University, School of Medicine, Stanford, CA, USA) at 4°C over night. Hermes I was detected the next day using Vectastain Elite ABC kit anti-rat rabbit antibody IgG (Vector Laboratories, Inc., Berlingame, CA, USA) and Western Blotting Luminol Reagent (Santa Cruz Biotechnology, Inc., Santa

Cruz, CA, USA) on Amersham Hyperfilm ECL (GE Healthcare Ltd., Buckinghamshire, UK).

6.2.14 Cytotoxicity tests

For cytotoxicity tests A549 and Calu-3 cells were seeded on 96 flat bottom well plates at a density of 5,000 and 25,000 cells per well, respectively. Cells were incubated with different concentrations of non-modified and 15% HA-DOPE liposomes and their lipoplexes at +/- ratios of 2:1 and 8:1 in serum-free RPMI cell culture medium without antibiotics for 3 hours under cell culture conditions. Lipoplexes of +/- 2:1 and +/- 8:1 corresponded to about 10 µg/ml and 50 µg/ml liposomes, respectively. Lipofectamine 2000 (LF 2000) was used for comparison. The required amount of LF 2000 was adjusted for the transfection of 100 nM siRNA as recommended by the manufacturer. This amount was regarded to be equal to the amount of lipids that is used for lipoplexes at the +/- ratio of 8:1. The different LF 2000 concentrations were adjusted accordingly.

MTT cytotoxicity test

Cells were incubated with different liposome concentrations and lipoplexes 1 day after seeding. After three hours of incubation, the suspensions were replaced by the respective normal cell culture medium (see above). Cells were allowed to grow for another 48 hours under cell culture conditions. Afterwards 25 µl of a 5 mg/ml 3-(4,5-dimethyl-2-thiazolyl)-2,5-diphenyl-2H-tetrazolium bromide (MTT; Sigma) in PBS were added to each well. Medium was removed after 2 hours of incubation under cell culture conditions and 200 µl of pure dimethylsulfoxide (DMSO) was added to each well for cell lysis and dissolution of formazan crystals. Absorbance was measured at 570 nm. Metabolic activity as a measure for cell survival was calculated in comparison with non-treated cells according to the formula: $(\text{mean abs}_{\text{treated cells}} / \text{mean abs}_{\text{non-treated cells}}) \times 100$. Each concentration was measured in triplicate.

LDH cytotoxicity test

Cells were incubated with different liposome concentrations and lipoplexes 3 days after seeding. Liposome and lipoplex suspensions were prepared as described above but with phenol red- free RPMI cell culture medium (Gibco). After incubation for 3 hours, 100 μ l samples from the supernatant of each well were taken and analyzed for LDH activity according to the manufacturer's instructions of the Cytotoxicity Detection Kit^{Plus} (LDH) (Roche Diagnostics, Meylan, France). Absorbance was measured at 492 nm. LDH release from cells incubated with liposomes or lipoplexes was referred to the spontaneous LDH release from non-treated cells. Background controls for non-specific reactions included all incubation media without cells. Each concentration was measured in triplicates.

6.2.15 Flow cytometry

A549 and Calu-3 cells were seeded on 6 well plates at a density of 250,000 cells per well. Lipoplexes were prepared as described above with FAM-labeled siRNA in serum-free RPMI cell culture medium. Cells were incubated with Lipoplexes of non-modified and 15% HA-DOPE liposomes at +/- ratios of 2:1 and 8:1 at a final siRNA concentration of 100 nM for three hours. Afterwards they were washed once with calcium and magnesium containing PBS (Ca/Mg-PBS; Gibco). Cells were detached with trypsin/EDTA (Lonza). After inactivation of trypsin with serum-free RPMI cell culture medium without phenol red, cells were pelleted and resuspended in PBS without calcium and magnesium. To be able to distinguish between internalized and extracellularly bound lipoplexes, half of the cells were incubated with 0.4% trypan blue in Ca/Mg-PBS and washed twice with normal PBS prior to trypsinization. Fluorescence intensities were measured using a FACSCalibur flow cytometer from Becton Dickinson (BD) Biosciences (Franklin Lakes, NJ USA) using the software CellQuestTM Pro Version 4.02 (BD Biosciences). The instrument was adjusted using non-treated cells.

6.2.16 Determination of telomerase activity by the TRAP-qPCR assay

A549 cells were seeded at a density of 100,000 and Calu-3 cells at 500,000 cells per well on 6 well plates. One day after seeding cells were incubated with lipoplexes of non-modified and 15% HA-DOPE liposomes at +/- ratios of 2:1 and 8:1 in serum-free RPMI cell culture medium at a final siRNA concentration of 100 nM for 3 hours. LF 2000 was used for comparison. Non-specific effects were examined with liposomes without siRNA and lipoplexes prepared with a nonsense sequence.

Following incubation the medium was exchanged with normal cell culture medium and cells were kept under cell culture condition for further 48 hours. Afterwards, cells were washed once with cold PBS (4°C), detached by scrapping, pelleted and lysed in a non-denaturing lysis buffer (10 mM Tris-HCl pH 7.4, 1 mM magnesium chloride, 1 mM EGTA, 5 mM beta-mercaptoethanol, 1% Triton X100 and 10% glycerol). Protein concentrations were determined with the Bio-Rad Protein Assay (Bio-Rad Laboratories Inc., Marnes-la-Coquette, France). Telomerase activity was determined by the *telomeric repeat amplification protocol* (TRAP assay) adapted for quantitative real-time PCR (qPCR) [148, 149]. The protein concentration of each sample was adjusted to 100 ng/μl with lysis buffer. The TRAP-qPCR was performed with a LightCycler 1.5 (Roche Diagnostics, Meylan, France) using the LightCycler FastStart DNA Master^{Plus} SYBR Green I kit (Roche Diagnostics, Meylan, France). The master mix was prepared according to the manufactures protocol. Each sample (20 μl) contained 100 ng of protein extract, 100 ng TS primer (5'-AATCCGTCGAGCAGAGTT-3') and 50 ng ACX primer (5'-GCGCGGCTTACCCTTACCCTTACCCTAACC-3') [99] (both from Eurogentec, Seraing, Belgium). The TRAP-qPCR was run under the following conditions: 30 minutes at 30°C for the elongation of TS primer by telomerase; 10 minutes at 95°C for the inactivation of telomerase and activation of polymerase; amplification of telomerase products during 40 cycles of 10 seconds at 95°C, 5 seconds at 62°C, 15 seconds at 72°C, final cooling step for 30 seconds at 40°C. Fluorescence intensities were acquired during amplification after each cycle. A calibration line was established by

serial dilution of protein extract from non-treated cells. The slope and y-intercept were determined after plotting \log_{10} amount protein versus the cycle threshold value. Relative telomerase activity (RTA) was determined according to equation 6-1:

$$RTA = 10^{\frac{Ct_{\text{sample}} - Y_{\text{intercept}}}{\text{slope}}} \quad \text{Equation 6-1}$$

where Ct_{sample} is the cycle threshold value for the respective sample and $Y_{\text{intercept}}$ and slope are calculated from regression line [149]. RTAs of cells incubated with liposomes or lipoplexes were normalized to those of non-treated cells.

6.3 Results

6.3.1 Properties of liposomes and lipoplexes

The ethanol injection method allowed the preparation of nano-sized HA-DOPE modified liposomes with a conjugate content of up to 20% ($W_{\text{HA-DOPE}}/W_{\text{total lipids}}$). The sizes ranged from 110 to 160 nm. There was a gradual increase in size with increasing HA-DOPE content (Figure 6-1 A). Higher amounts of the conjugate resulted in the formation of agglomerates (data not shown). The size distribution of non-modified liposomes and liposomes with lower amounts of HA-DOPE (1 – 10%) was rather heterogeneous which was reflected by polydispersity indices (PDIs) of around 0.4. This improved to values around 0.25 when 15 and 20% of conjugate were used (data not shown). Zeta potential values (ZPs) were in the range of +50 to +60 mV for all liposome preparations at pH-values of about 6.5 (Figure 6-1 A).

The formation of complexes with siRNA at +/- charge ratios of 1:1 to 8:1 resulted in lipoplexes with sizes around and below 200 nm and PDIs smaller than 0.25 for most of the preparations (Figure 6-1 B – F). The ZP measurements of lipoplexes clearly revealed the differences in the degree of liposome modifications. At the +/- ratio of 1:1 all lipoplexes were strongly negatively charged (≤ -40 mV; B). However, at +/- 2:1 lipoplexes prepared with non-modified liposomes were positively charged while ZPs decreased with increasing amounts of HA-DOPE for lipoplexes with modified liposomes (Figure 6-1 C). This trend was also observed at higher +/- ratios (Figure 6-1 D-F). The pH values for lipoplexes were in the range of 6.5 to 7.0.

Agglomeration occurred for lipoplexes in the range of -20 to +20 mV, demonstrating that electrostatic repulsion in this range is not sufficient to maintain the colloidal stability. 20% HA-DOPE liposomes were identified as a critical formulation because they formed agglomerates at +/- charge ratios of 4:1, 6:1 and 8:1.

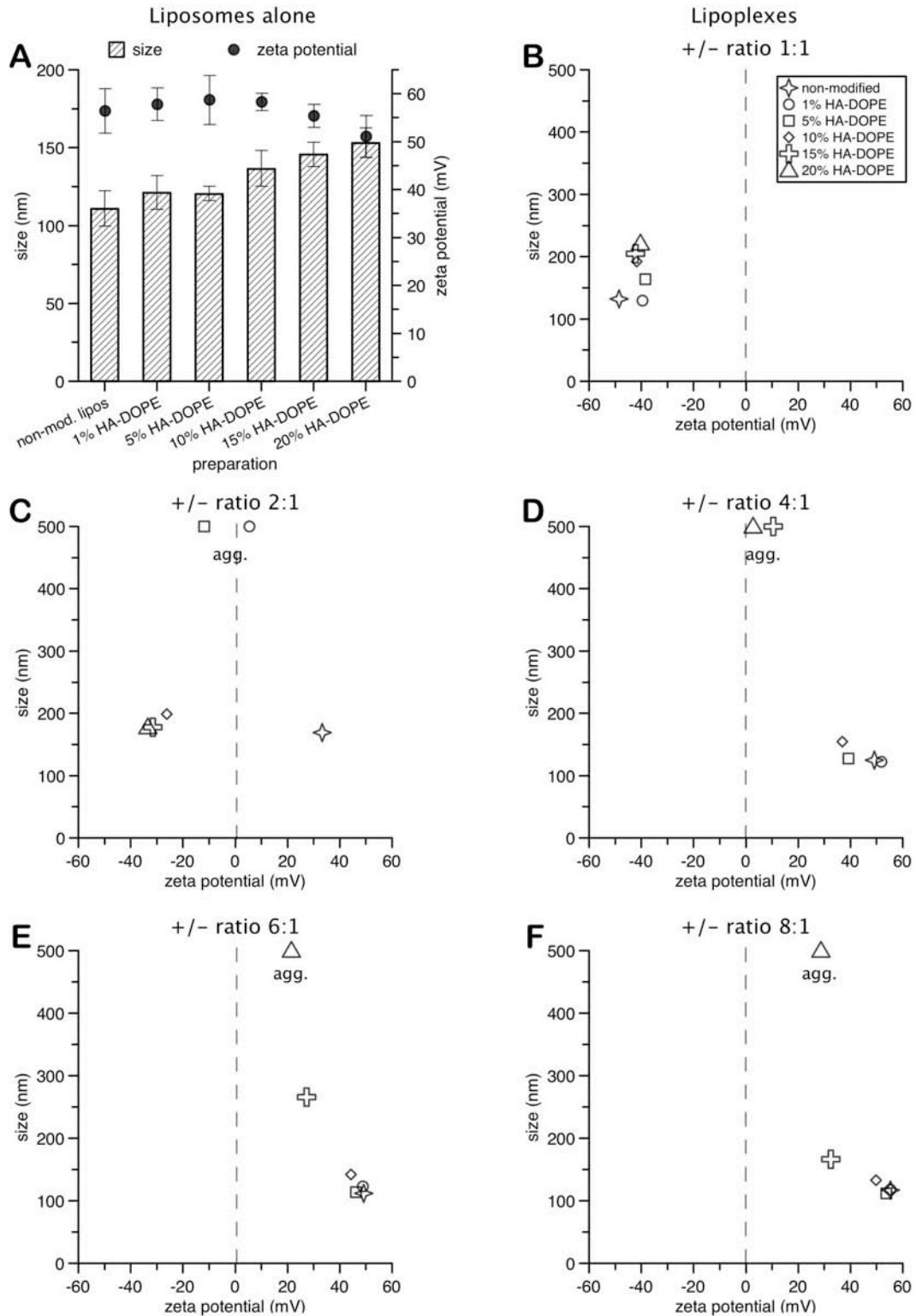


Figure 6-1: Properties of HA-modified DOTAP/DOPE liposomes prepared by the ethanol injection method. A: liposomes alone with different amounts of HA-DOPE conjugate (expressed in percent as $(W_{\text{HA-DOPE conjugate}}/W_{\text{total lipids}}) \times 100$) B-F: lipoplexes at varying +/- ratios with siRNA. Sizes for lipoplexes that formed agglomerates (agg.) were reduced to 500 nm for better representation. $n \geq 3$

6.3.2 Binding of siRNA

The binding experiments revealed that the modification of DOTAP/DOPE liposomes with the HA-DOPE conjugate did not compromise the binding efficiency of siRNA. In water as dispersion medium, almost complete binding was achieved at the +/- ratio of 2:1 for all preparations (Figure 6-2). Interestingly, with increasing +/- ratios the binding efficiency remained constant for lipoplexes prepared with higher HA-DOPE content, while it decreased slightly for non-modified liposomes and those with a lower HA-DOPE content.

As partial conclusion from the results of liposome and lipoplex characterization and binding experiments, 15% HA-DOPE liposomes and the corresponding lipoplex preparations at charge ratios of +/- 2:1 (negative ZP) and +/- 8:1 (positive ZP) were chosen for further experiments. Non-modified liposomes and their respective lipoplexes were used for comparison.

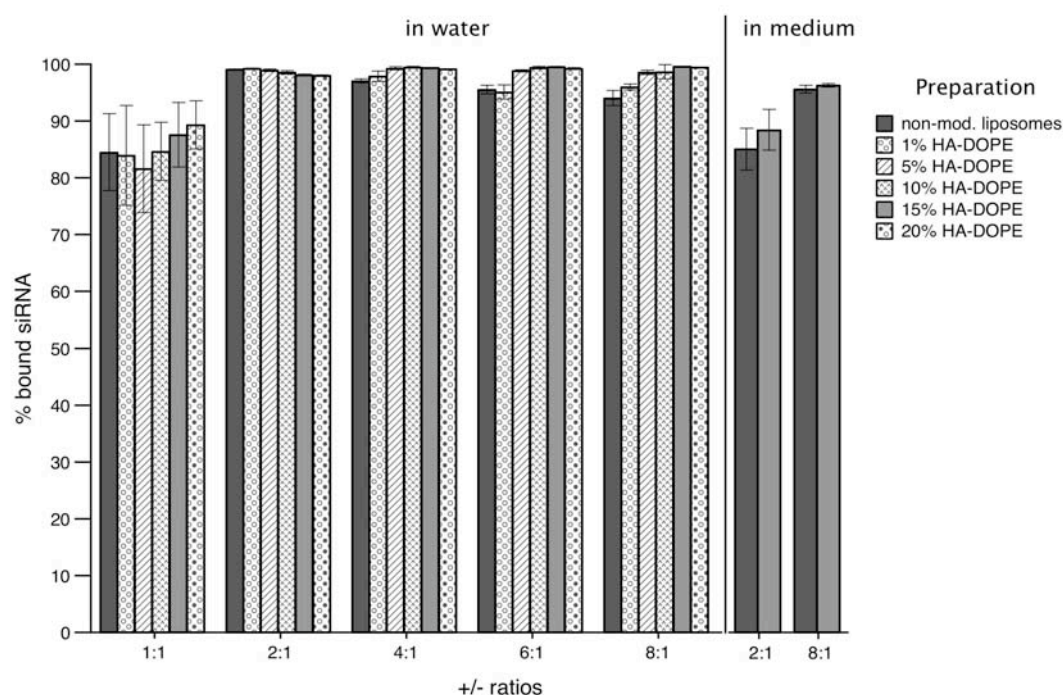


Figure 6-2: Binding efficiency of siRNA at different +/- ratios with different liposome preparations. The modification of DOTAP/DOPE liposomes with HA-DOPE does not influence the binding of siRNA. In serum-free cell culture medium binding of siRNA with HA-modified liposomes is even higher than with non-modified liposomes. n = 3

6.3.3 Influence of cell culture medium as dispersion medium

All results reported so far were obtained from dispersions in MilliQ water. However, since cell culture experiments (see below) were performed in serum-free RPMI cell culture medium, its influence on liposome/lipoplex properties was further tested.

As can be seen in Figure 6-2 the binding efficiency of HA-modified liposomes in cell culture medium decreased to about 85% for +/- 2:1 lipoplexes but was almost the same as in water for +/- 8:1. Again, in comparison with the non-modified liposomes, the modification did not compromise the binding efficiency.

The effect of cell culture medium on the colloidal stability of liposomes and lipoplexes was tested in repeated measurements by dynamic light scattering over two hours. HA-modified liposomes alone agglomerated upon dispersion in cell culture medium almost immediately. In contrast, non-modified liposomes alone seemed to be more stable (Figure 6-3 A). However, in complex with siRNA at either ratio (+/- 2:1 and +/- 8:1) the HA-modified liposomes were stable over the time of the measurement while lipoplexes of non-modified liposomes quickly formed agglomerates (Figure 6-3 B).

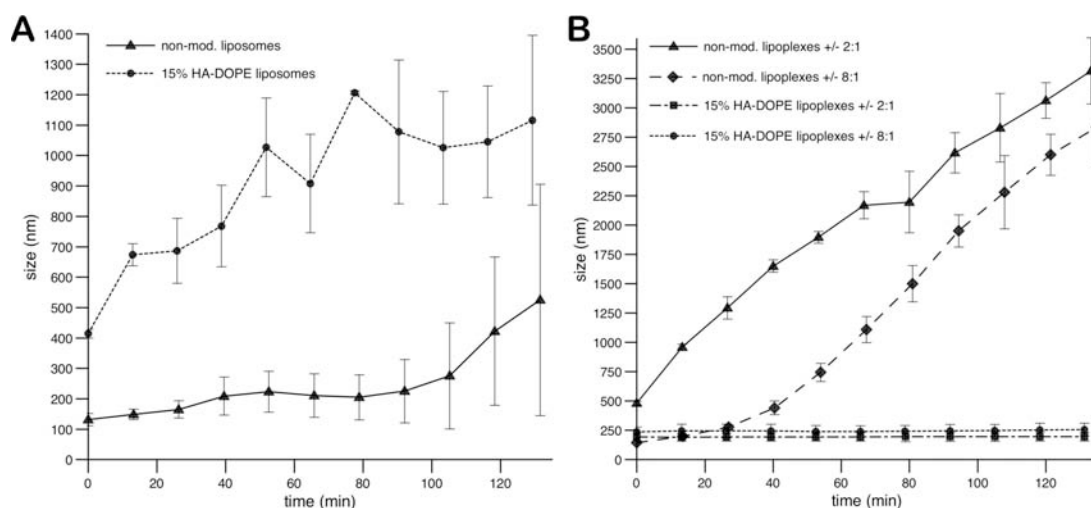


Figure 6-3 Colloidal stability of non-modified and HA-modified liposomes (A) and lipoplexes at +/- ratios of 2:1 and 8:1 (B) in serum-free cell culture medium measured over 2 hours by dynamic light scattering. Although non-modified liposomes appeared to be more stable than HA-modified liposomes both preparations tend to form agglomerates over time (A). In complex with siRNA HA-modified liposomes were stable while lipoplexes of non-modified liposomes quickly formed agglomerates. n = 3

6.3.4 Protection of siRNA in lipoplexes

The exposure of lipoplexes to double-stranded RNA-degrading RNase V1 revealed that the modification with HA-DOPE does not affect the protection of siRNA from degradation compared to non-modified lipoplexes (Figure 6-4 A). Only a slight degradation occurred for both preparations at either charge ratio (+/- 2:1 and +/- 8:1) and was not shown to be related to the treatment of lipoplexes after incubation.

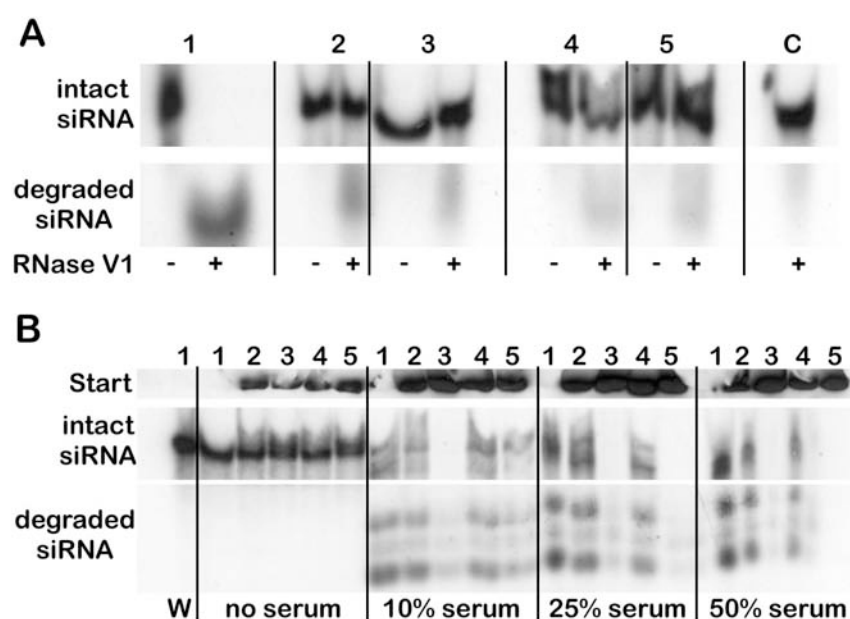


Figure 6-4: Protection of siRNA in complexes with either non-modified or HA-modified liposomes from degradation by RNase V1 (A) and human serum at different concentrations in cell culture medium (B). 1 = siRNA only; 2 = non-modified lipoplexes +/- 2:1; 3 = non-modified lipoplexes +/- 8:1; 4 = HA-modified lipoplexes +/- 2:1; 5 = HA-modified lipoplexes +/- 8:1; C = post-incubation degradation control; W = siRNA in water. (A) The modification with HA-DOPE did not compromise the siRNA stability in complex. (B) The presence of serum even at high concentrations does not seem to influence the stability of lipoplexes prepared at a charge ratio of +/-8:1 of either non-modified or HA-modified lipoplexes.

A similar result was observed when lipoplexes were dispersed in cell culture medium with different concentrations of human serum. In this experiment lipoplexes were not lysed after incubation but submitted directly to electrophoresis. This allows to investigate both the lipoplex stability and the protection of siRNA from degradation in the presence of human serum. The results show that even in 50% of serum lipoplex stability, and hence siRNA degradation, of HA-modified lipoplexes was comparable to non-modified

lipoplexes (Figure 6-4 B). One remarkable result was that lipoplexes at charge ratios of +/- 8:1 appeared to be significantly more stable in the presence of serum than under serum-free conditions. Using fluorescence microscopy and lipoplexes prepared with fluoresceinamine (FAM) - labeled siRNA at a charge ratio of +/- 8:1, it was verified that this observation was not due to the formation of large agglomerates that hinder a migration of siRNA. In contrast, non-modified lipoplexes in serum-free medium formed agglomerates that could be observed by microscopy (200 x magnification) while HA-modified did not, which is in good agreement with the size measurements shown in Figure 6-3. However, in medium containing 50% of human serum no agglomeration for both kinds of preparations was observed (data not shown).

6.3.5 Uptake of lipoplexes

The uptake of lipoplexes prepared with fluorescently labeled siRNA into lung cancer cells was studied by flow cytometry with CD44-expressing A549 and CD44-deficient Calu-3 cells (western blot in Figure 6-5 A). As can be seen in Figure 6-5 B ii and iv, the incubation of CD44-positive A549 cells with HA-modified lipoplexes resulted in a shift to higher fluorescence values indicating a higher cell association and uptake compared to non-modified lipoplexes. Interestingly, the uptake was higher at the +/- ratio of 2:1 than at 8:1. In contrast, such clear differences were not found for CD44-negative Calu-3 cells (Figure 6-5 B vi and vii). The incubation with LF2000 and siRNA resulted in a very heterogeneous uptake profile in both cell lines ranging from a population of non-transfected cells to cells that showed a very high uptake. Uptake profiles for cells treated with non-modified liposomes at either ratio were comparable, which demonstrates that the maximal transfection efficiency for this preparation is already reached at the +/- 2:1 ratio.

Cells incubated with trypan blue prior to measurements to quench extracellular fluorescence showed comparable profiles that slightly shifted to lower intensity values (data not shown).

Transfection was much more efficient in A549 cells than in Calu-3 cells for both HA-modified and non-modified liposomes. As can be seen in Table 6-1 after quenching the extracellular fluorescence with trypan blue at least 75% of A549 cell took up the lipoplexes. Best results were obtained with HA-modified

lipoplexes at a +/- ratio of 2:1. In Calu-3 cells the highest uptake was also found for this preparation. But only about 30% of cells took up the lipoplexes.

Table 6-1: Quantification of cells transfected with lipoplexes (compare Figure 6-5 B). Trypan blue – quenching was used to distinguish internalized lipoplexes from extracellularly bound lipoplexes. Uptake was considerably higher in A549 cells compared to Calu-3 cells. Best results were obtained for HA-modified liposomes at a +/- ratio of 2:1 with siRNA for both cell lines.

| cells treated with: | % of cells above fluorescence threshold | | | |
|--------------------------------|---|----------------------------|--------|----------------------------|
| | A549 | | Calu-3 | |
| | normal | incubated with trypan blue | normal | incubated with trypan blue |
| non-treated cells | 0.4 | - | 0.8 | - |
| siRNA only | 0.5 | - | 0.5 | - |
| non-modified liposomes +/- 2:1 | 92.0 | 76.5 | 37.8 | 20.4 |
| non-modified liposomes +/- 8:1 | 92.6 | 73.8 | 35.8 | 18.5 |
| 15% HA-DOPE liposomes +/- 2:1 | 99.5 | 92.6 | 47.9 | 30.1 |
| 15% HA-DOPE liposomes +/- 8:1 | 96.7 | 79.7 | 34.2 | 15.1 |
| Lipofectamine 2000 | 70.2 | 72.7 | 40.9 | 33.8 |

Next page:

Figure 6-5: A: Detection of the CD44 receptor in A549 and Calu-3 lung cancer cells by western blot with the monoclonal antibody Hermes-I. A549 cells are CD44 positive while Calu-3 cells do not express this receptor. The faint band in the Calu-3 lane at about 72 kDa is due to a non-specific binding of the secondary antibody. B: Results from flow cytometry with A549 (i – iv) and Calu-3 (v – viii) cells after incubation with lipoplexes prepared with FAM-labeled siRNA. In contrast to CD44-negative Calu-3 cells (vi and vii) CD44-positive A549 cells showed a clear shift to higher fluorescence intensities for the HA-modified liposomes (ii and iii). Incubation with Lipofectamine 2000 resulted in a very heterogeneous distribution for both cells cell lines (iv and viii). Incubation with siRNA alone did not increase the fluorescence intensities (i and v).

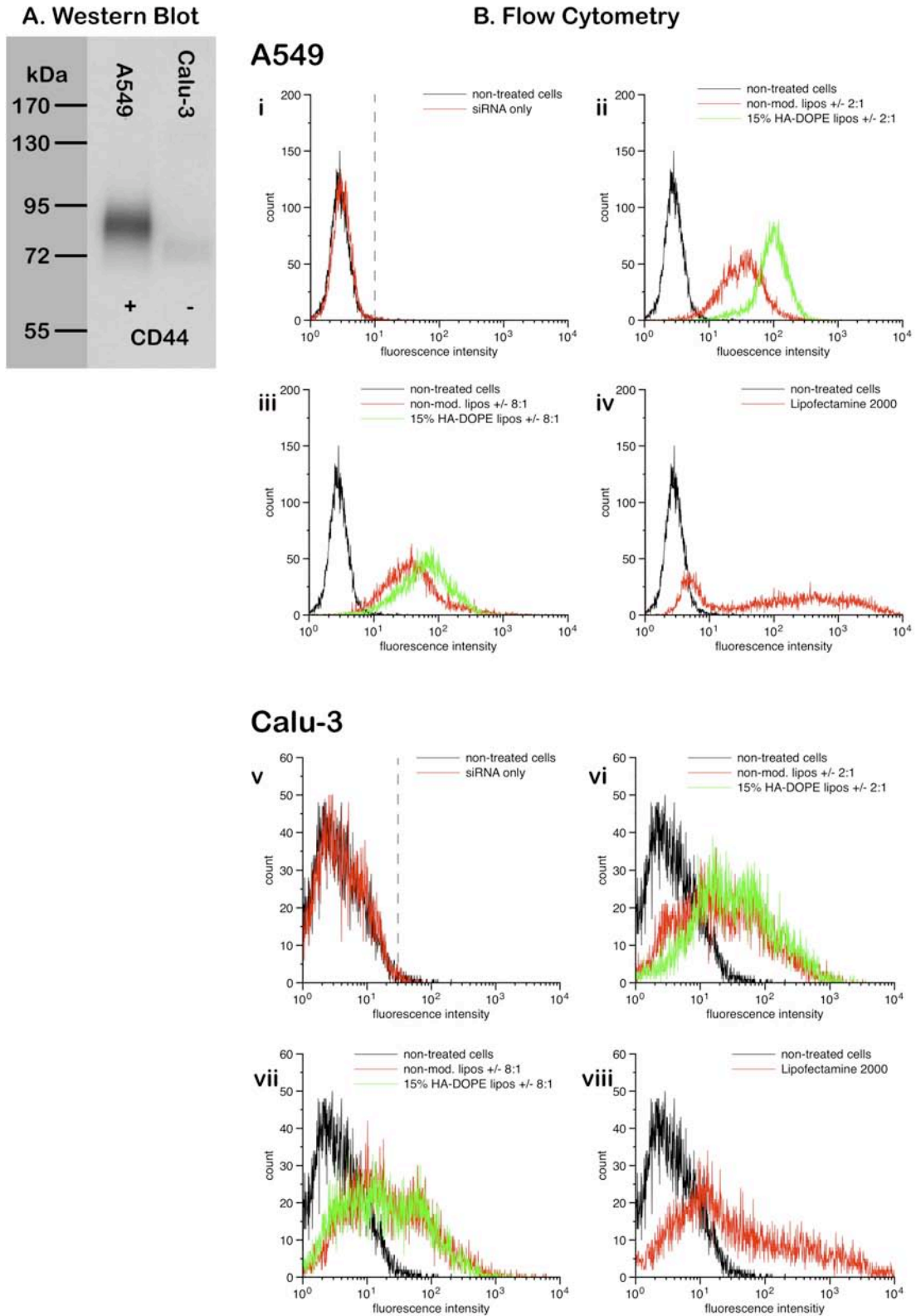


Figure 6-5

6.3.6 Cytotoxicity of liposomes and lipoplexes

In the MTT (for metabolic activity) and LDH (for membrane integrity) assay both liposomal preparations without siRNA showed a cytotoxic effect in both cell lines at higher concentrations while LF 2000 only slightly reduced metabolic activity (MTT) and did not influence membrane permeability (LDH). In the LDH assay the treatment with 15% HA-DOPE liposomes resulted in a higher release of LDH than with non-modified liposomes. A549 cells appeared to be more sensitive than Calu-3 cells (Figure 6-6). However, no cytotoxicity was observed with lipoplexes of non-modified and HA-modified liposomes at +/- ratios of 2:1 (approx. 10 $\mu\text{g/ml}$ lipids) and 8:1 (approx. 50 $\mu\text{g/ml}$ lipids) as well as for LF 2000 + siRNA for both cell lines (Figure 6-6 B).

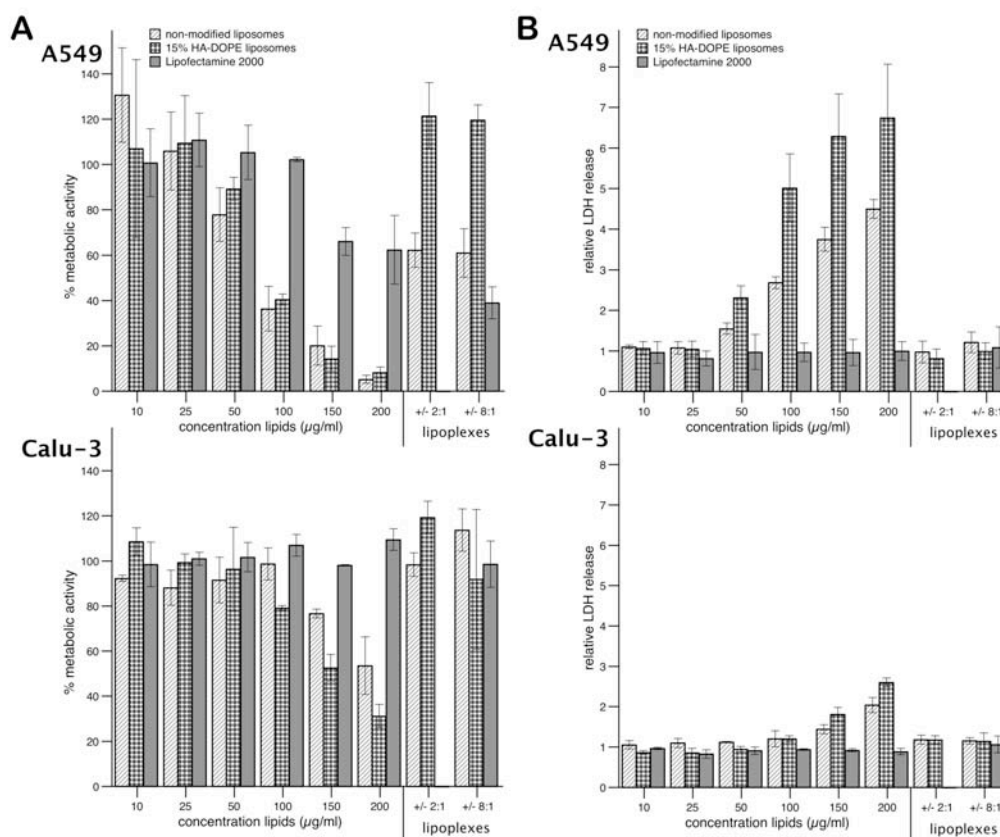


Figure 6-6: A: MTT cytotoxicity assay with A549 and Calu-3 cells after treatment with non-modified and HA-modified liposomes and lipoplexes in comparison with Lipofectamine 2000. Measured values were referred to cells that were treated under the same conditions but without liposomes or lipoplexes. B: LDH release from A549 and Calu-3 cells after treatment with non-modified and HA-modified liposomes and lipoplexes in comparison with Lipofectamine 2000. The values are referred to the LDH release of cells that were treated under the same conditions but without liposomes or lipoplexes. Lipoplexes of +/- 2:1 and +/- 8:1 corresponded to about 10 $\mu\text{g/ml}$ and 50 $\mu\text{g/ml}$ liposomes, respectively. Each concentration was measured in triplicate.

In the MTT assay the same was true for Calu-3 cells. However, for A549 cells there was a big difference between lipoplexes prepared with HA-modified liposomes and non-modified liposomes. The HA-modified lipoplexes were not cytotoxic while the treatment with non-modified lipoplexes resulted in a decrease of mitochondrial activity of about 40% for each preparation. When LF 2000 + siRNA was used an even stronger reduction in mitochondrial activity of about 60% was observed (Figure 6-6 A).

6.3.7 Inhibition of telomerase activity

In A549 cells telomerase activity was successfully inhibited after a treatment with lipoplexes prepared with anti-hTERT siRNA (Figure 6-7). The reduction in telomerase activity was stronger for lipoplexes prepared at a +/- ratio of 8:1 (15 – 20% of control) than 2:1 (25 – 30% of control). However, there was no longer any difference between HA-modified liposomes and non-modified liposomes. Also, treatment with lipoplexes containing the nonsense sequence and liposomes without siRNA at a concentration corresponding to the +/- ratio 8:1 still exhibited a moderate (60-80% of control) reduction of telomerase activity. This effect was even more pronounced for preparations with non-modified liposomes. When LF 2000 was used as transfection reagent inhibition of telomerase activity by anti-hTERT siRNA was even stronger (about 10% of control), suggesting a significant contribution of direct inhibitory effects exerted by the transfection reagents.

Calu-3 cells appeared to be less sensitive to the treatment with lipoplexes. Higher inhibition was obtained with HA-modified lipoplexes at a +/- ratio of 8:1. However, telomerase activity was only reduced by maximally 50%. Non-specific reduction of telomerase activity was also found for liposomes alone and lipoplexes with nonsense siRNA, but they were less pronounced compared to A549 cells. Again, however, transfection with LF 2000 resulted in a similar, but still only moderate reduction in telomerase activity for no, non-sense and anti-hTERT siRNA.

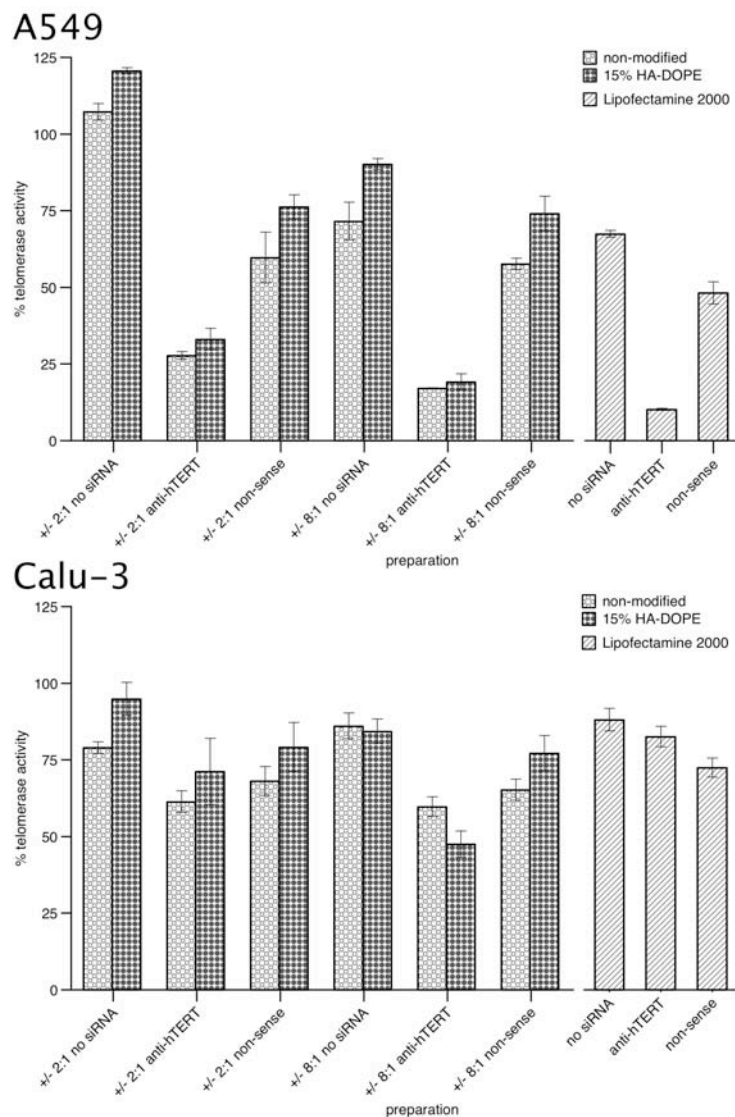


Figure 6-7: Inhibition of telomerase activity in A549 and Calu-3 cells determined by the TRAP-qPCR assay after treatment with non-modified and HA-modified liposomes in comparison with Lipofectamine 2000. “+/- x:1 no siRNA” = cells were incubated with liposomes alone at the same concentrations used for the respective lipoplexes.

6.4 Discussion

In our study, we demonstrated that cationic DOTAP/DOPE liposomes in a size range below 200 nm modified with the large negatively charged polysaccharide hyaluronic acid (HA) can be successfully prepared by the ethanol injection method. Surprisingly, zeta potential values of the HA-modified liposomes alone (Figure 6-1 A) did not differ from non-modified liposomes. Since the pK_a -value for HA is about 3.0 and the pH-values for the different preparations were in the range of pH 6.5, a decrease of ZPs was expected with increasing concentrations of the HA-DOPE conjugate because of the negatively charged carboxylic groups of the polymer. However, the differences became apparent when complexes with siRNA were formed. The gradual decrease in zeta potential values for lipoplexes with +/- ratios $\geq 2:1$ with increasing amounts of the HA-DOPE conjugate demonstrates that HA is present on the surface (Figure 6-1 B – F).

Although hyaluronic acid is a large negatively charged polymer that might interact with the positively charged liposomes, the modification was shown to have no negative influence on such important properties like the binding of siRNA, its protection in the complex from degradation by RNase V1 or complex stability in the presence of serum. On the contrary, binding of siRNA and especially the colloidal stability of HA-modified lipoplexes in serum-free cell culture medium were considerably improved compared to non-modified liposomes. These results indicate that i) despite the modification with HA the cationic liposome surface is still fully accessible for siRNA, which results in the high complexation efficiency and protection and ii) the modification might be regarded as a stabilizer comparable to polyethylene glycol [150]. Peer and Margalit reported in their experiments with neutral liposomes a prolonged systemic circulation in mice, which they attributed to a “hydrophilic coat effect” due to the modification with HA [138, 139]. The presence of the negatively charged polymer on the liposomes might reduce the interaction with counter ions from the solution. Additionally, a steric repulsion between the vesicles seems to be very likely.

The modification also improved the cytotoxic profile of DOTAP/DOPE liposomes. As could be shown in the MTT and LDH assay with A549 cells,

lipoplexes prepared with HA-modified liposomes strongly reduced the toxicity compared to lipoplexes prepared with non-modified liposomes or LF 2000. Since HA is endogenous to the human body and therefore fully biocompatible, the presence of the polymer on the liposome surface might avoid the direct contact of the cationic liposome with the negatively charged cell surface and hence reduce their cytotoxic potential.

In our uptake studies we were able to demonstrate that the HA-modified liposomes considerably improve the uptake of lipoplexes into CD44-expressing A549 lung cancer cells compared to non-modified liposomes and that this difference was not found for CD44-deficient Calu-3 cells (Figure 6-5 B and Table 6-1). However, the uptake of HA-modified lipoplexes in A549 cells at the +/- ratio 8:1 was lower compared to +/- 2:1. In the latter case, the loading of siRNA per lipoplex was reduced because of the increased liposome concentration. Zeta potential measurements demonstrated that at +/- 2:1 the surface charge of lipoplexes is strongly negative (about -35 mV), indicating an excess of siRNA on the liposomal surface (Figure 6-1 C). At +/- 8:1 the surface charge is positive (about +25 mV), which shows that the liposome surface is not fully covered. Since the siRNA concentration was kept constant at 100 nM throughout the experiments, the +/- 8:1 preparation contained an increased concentration of lipoplexes with reduced siRNA content compared to the +/- 2:1 preparation with higher siRNA loading and lower total lipoplex concentration. Given that both preparations were used under the same conditions and that the uptake of HA-modified liposomes via interaction with the CD44 receptor is a saturable process [151], +/- 2:1 complexes were more efficient.

The results from the uptake studies, however, were not consistent with the measurements of the TRAP assay. Although telomerase activity was reduced in transfected A549 cells, and to a lesser extent also in Calu-3 cells, the expected difference between non-modified and HA-modified liposomes was not found. This result can most likely be attributed to some non-specific effects exerted by the lipidic transfection agents and the siRNA concentration used in these experiments. Since siRNA has been reported to be able to induce concentration-dependent activation of the interferon system [152] and

changes in the levels of non-targeted proteins [153, 154], especially in combination with cationic lipids [155], further studies regarding the use of cationic lipids for siRNA-transfection and gene silencing as well as an optimization of siRNA concentrations appear to be necessary.

6.5 Conclusion

We successfully prepared cationic DOTAP/DOPE liposomes modified with the large negatively charged polymer hyaluronic acid as nano-sized carriers for siRNA. This modification did not influence the capability of the DOTAP/DOPE liposomes to efficiently bind and protect siRNA. On the contrary, it significantly improved such important properties like stability in high-salt cell culture medium, reduced cytotoxicity and allowed the targeting of CD44-expressing lung cancer cells. Our results are an encouraging starting point for further *in vitro* and *in vivo* studies where the efficacy of this system will be tested.

Chapter 7

Summary and Outlook

The work presented in this thesis dealt with three different strategies for the treatment of non-small lung cancer by telomerase inhibition. In this context important steps in the preclinical evaluation of new drug substances and drug carrier systems based on cell culture models were investigated.

The results from the characterization of the potential drug candidate and model substance BRACO19 are important for future studies like animal experiments or clinical trials. Problems like therapy failure that might occur during such investigations can be explained by the findings described in this dissertation. Our results demonstrate that an appropriate formulation is required for BRACO19 and related substances to improve its permeability across biological barriers and prevent the rapid decomposition in physiological media.

The oligonucleotide-based telomerase inhibitors 2OMR and siRNA are promising candidates that might be used in drugs of the next generation. The strategies presented here for their (targeted) delivery into lung cancer cells are an important step towards their therapeutic application. Since the problems of their poor uptake and stability have been extensively described in the literature, our studies were focused on the characterization and optimization of potential carrier systems to improve the uptake and reduce inactivation due to an early degradation.

The work with the cationic chitosan/PLGA nanoparticles as a carrier system for 2OMR demonstrated the necessity for an accurate optimization of the particle formulation for further studies. Particle properties strongly depended on the ratio of the anionic polymer PLGA and the cationic polymer chitosan. The simple criterion “cationic particles improve the uptake” is not applicable for the combination of these two polymers. As could be shown by the experiments a certain amount of chitosan in the particle preparation is required for the optimal uptake of 2OMR into lung cancer cells. Since an increase of the chitosan concentration did not result in further uptake improvements the optimum formulation for chitosan/PLGA nanoparticles has

been found. Another important result of these experiments was that nanoplexes were almost only taken up by lung cancer cells and not by non-malignant cells although they were not specifically modified for the targeting of this cell type. This indicates that a treatment with nanoplexes of 2OMR and chitosan/PLGA nanoparticles does not affect healthy cells. Together with the specific inhibition of telomerase activity, side effects in such a therapeutic approach should be reduced to a minimum.

The strategy of a targeted uptake of nano-sized surface modified carrier systems into lung cancer cells was employed for the delivery of siRNA via hyaluronic acid modified cationic liposomes. This targeting was intended to improve the uptake of lipoplexes into tumors that overexpress the CD44 receptor. In these studies the optimization of the liposome formulation was also an important prerequisite for further experiments. Since the large polymer hyaluronic acid is negatively charged under physiological conditions, one major concern was that the preparation of modified cationic liposomes is not easily feasible. However, the binding and stability experiments revealed that these concerns were not justified. The modified liposomes were as efficient in binding siRNA as non-modified liposomes and showed an improved stability in physiological cell culture medium and a reduced cytotoxicity. The aim of targeting CD44-expressing lung cancer cells was successfully accomplished. The results from these experiments are a good basis for further studies with this kind of modified siRNA carrier system.

In summary, the inhibition of telomerase activity via siRNA appears to be the most promising strategy for the treatment of non-small cell lung cancer by telomerase inhibition.

BRACO19's mechanism, the induction of dysfunctional telomeres by G-quadruplex stabilization, is a new and interesting approach for cancer treatment. However, it has to be considered that this molecule and other substances with the same mechanism are not selective for telomeres but can also bind to other guanine-rich regions of the DNA that form G-quadruplex structures [52]. Even if the problems described in Chapters 2 and 3 might be solved by suitable formulations of the drug, the effects of binding to DNA

regions other than the telomeres still needs to be addressed to learn more about possible unwanted side effects. Also, it still needs to be clarified how the induced telomere dysfunction affects healthy cell types like stem cells or germ cells that have a high proliferative capacity.

The strategy of telomerase inhibition using oligonucleotides should be preferred because they allow the design of highly specific and selective sequences. Therefore, unwanted side effects can most probably be reduced to a minimum. Regarding the work described here, siRNA is the more promising approach because of two reasons:

- i) siRNA does not have to enter the nucleus of a cell to be effective but only needs to be released into the cytoplasm after transfection. In comparison with 2OMR, which has to reach the nucleus to bind to the template region of hTR, siRNA has one barrier less to overcome.
- ii) siRNA is effective at much lower concentrations than 2OMR. The factor for the experiments presented here is 40 (4 μ M 2OMR vs. 0.1 μ M siRNA). Considering values from literature, this factor could even be increased to 100 to 1000 with a highly specific sequence under optimized conditions. With regard to a possible therapeutic application in humans a treatment with siRNA would require less oligonucleotides and less of the carrier system than 2OMR.

For the continuation of this project with siRNA as an inhibitor of telomerase activity the following steps need to be considered.

First a screening of several siRNA sequences is necessary to identify the one with the highest selectivity and inhibitory potential, followed by an optimization of siRNA concentrations to avoid non-specific effects on protein biosynthesis as observed in these experiments. Afterwards the carrier system has to be optimized to reduce non-specific effects on telomerase activity and to avoid cytotoxicity at higher concentrations. The carrier should also be suitable for an application as an aerosol, to fulfill the final aim of the project of an inhalative treatment of lung cancer.

Additionally, the test systems have to be changed or extended. In all parts of this thesis *in vitro* cell culture models, either derived from tumor or non-malignant tissue, were an essential part to investigate the new strategies.

Cell culture models are suitable systems to provide information about processes that occur at the site of interest. However, it has to be kept in mind that these models are only able to simulate the situation when the drug substance or the drug loaded carrier system reached the target tissue. To learn more about the distribution, uptake or efficacy of the preparation, further studies should include more complex models like the isolated perfused lung or animal experiments.

Chapter 8

Zusammenfassung und Ausblick

Im Rahmen der hier vorgestellten Doktorarbeit wurden drei verschiedene Strategien zur Therapie des nicht-kleinzelligen Lungenkarzinoms mit Telomeraseinhibitoren behandelt. Hierbei wurden wichtige Phasen der präklinischen Erprobung neuer Wirkstoffe und Wirkstoffträgersysteme auf Basis von Zellkulturmodellen durchschritten.

Die Daten, die bei der Charakterisierung des potentiellen Wirkstoffkandidaten, bzw. der Modellsubstanz, BRACO19 erhalten wurden stellen wichtige Informationen für das weitere Verständnis von eventuelle auftretenden Problemen in späteren Phasen seiner Erprobung in Tierversuchen oder klinischen Studien dar. Die vorliegenden Ergebnisse zeigen deutlich, dass für eine weitere Erprobung von BRACO19 oder von seiner Struktur abgeleiteten Substanzen der Einfluss der Formulierung eine große Rolle spielen wird, um die aufgezeigten Probleme der sehr schlechten Permeabilität und raschen Zersetzung zu umgehen.

Die Oligonukleotid-basierten Wirkstoffe 2OMR und siRNA sind viel versprechende Substanzen, die in Arzneimitteln der nächsten Generation zur Anwendung kommen könnten. Die hier vorgestellten Strategien zur Verbesserung der (gezielten) Aufnahme in Lungenkrebszellen sind ein wichtiger Schritt in Richtung ihrer therapeutischen Verwendung. Da die Problematik mit Hinblick auf ihre Aufnahme- und Stabilitätseigenschaften bereits ausführlich in der Literatur beschrieben wurde, lag der Schwerpunkt der hier vorgestellten Arbeiten auf der Charakterisierung und Optimierung möglicher Trägersysteme, die die Aufnahme in die Zellen verbessern und eine frühzeitige Inaktivierung durch Abbau verhindern.

Bei den kationischen Chitosan/PLGA Nanopartikeln als Trägersystem für die 2OMR zeigte sich die Notwendigkeit einer sorgfältigen Optimierung der Formulierung für weitere Arbeiten. Die Kombination aus dem anionischen Polymer PLGA und dem kationischen Polymer Chitosan führt je nach Mengenverhältnissen zu Partikeln mit unterschiedlichen Eigenschaften. Das einfache Kriterium "kationische Partikel führen zur Aufnahmeverbesserung" ist

bei der Verwendung dieser zwei Polymersorten nicht ausreichend. Wie die Versuche zeigten, ist zunächst eine gewisse Menge an Chitosan in der Partikelzubereitung notwendig, um eine größtmögliche Aufnahme von 2OMR in Lungenkrebszellen zu erreichen. Das eine weitere Steigerung der Chitosankonzentration jedoch nicht in einer weiteren Aufnahmeerhöhung resultiert, deutet darauf hin, dass die optimale Partikelformulierung gefunden wurde. Ein weiteres wichtiges Ergebnis dieser Versuche war die Erkenntnis, dass die Nanoplexe fast nur in Krebszellen aufgenommen wurden, obwohl sie nicht speziell modifiziert waren, um diesem Zelltyp gezielt zu erkennen. Dies lässt darauf schließen, dass normale, gesunde Zellen von einer Behandlung mit den 2OMR-Chitosan/PLGA-Nanoplexten wenig beeinflusst werden dürften und Nebenwirkungen, die durch die Verwendung des spezifischen Telomeraseinhibitors bereits gering sein sollten, auf ein Minimum reduziert werden.

Die Strategie der gezielten Aufnahme nanoskaliger oberflächenmodifizierter Trägersysteme in Krebszellen wurde für das Delivery von siRNA mittels Hyaluronsäure modifizierten kationischen Liposomen verfolgt. Dieses Targeting soll eine verstärkte Aufnahme der Lipoplexe in Tumore gewährleisten, die den CD44-Rezeptor überexprimieren. Somit können höhere Wirkstoffkonzentrationen im erkrankten Gewebe erreicht werden und gesundes Gewebe bleibt möglichst von der Therapie verschont. Auch hier war die Optimierung der Formulierung zunächst eine wichtige Voraussetzung für weitere Versuche. Da Hyaluronsäure unter physiologischen Bedingungen ein negativ geladenes Polymer ist, war zu befürchten, dass eine Modifizierung der verwendeten kationischen DOTAP/DOPE Liposomen nicht ohne weiteres möglich ist. Die Bindungs- und Stabilitätsversuche ergaben aber, dass diese Befürchtungen unbegründet waren. Die modifizierten Liposomen zeigten die gleiche Bindungseffizienz wie nicht modifizierte Liposomen und wiesen darüber hinaus eine höhere Stabilität in physiologischen Zellkulturmedium auf sowie eine reduzierte Zytotoxizität. Das Ziel der verbesserten Aufnahmeeffizienz von siRNA in CD44-überexprimierende Lungenkrebszellen durch die Modifizierung der Liposomen mit Hyaluronsäure wurde erreicht und muss nun in weiteren Versuchen hinsichtlich seiner Wirkung getestet werden.

Zusammenfassend betrachtet stellt die siRNA-basierte Strategie zur Behandlung von Lunkenkrebs mit Telomeraseinhibitoren die vielversprechendste Variante dar.

Der Wirkmechanismus von BRACO19 über die G-Quadruplexstabilisierung bis zu dysfunktionalen Telomeren ist ein neuer interessanter Weg zur Behandlung von Krebs. Allerdings muss man hierbei beachten, dass diese Substanzklasse nicht selektiv auf Telomere ausgerichtet ist, sondern auch in anderen Guanin-reichen Regionen der DNA, in denen sich G-Quadruplex-Strukturen bilden können [52], binden kann. Selbst wenn die in Kapitel 2 und 3 beschriebenen Probleme durch galenischen Maßnahmen umgangen werden, gilt es abzuklären, in wie weit diese Vorgehensweise durch Bindung des Wirkstoffs in anderen Bereichen als Telomere zu eventuellen unerwünschten Wirkungen führt. Außerdem muss gründlich untersucht werden, wie sich die herbeigeführte Telomerdysfunktion auf andere häufig teilende Zelltypen, wie zum Beispiel Keimzellen oder Stammzellen, auswirkt. Die Strategie der Telomerasehemmung mit Hilfe von Oligonukleotiden ist vorzuziehen, weil durch eine sorgfältige Sequenzauswahl eine hohe Spezifität und Selektivität gegeben ist, was die Gefahr von möglichen unerwünschten Wirkungen stark reduziert. Die siRNA ist dabei aus folgenden zwei Gründen der aussichtsreichere Kandidat:

- i) siRNA muss zur Entfaltung ihrer Wirkung nicht in den Zellkern gelangen. Die Freisetzung aus dem Trägersystem in das Zytoplasma ist hierfür ausreichend. Damit besteht für diese Vorgehensweise eine Barriere weniger im Vergleich zur 2OMR, die bis in den Zellkern gelangen muss, um an die Template Region der hTR zu binden.
- ii) siRNA ist in wesentlich geringeren Konzentrationen wirksam als 2OMR. Der Faktor in den hier durchgeführten Versuchen beträgt 40 (4 μM 2OMR vs. 0,1 μM siRNA). Ein Blick in die Literatur zeigt, dass dieser Faktor bei Auswahl einer hochspezifischen Sequenz unter optimierten Bedingungen auf 100 bis 1000 erhöht werden kann. Im Umkehrschluss bedeutet dies mit Hinblick auf eine mögliche Anwendung am Menschen, dass geringere Konzentrationen an siRNA und Trägersystem zum Einsatz kommen würden.

Zur Fortführung des Projektes mit siRNA zur Telomerasehemmung sollte in folgenden Schritten vorgegangen werden.

Zuerst ist ein Screening weiterer siRNA Sequenzen nötig um diejenige mit der größten Selektivität und Hemmeffizienz zu identifizieren. Anschließend muss die Konzentration so optimiert werden, dass unspezifische Effekte auf die Proteinbiosynthese, wie sie in den hier beschriebenen Versuchen beobachtet wurden, vermieden werden. Das Trägersystem sollte dahingehend optimiert werden, dass keine Effekte auf die Telomeraseaktivität zu finden sind und auch bei höheren Konzentrationen keine Toxizität auftritt. Außerdem sollte es so ausgelegt sein, dass eine Überführung in ein Aerosol möglich ist, um das Ziel der Studien der inhalativen Applikation zu erreichen.

Zusätzlich müssen die Testsysteme verändert bzw. erweitert werden. In allen Teilen dieser Arbeit war die Verwendung von *in vitro* Zellkulturmodellen, die sich entweder aus Tumor- oder nicht malignen Gewebe ableiteten, ein wichtiger Bestandteil zur Untersuchung der vorgestellten Strategien. Diese Zellkulturmodelle lieferten gute Informationen zum Verständnis im betrachteten Zielgewebe. Hierbei muss jedoch beachtet werden, dass die Modelle nur Momentanaufnahmen darstellen, die diejenigen Zustände simulieren, wenn der Wirkstoff, bzw. das mit Wirkstoff beladene Trägersystem das Zielgewebe erreicht hat. In den weiterführenden Studien ist daher zur Erlangung tiefer greifender Information über die Verteilung, Aufnahme und Wirksamkeit der Zubereitung die Verwendung von komplexeren Modellen, wie zum Beispiel die isoliert perfundierten Lunge oder der Tierversuch, notwendig.

Abbreviations

| | |
|---------|---|
| 2OMR | 2'-O-methyl-RNA |
| AB | apical to basolateral direction (in transport studies) |
| ALT | alternative lengthening of telomeres |
| ATCC | American Type Culture Collection |
| BA | basolateral to apical direction (in transport studies) |
| BSA | bovine serum albumin |
| BSS | balanced salt solution |
| CPNP | chitosan/PLGA nanoparticles |
| Dil | 1,1'-Dioctadecyl-3,3,3',3'-tetramethylindocarbocyanine perchlorate |
| DOPE | 1,2-dioleoyl-sn-glycero-3-phosphoethanolamine |
| DOTAP | 1,2-dioleoyl-3-trimethylammonium-propane |
| FAM | carboxyfluoresceinamine |
| FCS | fetal calf serum |
| HA | hyaluronic acid |
| hAEpC | primary human alveolar epithelial cells |
| HBSS | Hank's balanced salt solution |
| HSA | human serum albumin |
| hTERT | human telomerase reverse transcriptase |
| hTR | human telomerase RNA |
| IAM | immobilized artificial membrane |
| LDH | lactate dehydrogenase |
| LF 2000 | Lipofectamine 2000 [®] |
| MTT | methyl-thiazolyl-tetrazolium |
| NEAA | non-essential amino acids |
| NSCLC | non-small cell lung cancer |
| PBS | phosphate buffered saline |
| PDI | polydispersity index |
| PLGA | poly(lactic-co-glycolic acid) |
| PVA | polyvinyl alcohol |
| RNAi | RNA interference |
| SAGM | small airway growth medium |
| SCLC | small cell lung cancer |
| SDS | sodium dodecylsulfate |
| SEC | size exclusion chromatography |
| siRNA | small interfering RNA |
| TEAC | tetraethylammonium chloride |
| TEER | transepithelial electrical resistance |
| TNM | classification of malignant tumors; T = tumor size, N = involvement of regional lymph nodes, M = distant metastasis |
| TRAP | telomeric repeat amplification protocol |
| ZP | zeta potential |

References

1. Jemal, A., Siegel, R., Ward, E., Hao, Y., Xu, J., Murray, T., Thun, M. J. *Cancer statistics, 2008*. (2008) *CA Cancer J. Clin.*, 58(2), 71-96
2. Batzler, W. U., Giersiepen, K., Hentschel, S., Husmann, G., Kaatsch, P., Katalinic, A., Kieschke, J., Kraywinkel, K., Meyer, M., Stabenow, R., Stegmaier, C., Bertz, J., Haberland, J., Wolf, U. *Krebs in Deutschland 2003-2004, Häufigkeiten und Trends*. (2008) *Krebs in Deutschland*, 1-113
3. Beasley, M. B., Brambilla, E., Travis, W. D. *The 2004 World Health Organization classification of lung tumors*. (2005) *Semin. Roentgenol.*, 40(2), 90-97
4. Micke, P., Faldum, A., Metz, T., Beeh, K.-M., Bittinger, F., Hengstler, J.-G., Buhl, R. *Staging small cell lung cancer: Veterans Administration Lung Study Group versus International Association for the Study of Lung Cancer--what limits limited disease?* (2002) *Lung cancer (Amsterdam, Netherlands)*, 37(3), 271-276
5. Serke, M., Schönfeld, N. *[Diagnosis and staging of lung cancer]*. (2007) *Dtsch. Med. Wochenschr.*, 132(21), 1165-1169
6. Wynants, J., Stroobants, S., Dooms, C., Vansteenkiste, J. *Staging of lung cancer*. (2007) *Radiologic Clinics of North America*, 45(4), 609-25, v
7. Lababede, O., Meziane, M. A., Rice, T. W. *TNM staging of lung cancer: a quick reference chart*. (1999) *Chest*, 115(1), 233-235
8. Ettinger, D. S., Akerley, W., Bepler, G., Chang, A., Cheney, R. T., Chirieac, L. R., D'Amico, T. A., Demmy, T. L., Feigenberg, S. J., Figlin, R. A., Govindan, R., Grannis Jr., F. W., Jahan, T., Jahanzeb, M., Kessinger, A., Komaki, R., Kris, M. G., Langer, C. J., Le, Q. T., Martins, R., Otterson, G. A., Patel, J. D., Robert, F., Sugarbaker, D. J., Wood, D. E. *Non-Small Cell Lung Cancer*. (2008) *NCCN Clinical Practice Guidelines in Oncology*, V.2.2008
9. Heigener, D. F., Reck, M., Gatzemeier, U. *[Non-small cell lung cancer - diagnostics and stage-adapted therapy]*. (2007) *Med. Klin. (Munich)*, 102(12), 981-8; quiz 989-90

References

10. Tatsumura, T., Koyama, S., Tsujimoto, M., Kitagawa, M., Kagamimori, S. *Further study of nebulisation chemotherapy, a new chemotherapeutic method in the treatment of lung carcinomas: fundamental and clinical.* (1993) Br. J. Cancer, 68(6), 1146-1149
11. Tatsumura, T., Yamamoto, K., Murakami, A., Tsuda, M., Sugiyama, S. *[New chemotherapeutic method for the treatment of tracheal and bronchial cancers--nebulization chemotherapy].* (1983) Gan No Risho, 29(7), 765-770
12. Otterson, G. A., Villalona-Calero, M. A., Sharma, S., Kris, M. G., Imondi, A., Gerber, M., White, D. A., Ratain, M. J., Schiller, J. H., Sandler, A., Kraut, M., Mani, S., Murren, J. R. *Phase I study of inhaled Doxorubicin for patients with metastatic tumors to the lungs.* (2007) Clin. Cancer Res., 13(4), 1246-1252
13. Wittgen, B. P. H., Kunst, P. W. A., van der Born, K., van Wijk, A. W., Perkins, W., Pilkiewicz, F. G., Perez-Soler, R., Nicholson, S., Peters, G. J., Postmus, P. E. *Phase I study of aerosolized SLIT cisplatin in the treatment of patients with carcinoma of the lung.* (2007) Clin. Cancer Res., 13(8), 2414-2421
14. Verschraegen, C. F., Gilbert, B. E., Loyer, E., Huaranga, A., Walsh, G., Newman, R. A., Knight, V. *Clinical evaluation of the delivery and safety of aerosolized liposomal 9-nitro-20(s)-camptothecin in patients with advanced pulmonary malignancies.* (2004) Clin. Cancer Res., 10(7), 2319-2326
15. Albanell, J., Lonardo, F., Rusch, V., Engelhardt, M., Langenfeld, J., Han, W., Klimstra, D., Venkatraman, E., Moore, M. A., Dmitrovsky, E. *High telomerase activity in primary lung cancers: association with increased cell proliferation rates and advanced pathologic stage.* (1997) J. Natl. Cancer Inst., 89(21), 1609-1615
16. Chen, K. Y., Lee, L. N., Yu, C. J., Lee, Y. C., Kuo, S. H., Yang, P. C. *Elevation of telomerase activity positively correlates to poor prognosis of patients with non-small cell lung cancer.* (2005) Cancer Lett., 240(1), 148-156

-
17. Marchetti, A., Bertacca, G., Buttitta, F., Chella, A., Quattrocchio, G., Angeletti, C. A., Bevilacqua, G. *Telomerase activity as a prognostic indicator in stage I non-small cell lung cancer.* (1999) *Clin. Cancer Res.*, 5(8), 2077-2081
 18. Taga, S., Osaki, T., Ohgami, A., Imoto, H., Yasumoto, K. *Prognostic impact of telomerase activity in non-small cell lung cancers.* (1999) *Ann. Surg.*, 230(5), 715-720
 19. Hayflick, L., Moorhead, P. S. *The serial cultivation of human diploid cell strains.* (1961) *Exp. Cell Res.*, 25, 585-621
 20. Hayflick, L. *The limited in vitro lifetime of human diploid cell strains.* (1965) *Exp. Cell Res.*, 37, 614-636
 21. Harley, C. B., Futcher, A. B., Greider, C. W. *Telomeres shorten during ageing of human fibroblasts.* (1990) *Nature*, 345(6274), 458-460
 22. Greider, C. W., Blackburn, E. H. *Identification of a specific telomere terminal transferase activity in Tetrahymena extracts.* (1985) *Cell*, 43(2 Pt 1), 405-413
 23. Bodnar, A. G., Ouellette, M., Frolkis, M., Holt, S. E., Chiu, C. P., Morin, G. B., Harley, C. B., Shay, J. W., Lichtsteiner, S., Wright, W. E. *Extension of life-span by introduction of telomerase into normal human cells.* (1998) *Science*, 279(5349), 349-352
 24. Vaziri, H., Benchimol, S. *Reconstitution of telomerase activity in normal human cells leads to elongation of telomeres and extended replicative life span.* (1998) *Curr. Biol.*, 8(5), 279-282
 25. Blackburn, E. H., Gall, J. G. *A tandemly repeated sequence at the termini of the extrachromosomal ribosomal RNA genes in Tetrahymena.* (1978) *J. Mol. Biol.*, 120(1), 33-53
 26. Moyzis, R. K., Buckingham, J. M., Cram, L. S., Dani, M., Deaven, L. L., Jones, M. D., Meyne, J., Ratliff, R. L., Wu, J. R. *A highly conserved repetitive DNA sequence, (TTAGGG)_n, present at the telomeres of human chromosomes.* (1988) *Proc. Natl. Acad. Sci. U.S.A.*, 85(18), 6622-6626

References

27. Griffith, J. D., Comeau, L., Rosenfield, S., Stansel, R. M., Bianchi, A., Moss, H., de Lange, T. *Mammalian telomeres end in a large duplex loop.* (1999) *Cell*, 97(4), 503-514
28. Palm, W., de Lange, T. *How shelterin protects Mammalian telomeres.* (2008) *Annu. Rev. Genet.*, 42, 301-334
29. Huffman, K. E., Levene, S. D., Tesmer, V. M., Shay, J. W., Wright, W. E. *Telomere shortening is proportional to the size of the G-rich telomeric 3'-overhang.* (2000) *J. Biol. Chem.*, 275(26), 19719-19722
30. Sfeir, A. J., Chai, W., Shay, J. W., Wright, W. E. *Telomere-end processing the terminal nucleotides of human chromosomes.* (2005) *Mol. Cell*, 18(1), 131-138
31. Deng, Y., Chan, S., Chang, S. *Telomere dysfunction and tumour suppression: the senescence connection.* (2008) *Nat. Rev. Cancer*, 8(6), 450-458
32. Phatak, P., Burger, A. M. *Telomerase and its potential for therapeutic intervention.* (2007) *Br. J. Pharmacol.*, 152(7), 1003-1011
33. Wang, J., Xie, L. Y., Allan, S., Beach, D., Hannon, G. J. *Myc activates telomerase.* (1998) *Genes Dev.*, 12(12), 1769-1774
34. Wu, K. J., Grandori, C., Amacker, M., Simon-Vermot, N., Polack, A., Lingner, J., Dalla-Favera, R. *Direct activation of TERT transcription by c-MYC.* (1999) *Nat. Genet.*, 21(2), 220-224
35. Feng, J., Funk, W. D., Wang, S. S., Weinrich, S. L., Avilion, A. A., Chiu, C. P., Adams, R. R., Chang, E., Allsopp, R. C., Yu, J. *The RNA component of human telomerase.* (1995) *Science*, 269(5228), 1236-1241
36. Lingner, J., Hughes, T. R., Shevchenko, A., Mann, M., Lundblad, V., Cech, T. R. *Reverse transcriptase motifs in the catalytic subunit of telomerase.* (1997) *Science*, 276(5312), 561-567
37. Cohen, S. B., Graham, M. E., Lovrecz, G. O., Bache, N., Robinson, P. J., Reddel, R. R. *Protein composition of catalytically active human telomerase from immortal cells.* (2007) *Science*, 315(5820), 1850-1853
38. Flores, I., Benetti, R., Blasco, M. A. *Telomerase regulation and stem cell behaviour.* (2006) *Curr. Opin. Cell Biol.*, 18(3), 254-260

-
39. Wright, W. E., Piatyszek, M. A., Rainey, W. E., Byrd, W., Shay, J. W. *Telomerase activity in human germline and embryonic tissues and cells.* (1996) *Dev. Genet.*, 18(2), 173-179
 40. Kim, N. W., Piatyszek, M. A., Prowse, K. R., Harley, C. B., West, M. D., Ho, P. L., Coviello, G. M., Wright, W. E., Weinrich, S. L., Shay, J. W. *Specific association of human telomerase activity with immortal cells and cancer.* (1994) *Science*, 266(5193), 2011-2015
 41. Shay, J. W., Bacchetti, S. *A survey of telomerase activity in human cancer.* (1997) *Eur. J. Cancer*, 33(5), 787-791
 42. Hanahan, D., Weinberg, R. A. *The hallmarks of cancer.* (2000) *Cell*, 100(1), 57-70
 43. Bollmann, F. M. *Targeting ALT: the role of alternative lengthening of telomeres in pathogenesis and prevention of cancer.* (2007) *Cancer Treat. Rev.*, 33(8), 704-709
 44. Cesare, A. J., Reddel, R. R. *Telomere uncapping and alternative lengthening of telomeres.* (2008) *Mech. Ageing Dev.*, 129(1-2), 99-108
 45. Damm, K., Hemmann, U., Garin-Chesa, P., Huel, N., Kauffmann, I., Priepke, H., Niestroj, C., Daiber, C., Enenkel, B., Guilliard, B., Lauritsch, I., Müller, E., Pascolo, E., Sauter, G., Pantic, M., Martens, U. M., Wenz, C., Lingner, J., Kraut, N., Rettig, W. J., Schnapp, A. *A highly selective telomerase inhibitor limiting human cancer cell proliferation.* (2001) *EMBO J.*, 20(24), 6958-6968
 46. Gomez, D. E., Tejera, A. M., Olivero, O. A. *Irreversible telomere shortening by 3'-azido-2',3'-dideoxythymidine (AZT) treatment.* (1998) *Biochem. Biophys. Res. Commun.*, 246(1), 107-110
 47. Asai, A., Oshima, Y., Yamamoto, Y., Uochi, T. A., Kusaka, H., Akinaga, S., Yamashita, Y., Pongracz, K., Pruzan, R., Wunder, E., Piatyszek, M., Li, S., Chin, A. C., Harley, C. B., Gryaznov, S. *A novel telomerase template antagonist (GRN163) as a potential anticancer agent.* (2003) *Cancer Res.*, 63(14), 3931-3939
 48. Pitts, A. E., Corey, D. R. *Inhibition of human telomerase by 2'-O-methyl-RNA.* (1998) *Proc. Natl. Acad. Sci. U. S. A.*, 95(20), 11549-11554

References

49. Dikmen, Z. G., Gellert, G. C., Jackson, S., Gryaznov, S., Tressler, R., Dogan, P., Wright, W. E., Shay, J. W. *In vivo inhibition of lung cancer by GRN163L: a novel human telomerase inhibitor.* (2005) *Cancer Res.*, 65(17), 7866-7873
50. Gellert, G. C., Dikmen, Z. G., Wright, W. E., Gryaznov, S., Shay, J. W. *Effects of a novel telomerase inhibitor, GRN163L, in human breast cancer.* (2006) *Breast Cancer Res. Treat.*, 96(1), 73-81
51. Herbert, B. S., Gellert, G. C., Hochreiter, A., Pongracz, K., Wright, W. E., Zielinska, D., Chin, A. C., Harley, C. B., Shay, J. W., Gryaznov, S. M. *Lipid modification of GRN163, an N3'-->P5' thio-phosphoramidate oligonucleotide, enhances the potency of telomerase inhibition.* (2005) *Oncogene*, 24(33), 5262-5268
52. Burge, S., Parkinson, G. N., Hazel, P., Todd, A. K., Neidle, S. *Quadruplex DNA: sequence, topology and structure.* (2006) *Nucleic Acids Res.*, 34(19), 5402-5415
53. Cuesta, J., Read, M. A., Neidle, S. *The design of G-quadruplex ligands as telomerase inhibitors.* (2003) *Mini. Rev. Med. Chem.*, 3(1), 11-21
54. Riou, J. F. *G-quadruplex interacting agents targeting the telomeric G-overhang are more than simple telomerase inhibitors.* (2004) *Curr. Med. Chem. Anticancer Agents*, 4(5), 439-443
55. Brunsvig, P. F., Aamdal, S., Gjertsen, M. K., Kvalheim, G., Markowski-Grimsrud, C. J., Sve, I., Dyrhaug, M., Trachsel, S., Møller, M., Eriksen, J. A., Gaudernack, G. *Telomerase peptide vaccination: a phase I/II study in patients with non-small cell lung cancer.* (2006) *Cancer Immunol. Immunother.*, 55(12), 1553-1564
56. Vonderheide, R. H. *Universal tumor antigens for cancer vaccination: targeting telomerase for immunoprevention.* (2007) *Discov. Med.*, 7(39), 103-108
57. Vonderheide, R. H., Domchek, S. M., Schultze, J. L., George, D. J., Hoar, K. M., Chen, D. Y., Stephans, K. F., Masutomi, K., Loda, M., Xia, Z., Anderson, K. S., Hahn, W. C., Nadler, L. M. *Vaccination of cancer patients against telomerase induces functional antitumor CD8+ T lymphocytes.* (2004) *Clin. Cancer Res.*, 10(3), 828-839

-
58. Bilisland, A. E., Anderson, C. J., Fletcher-Monaghan, A. J., McGregor, F., Evans, T. R., Ganly, I., Knox, R. J., Plumb, J. A., Keith, W. N. *Selective ablation of human cancer cells by telomerase-specific adenoviral suicide gene therapy vectors expressing bacterial nitroreductase.* (2003) *Oncogene*, 22(3), 370-380
 59. Plumb, J. A., Bilisland, A., Kakani, R., Zhao, J., Glasspool, R. M., Knox, R. J., Evans, T. R., Keith, W. N. *Telomerase-specific suicide gene therapy vectors expressing bacterial nitroreductase sensitize human cancer cells to the pro-drug CB1954.* (2001) *Oncogene*, 20(53), 7797-7803
 60. Fujiwara, T., Urata, Y., Tanaka, N. *Telomerase-specific oncolytic virotherapy for human cancer with the hTERT promoter.* (2007) *Curr. Cancer Drug Targets*, 7(2), 191-201
 61. Agarwal, M., Pandita, S., Hunt, C. R., Gupta, A., Yue, X., Khan, S., Pandita, R. K., Pratt, D., Shay, J. W., Taylor, J. S., Pandita, T. K. *Inhibition of telomerase activity enhances hyperthermia-mediated radiosensitization.* (2008) *Cancer Res.*, 68(9), 3370-3378
 62. Fujiwara, T., Kagawa, S., Kishimoto, H., Endo, Y., Hioki, M., Ikeda, Y., Sakai, R., Urata, Y., Tanaka, N., Fujiwara, T. *Enhanced antitumor efficacy of telomerase-selective oncolytic adenoviral agent OBP-401 with docetaxel: preclinical evaluation of chemovirotherapy.* (2006) *Int. J. Cancer*, 119(2), 432-440
 63. Gomez-Millan, J., Goldblatt, E. M., Gryaznov, S. M., Mendonca, M. S., Herbert, B. S. *Specific telomere dysfunction induced by GRN163L increases radiation sensitivity in breast cancer cells.* (2007) *Int. J. Radiat. Oncol. Biol. Phys.*, 67(3), 897-905
 64. Misawa, M., Tauchi, T., Sashida, G., Nakajima, A., Abe, K., Ohyashiki, J. H., Ohyashiki, K. *Inhibition of human telomerase enhances the effect of chemotherapeutic agents in lung cancer cells.* (2002) *Int. J. Oncol.*, 21(5), 1087-1092
 65. Tauchi, T., Ohyashiki, J. H., Ohyashiki, K. *Telomerase inhibition combined with other chemotherapeutic reagents to enhance anti-cancer effect.* (2008) *Methods Mol. Biol.*, 405, 181-189

References

66. Ward, R. J., Autexier, C. *Pharmacological telomerase inhibition can sensitize drug-resistant and drug-sensitive cells to chemotherapeutic treatment.* (2005) *Mol. Pharmacol.*, 68(3), 779-786
67. Gowan, S. M., Harrison, J. R., Patterson, L., Valenti, M., Read, M. A., Neidle, S., Kelland, L. R. *A G-quadruplex-interactive potent small-molecule inhibitor of telomerase exhibiting in vitro and in vivo antitumor activity.* (2002) *Mol. Pharmacol.*, 61(5), 1154-1162
68. Amidon, G. L., Lennernäs, H., Shah, V. P., Crison, J. R. *A theoretical basis for a biopharmaceutic drug classification: the correlation of in vitro drug product dissolution and in vivo bioavailability.* (1995) *Pharm. Res.*, 12(3), 413-420
69. Elbashir, S. M., Harborth, J., Lendeckel, W., Yalcin, A., Weber, K., Tuschl, T. *Duplexes of 21-nucleotide RNAs mediate RNA interference in cultured mammalian cells.* (2001) *Nature*, 411(6836), 494-498
70. Elbashir, S. M., Lendeckel, W., Tuschl, T. *RNA interference is mediated by 21- and 22-nucleotide RNAs.* (2001) *Genes Dev.*, 15(2), 188-200
71. Blackburn, E. H. *Telomeres and telomerase: their mechanisms of action and the effects of altering their functions.* (2005) *FEBS Lett.*, 579(4), 859-862
72. Shay, J. W., Wright, W. E. *Senescence and immortalization: role of telomeres and telomerase.* (2004) *Carcinogenesis*, 26(5), 867-874
73. Piotrowska, K., Kleideiter, E., Mürdter, T. E., Taetz, S., Baldes, C., Schaefer, U. F., Lehr, C. M., Klotz, U. *Optimization of the TRAP assay to evaluate specificity of telomerase inhibitors.* (2005) *Lab. Invest.*, 85(12), 1565-1569
74. Burger, A. M., Dai, F., Schultes, C. M., Reszka, A. P., Moore, M. J., Double, J. A., Neidle, S. *The G-quadruplex-interactive molecule BRACO-19 inhibits tumor growth, consistent with telomere targeting and interference with telomerase function.* (2005) *Cancer Res.*, 65(4), 1489-1496
75. Cozens, A. L., Yezzi, M. J., Kunzelmann, K., Ohrui, T., Chin, L., Eng, K., Finkbeiner, W. E., Widdicombe, J. H., Gruenert, D. C. *CFTR expression*

-
- and chloride secretion in polarized immortal human bronchial epithelial cells.* (1994) *Am. J. Respir. Cell Mol. Biol.*, 10(1), 38-47
76. Forbes, B., Shah, A., Martin, G. P., Lansley, A. B. *The human bronchial epithelial cell line 16HBE14o- as a model system of the airways for studying drug transport.* (2003) *Int. J. Pharm.*, 257(1-2), 161-167
77. Florea, B. I., Cassara, M. L., Junginger, H. E., Borchard, G. *Drug transport and metabolism characteristics of the human airway epithelial cell line Calu-3.* (2003) *J. Control. Release*, 87(1-3), 131-138
78. Foster, K. A., Avery, M. L., Yazdani, M., Audus, K. L. *Characterization of the Calu-3 cell line as a tool to screen pulmonary drug delivery.* (2000) *Int. J. Pharm.*, 208(1-2), 1-11
79. Elbert, K. J., Schafer, U. F., Schafers, H. J., Kim, K. J., Lee, V. H., Lehr, C. M. *Monolayers of human alveolar epithelial cells in primary culture for pulmonary absorption and transport studies.* (1999) *Pharm. Res.*, 16(5), 601-608
80. Fuchs, S., Hollins, A. J., Laue, M., Schaefer, U. F., Roemer, K., Gumbleton, M., Lehr, C. M. *Differentiation of human alveolar epithelial cells in primary culture: morphological characterization and synthesis of caveolin-1 and surfactant protein-C.* (2003) *Cell Tissue Res.*, 311(1), 31-45
81. Artursson, P., Palm, K., Luthman, K. *Caco-2 monolayers in experimental and theoretical predictions of drug transport.* (2001) *Adv. Drug Deliv. Rev.*, 46(1-3), 27-43
82. Harrison, R. J., Cuesta, J., Chessari, G., Read, M. A., Basra, S. K., Reszka, A. P., Morrell, J., Gowan, S. M., Incles, C. M., Tanious, F. A., Wilson, W. D., Kelland, L. R., Neidle, S. *Trisubstituted acridine derivatives as potent and selective telomerase inhibitors.* (2003) *J. Med. Chem.*, 46(21), 4463-4476
83. Ehrhardt, C., Kim, K. J., Lehr, C. M. *Isolation and culture of human alveolar epithelial cells.* (2005) *Methods Mol. Med.*, 107, 207-216
84. Ehrhardt, C., Kneuer, C., Bies, C., Lehr, C. M., Kim, K. J., Bakowsky, U. *Salbutamol is actively absorbed across human bronchial epithelial cell layers.* (2005) *Pulm. Pharmacol. Ther.*, 18(3), 165-170

References

85. Hamilton, K. O., Backstrom, G., Yazdanian, M. A., Audus, K. L. *P-glycoprotein efflux pump expression and activity in Calu-3 cells.* (2001) *J. Pharm. Sci.*, 90(5), 647-658
86. Qadir, M., O'Loughlin, K. L., Fricke, S. M., Williamson, N. A., Greco, W. R., Minderman, H., Baer, M. R. *Cyclosporin A is a broad-spectrum multidrug resistance modulator.* (2005) *Clin. Cancer Res.*, 11(6), 2320-2326
87. Koepsell, H., Schmitt, B. M., Gorboulev, V. *Organic cation transporters.* (2003) *Rev. Physiol. Biochem. Pharmacol.*, 150, 36-90
88. Bock, U., Flototto, T., Haltner, E. *Validation of cell culture models for the intestine and the blood-brain barrier and comparison of drug permeation.* (2004) *ALTEX*, 21 (Suppl 3), 57-64
89. Incles, C. M., Schultes, C. M., Kempfski, H., Koehler, H., Kelland, L. R., Neidle, S. *A G-quadruplex telomere targeting agent produces p16-associated senescence and chromosomal fusions in human prostate cancer cells.* (2004) *Mol. Cancer Ther.*, 3(10), 1201-1206
90. Loprevite, M., Favoni, R. E., de Cupis, A., Pirani, P., Merlo, F., Grossi, F., Ardizzoni, A. *Pre-clinical evaluation of new antineoplastic agents in NSCLC cell lines: evidence of histological subtype-dependent cytotoxicity.* (1999) *Int. J. Oncol.*, 15(4), 787-792
91. Smith, J. A., Ngo, H., Martin, M. C., Wolf, J. K. *An evaluation of cytotoxicity of the taxane and platinum agents combination treatment in a panel of human ovarian carcinoma cell lines.* (2005) *Gynecol. Oncol.*, 98(1), 141-145
92. Ravizza, R., Gariboldi, M. B., Passarelli, L., Monti, E. *Role of the p53/p21 system in the response of human colon carcinoma cells to Doxorubicin.* (2004) *BMC Cancer*, 4, 92
93. Kobayashi, S., Okada, S., Yoshida, H., Fujimura, S. *Indomethacin enhances the cytotoxicity of VCR and ADR in human pulmonary adenocarcinoma cells.* (1997) *Tohoku J. Exp. Med.*, 181(3), 361-370
94. Ong, S., Liu, H., Qiu, X., Bhat, G., Pidgeon, C. *Membrane partition coefficients chromatographically measured using immobilized artificial membrane surfaces.* (1995) *Anal. Chem.*, 67(4), 755-762

-
95. Pidgeon, C., Ong, S., Liu, H., Qiu, X., Pidgeon, M., Dantzig, A. H., Munroe, J., Hornback, W. J., Kasher, J. S., Glunz, L. *IAM chromatography: an in vitro screen for predicting drug membrane permeability*. (1995) *J. Med. Chem.*, 38(4), 590-594
96. Pendino, F., Tarkanyi, I., Dudognon, C., Hillion, J., Lanotte, M., Aradi, J., Ségal-Bendirdjian, E. *Telomeres and telomerase: Pharmacological targets for new anticancer strategies?* (2006) *Curr. Cancer Drug Targets*, 6(2), 147-180
97. Shay, J. W., Wright, W. E. *Telomerase therapeutics for cancer: challenges and new directions*. (2006) *Nat. Rev. Drug Discov.*, 5(7), 577-584
98. Taetz, S., Baldes, C., Mürdter, T. E., Kleideiter, E., Piotrowska, K., Bock, U., Haltner-Ukomadu, E., Mueller, J., Huwer, H., Schaefer, U. F., Klotz, U., Lehr, C. M. *Biopharmaceutical characterization of the telomerase inhibitor BRACO19*. (2006) *Pharm. Res.*, 23(5), 1031-1037
99. Kim, N. W., Wu, F. *Advances in quantification and characterization of telomerase activity by the telomeric repeat amplification protocol (TRAP)*. (1997) *Nucleic Acids Res.*, 25(13), 2595-2597
100. Goodell, J., Svensson, B., Ferguson, D. *Spectrophotometric determination and computational evaluation of the rates of hydrolysis of 9-amino-substituted acridines*. (2006) *J. Chem. Inf. Model.*, 46(2), 876-883
101. Read, M. A., Wood, A. A., Harrison, J. R., Gowan, S. M., Kelland, L. R., Dosanjh, H. S., Neidle, S. *Molecular modeling studies on G-quadruplex complexes of telomerase inhibitors: structure-activity relationships*. (1999) *J. Med. Chem.*, 42(22), 4538-4546
102. Harrison, R. J., Reszka, A. P., Haider, S. M., Romagnoli, B., Morrell, J., Read, M. A., Gowan, S. M., Incles, C. M., Kelland, L. R., Neidle, S. *Evaluation of by disubstituted acridone derivatives as telomerase inhibitors: the importance of G-quadruplex binding*. (2004) *Bioorg. Med. Chem. Lett.*, 14(23), 5845-5849
103. Moore, M. J., Schultes, C. M., Cuesta, J., Cuenca, F., Gunaratnam, M., Tanious, F. A., Wilson, W. D., Neidle, S. *Trisubstituted acridines as G-*

-
- quadruplex telomere targeting agents. Effects of extensions of the 3,6- and 9-side chains on quadruplex binding, telomerase activity, and cell proliferation.* (2006) *J. Med. Chem.*, 49(2), 582-599
104. De Cian, A., Cristofari, G., Reichenbach, P., De Lemos, E., Monchaud, D., Teulade-Fichou, M. P., Shin-Ya, K., Lacroix, L., Lingner, J., Mergny, J. L. *Reevaluation of telomerase inhibition by quadruplex ligands and their mechanisms of action.* (2007) *Proc. Natl. Acad. Sci. U. S. A.*,
105. Martins, C., Gunaratnam, M., Stuart, J., Makwana, V., Greciano, O., Reszka, A. P., Kelland, L. R., Neidle, S. *Structure-based design of benzylamino-acridine compounds as G-quadruplex DNA telomere targeting agents.* (2007) *Bioorg. Med. Chem. Lett.*, 17(8), 2293-2298
106. Herbert, B., Pitts, A. E., Baker, S. I., Hamilton, S. E., Wright, W. E., Shay, J. W., Corey, D. R. *Inhibition of human telomerase in immortal human cells leads to progressive telomere shortening and cell death.* (1999) *Proc. Natl. Acad. Sci. U. S. A.*, 96(25), 14276-14281
107. Ravi Kumar, M. N., Bakowsky, U., Lehr, C. M. *Preparation and characterization of cationic PLGA nanospheres as DNA carriers.* (2004) *Biomaterials*, 25(10), 1771-1777
108. Ravi Kumar, M. N., Mohapatra, S. S., Kong, X., Jena, P. K., Bakowsky, U., Lehr, C. M. *Cationic poly(lactide-co-glycolide) nanoparticles as efficient in vivo gene transfection agents.* (2005) *J. Nanosci. Nanotechnol.*, 4(8), 990-994
109. Nafee, N., Taetz, S., Schneider, M., Schaefer, U. F., Lehr, C. M. *Chitosan-coated PLGA nanoparticles for DNA/RNA delivery: effect of the formulation parameters on complexation and transfection of antisense oligonucleotides.* (2007) *Nanomedicine*, 3(3), 173-183
110. Mathias, N. R., Timoszyk, J., Stetsko, P., Megill, J., Smith, R., Wall, D. *Permeability characteristics of Calu-3 human bronchial epithelial cells: In vitro-in vitro correlation to predict lung absorption in rats.* (2002) *J. Drug Target.*, 10(1), 31-40
111. Beisner, J., Dong, M., Taetz, S., Piotrowska, K., Kleideiter, E., Friedel, G., Schaefer, U. F., Lehr, C. M., Klotz, U., Mürdter, T. E. *Efficient*

-
- Telomerase Inhibition in Human Non-Small Cell Lung Cancer Cells by Liposomal Delivery of 2'-O-methyl-RNA.* (2008) *J. Pharm. Sci.*, in press
112. Sorlier, P., Denuzière, A., Viton, C., Domard, A. *Relation between the degree of acetylation and the electrostatic properties of chitin and chitosan.* (2001) *Biomacromolecules*, 2(3), 765-772
113. Lorenz, M. R., Holzapfel, V., Musyanovych, A., Nothelfer, K., Walther, P., Frank, H., Landfester, K., Schrezenmeier, H., Mailänder, V. *Uptake of functionalized, fluorescent-labeled polymeric particles in different cell lines and stem cells.* (2006) *Biomaterials*, 27(14), 2820-2828
114. Gessner, A., Lieske, A., Paulke, B., Müller, R. *Influence of surface charge density on protein adsorption on polymeric nanoparticles: analysis by two-dimensional electrophoresis.* (2002) *Eur. J. Pharm. Biopharm.*, 54(2), 165-170
115. Lück, M., Paulke, B. R., Schröder, W., Blunk, T., Müller, R. H. *Analysis of plasma protein adsorption on polymeric nanoparticles with different surface characteristics.* (1998) *J. Biomed. Mater. Res.*, 39(3), 478-485
116. Fang, N., Chan, V. *Interaction of liposome with immobilized chitosan during main phase transition.* (2003) *Biomacromolecules*, 4(3), 581-588
117. Löhbach, C., Neumann, D., Lehr, C. M., Lamprecht, A. *Human vascular endothelial cells in primary cell culture for the evaluation of nanoparticle bioadhesion.* (2006) *J. Nanosci. Nanotechnol.*, 6(8), 1-7
118. Huang, M., Ma, Z., Khor, E., Lim, L. Y. *Uptake of FITC-chitosan nanoparticles by A549 cells.* (2002) *Pharm. Res.*, 19(10), 1488-1494
119. Huang, M., Khor, E., Lim, L. Y. *Uptake and cytotoxicity of chitosan molecules and nanoparticles: effects of molecular weight and degree of deacetylation.* (2004) *Pharm. Res.*, 21(2), 344-353
120. Gumbleton, M. *Caveolae as potential macromolecule trafficking compartments within alveolar epithelium.* (2001) *Adv. Drug Deliv. Rev.*, 49(3), 281-300
121. Bradbury, N. A., Clark, J. A., Watkins, S. C., Widnell, C. C., Smith, H. S., Bridges, R. J. *Characterization of the internalization pathways for the cystic fibrosis transmembrane conductance regulator.* (1999) *Am. J. Physiol.*, 276(4 Pt 1), L659-68

References

122. Grenha, A., Grainger, C. I., Dailey, L. A., Seijo, B., Martin, G. P., Remuñán-López, C., Forbes, B. *Chitosan nanoparticles are compatible with respiratory epithelial cells in vitro.* (2007) *Eur. J. Pharm. Sci.*,
123. Curotto, E., Aros, F. *Quantitative determination of chitosan and the percentage of free amino groups.* (1993) *Anal. Biochem.*, 211(2), 240-241
124. Messai, I., Delair, T. *Adsorption of chitosan onto poly(D,L-lactic acid) particles: A physico-chemical investigation.* (2005) *Macromol. Chem. Phys.*, 206(16), 1665-1674
125. Messai, I., Delair, T. *Cationic biodegradable particles: Comparison of one or two step processes.* (2006) *Colloids. Surf. A Physicochem. Eng. Asp.*, 278(1-3), 188-196
126. Toub, N., Malvy, C., Fattal, E., Couvreur, P. *Innovative nanotechnologies for the delivery of oligonucleotides and siRNA.* (2006) *Biomed. Pharmacother.*, 60(9), 607-620
127. Aagaard, L., Amarguioui, M., Sun, G., Santos, L. C., Ehsani, A., Prydz, H., Rossi, J. J. *A facile lentiviral vector system for expression of doxycycline-inducible shRNAs: knockdown of the pre-miRNA processing enzyme Drosha.* (2007) *Mol. Ther.*, 15(5), 938-945
128. Devi, G. R. *siRNA-based approaches in cancer therapy.* (2006) *Cancer Gene Ther.*, 13(9), 819-829
129. Cardoso, A. L., Simões, S., de Almeida, L. P., Pelisek, J., Culmsee, C., Wagner, E., Pedroso de Lima, M. C. *siRNA delivery by a transferrin-associated lipid-based vector: a non-viral strategy to mediate gene silencing.* (2007) *J. Gene Med.*, 9(3), 170-183
130. Schiffelers, R. M., Ansari, A., Xu, J., Zhou, Q., Tang, Q., Storm, G., Molema, G., Lu, P. Y., Scaria, P. V., Woodle, M. C. *Cancer siRNA therapy by tumor selective delivery with ligand-targeted sterically stabilized nanoparticle.* (2004) *Nucleic Acids Res.*, 32(19), e149
131. Li, S.-D., Huang, L. *Surface-modified LPD nanoparticles for tumor targeting.* (2006) *Ann. N. Y. Acad. Sci.*, 1082, 1-8

-
132. Luo, Y., Ziebell, M. R., Prestwich, G. D. *A hyaluronic acid-taxol antitumor bioconjugate targeted to cancer cells.* (2000) *Biomacromolecules*, 1(2), 208-218
133. Luo, Y., Bernshaw, N. J., Lu, Z.-R., Kopecek, J., Prestwich, G. D. *Targeted delivery of doxorubicin by HPMA copolymer-hyaluronan bioconjugates.* (2002) *Pharm. Res.*, 19(4), 396-402
134. Eliaz, R. E., Szoka Jr., F. C. *Liposome-encapsulated doxorubicin targeted to CD44: a strategy to kill CD44-overexpressing tumor cells.* (2001) *Cancer Res.*, 61(6), 2592-2601
135. Hornof, M., De La Fuente, M., Hallikainen, M., Tammi, R. H., Urtti, A. *Low molecular weight hyaluronan shielding of DNA/PEI polyplexes facilitates CD44 receptor mediated uptake in human corneal epithelial cells.* (2008) *J. Gene Med.*, 10(1), 70-80
136. Lee, H., Mok, H., Lee, S., Oh, Y. K., Park, T. G. *Target-specific intracellular delivery of siRNA using degradable hyaluronic acid nanogels.* (2007) *J. Controlled Release*, 119(2), 245-252
137. Mok, H., Park, J. W., Park, T. G. *Antisense oligodeoxynucleotide-conjugated hyaluronic acid/protamine nanocomplexes for intracellular gene inhibition.* (2007) *Bioconjug. Chem.*, 18(5), 1483-1489
138. Peer, D., Margalit, R. *Loading mitomycin C inside long circulating hyaluronan targeted nano-liposomes increases its antitumor activity in three mice tumor models.* (2003) *Int. J. Cancer*, 108(5), 780-789
139. Peer, D., Margalit, R. *Tumor-targeted hyaluronan nanoliposomes increase the antitumor activity of liposomal Doxorubicin in syngeneic and human xenograft mouse tumor models.* (2004) *Neoplasia*, 6(4), 343-353
140. Bastow, E. R., Byers, S., Golub, S. B., Clarkin, C. E., Pitsillides, A. A., Fosang, A. J. *Hyaluronan synthesis and degradation in cartilage and bone.* (2008) *Cell. Mol. Life Sci.*, 65(3), 395-413
141. Jothy, S. *CD44 and its partners in metastasis.* (2003) *Clin. Exp. Metastasis*, 20(3), 195-201
142. Ponta, H., Sherman, L., Herrlich, P. A. *CD44: from adhesion molecules to signalling regulators.* (2003) *Nat. Rev. Mol. Cell Biol.*, 4(1), 33-45

References

143. Turley, E. A., Noble, P. W., Bourguignon, L. Y. *Signaling properties of hyaluronan receptors.* (2001) *J. Biol. Chem.*, 277(7), 4589-4592
144. Surace, C., Arpicco, S., Marsaud, V., Bouclier, C., Dufay-Wojcicki, A., Cattel, L., Renoir, J. M., Fattal, E. *Lipoplexes targeting the CD44 hyaluronic acid receptor for efficient transfection of breast cancer cells.* submitted
145. Yerushalmi, N., Margalit, R. *Hyaluronic acid-modified bioadhesive liposomes as local drug depots: effects of cellular and fluid dynamics on liposome retention at target sites.* (1998) *Arch. Biochem. Biophys.*, 349(1), 21-26
146. Batzri, S., Korn, E. D. *Single bilayer liposomes prepared without sonication.* (1973) *Biochim. Biophys. Acta*, 298(4), 1015-1019
147. Kremer, J. M., Esker, M. W., Pathmamanoharan, C., Wiersema, P. H. *Vesicles of variable diameter prepared by a modified injection method.* (1977) *Biochemistry*, 16(17), 3932-3935
148. Hou, M., Xu, D., Björkholm, M., Gruber, A. *Real-time quantitative telomeric repeat amplification protocol assay for the detection of telomerase activity.* (2001) *Clin. Chem.*, 47(3), 519-524
149. Herbert, B. S., Hochreiter, A. E., Wright, W. E., Shay, J. W. *Nonradioactive detection of telomerase activity using the telomeric repeat amplification protocol.* (2006) *Nat. Protoc.*, 1(3), 1583-1590
150. Meyer, O., Kirpotin, D., Hong, K., Sternberg, B., Park, J. W., Woodle, M. C., Papahadjopoulos, D. *Cationic liposomes coated with polyethylene glycol as carriers for oligonucleotides.* (1998) *J. Biol. Chem.*, 273(25), 15621-15627
151. Eliaz, R. E., Nir, S., Szoka, F. C. *Interactions of hyaluronan-targeted liposomes with cultured cells: modeling of binding and endocytosis.* (2004) *Methods Enzymol.*, 387, 16-33
152. Sledz, C. A., Holko, M., de Veer, M. J., Silverman, R. H., Williams, B. R. G. *Activation of the interferon system by short-interfering RNAs.* (2003) *Nat. Cell Biol.*, 5(9), 834-839

-
153. Persengiev, S. P., Zhu, X., Green, M. R. *Nonspecific, concentration-dependent stimulation and repression of mammalian gene expression by small interfering RNAs (siRNAs)*. (2004) *RNA*, 10(1), 12-18
154. Scacheri, P. C., Rozenblatt-Rosen, O., Caplen, N. J., Wolfsberg, T. G., Umayam, L., Lee, J. C., Hughes, C. M., Shanmugam, K. S., Bhattacharjee, A., Meyerson, M., Collins, F. S. *Short interfering RNAs can induce unexpected and divergent changes in the levels of untargeted proteins in mammalian cells*. (2004) *Proc. Natl. Acad. Sci. U. S. A.*, 101(7), 1892-1897
155. Ma, Z., Li, J., He, F., Wilson, A., Pitt, B., Li, S. *Cationic lipids enhance siRNA-mediated interferon response in mice*. (2005) *Biochem. Biophys. Res. Commun.*, 330(3), 755-759

Danksagungen

Acknowledgements

Zuerst möchte ich Herrn Professor Claus-Michael Lehr für die Bereitstellung des sehr interessanten Themas danken sowie den vielen Möglichkeiten meine Ergebnisse auf nationalen und internationalen Kongressen zu präsentieren.

Dr. Christiane Baldes danke ich für ihre Betreuung, besonders für die gute Einführung in die Zellkultur und Hilfestellung bei molekularbiologischen Fragen und dass Du immer die Zeit hattest die verschiedensten Dinge mit mir zu erörtern.

Bei Dr. Ulrich Schäfer möchte ich mich neben der wissenschaftlichen Begleitung auch für die viele Hilfe im administrativen Bereich sowie seiner Unterstützung bei persönlichen Angelegenheiten bedanken.

Bei der Gruppe von Professor Ulrich Klotz vom Dr. Margarete Fischer-Bosch Institut für Klinische Pharmakologie in Stuttgart mit Dr. Elke Kleideiter, Dr. Kamilla Piotrowska, Dr. Thomas Mürdter, Dr. Julia Beisner und Meng Dong möchte ich mich sehr für die gute Zusammenarbeit im Rahmen des Telomeraseprojektes bedanken.

Dr. Udo Bock und Dr. Johanna Müller von Across Barriers danke ich für die HSA- und IAM-Chromatographiemessungen zur Charakterisierung von BRACO19.

Dr. Joseph Zapp, Dr. Stefan Boettcher und Dr. Dirk Neumann danke ich für ihre große Hilfe und Geduld bei der Suche nach den Zerfallsprodukten von BRACO19.

Meiner Kollegin Noha Nafee danke ich für die Einführung in die Kunst der Nanopartikelherstellung und die gute Zusammenarbeit während der Versuche mit den Chitosan/PLGA Nanopartikeln.

Dr. Marc Schneider danke ich für seine Unterstützung bei Fragen zur Konfokalmikroskopie und Partikelmessung sowie für die vielen konstruktiven Diskussionen und Anregungen bei den Versuchen mit den Chitosan/PLGA Nanopartikeln.

Weiterhin möchte ich mich bei unseren Technikern, insbesondere Petra König, Susanne Kossek, Heike Stunpf und Leon Muijs, für die Hilfe sowie Tips und Tricks rund um die Zellkultur bedanken.

Herrn Dr. Hanno Huwer von den SHG Kliniken Völklingen danke ich für die Bereitstellung von Lungengewebe zur Isolation von Primärzellen.

From Paris I would like to thank a lot Professor Elias Fattal for giving me the opportunity to spend one year in his group and for accepting to be the second referee of my thesis. I am also very grateful to Dr. Amélie Bochot for being my second supervisor during the year in Paris. Furthermore I would like to thank Claudio Surace for the preparation of the HA-DOPE conjugate and Dr. Véronique Massaud, Professor Jack-Michel Renoir, Dr. Hélène Chacun, Dr. Nicolas Tsapis, Dr. Saadia Kerdine-Römer and Dr. Valérie Nicolas for all their inestimable help and support in the laboratory.

It was a great time in Paris that I enjoyed a lot and will never forget!

Da sich kein Forschungsprojekt ohne entsprechende finanzielle Unterstützung durchführen lässt, möchte ich mich hiermit bei der Deutschen Krebshilfe e.V. für die Förderung des Telomeraseprojektes in Saarbrücken (Projekt Nr.: 10-2035-KI I) und dem GALENOS Netzwerk für das Stipendium zur Finanzierung meines Frankreichaufenthalts im Rahmen des EU Projektes "Towards a European PhD in Advanced Drug Delivery" (Marie Curie Contract MEST-CT-2004-404992) bedanken.

Ein besonderer Dank gilt natürlich meinen ehemaligen Kollegen, besonders Stephan, Barbara, Andi, Eva, Katharina, Frank und Michael. Mit eurer Hilfe war so manches leichter durchzustehen, egal ob es um rein wissenschaftliche Probleme ging oder um den immer mal wieder auftretenden Promotionsfrust loszuwerden. Die Zusammenarbeit mit euch hat mir sehr viel Spaß gemacht und gezeigt, dass ein gutes kollegiales Umfeld einen großen Einfluss auf das Gelingen von vielen Dingen hat.

Meinen Eltern Renate und Heinrich Tätz, den wahrscheinlich wichtigsten Personen, die zum Gelingen dieser Arbeit beigetragen haben, möchte ich ganz herzlich für die jahrelange moralische und finanzielle Unterstützung danken. Wann immer es Entscheidungen zu treffen galt, wusste ich, dass ich auf euren Rat zählen konnte. Bei der Umsetzung habt ihr stets zu mir gestanden und auch tatkräftig mitgeholfen. Danke für alles.

Publication List

Publications

Taetz, S., Baldes, C., Mürdter, T. E., Kleideiter, E., Piotrowska, K., Bock, U., Haltner-Ukomadu, E., Mueller, J., Huwer, H., Schaefer, U. F., Klotz, U., Lehr, C. M.; Biopharmaceutical characterization of the telomerase inhibitor BRACO19. (2006) *Pharm. Res.*, **23** (5), 1031-1037

Taetz, S., Mürdter, T. E., Zapp, J., Boettcher, S., Baldes, C., Kleideiter, E., Piotrowska, K., Schaefer, U. F., Klotz, U., Lehr, C. M.; Decomposition of the Telomere-Targeting agent BRACO19 in physiological media results in products with decreased inhibitory potential. (2008) *Int. J. Pharm.*, **357** (1-2), 6-14

Taetz, S., Nafee, N., Beisner, J., Piotrowska, K., Baldes, C., Mürdter, T. E., Huwer, H., Schneider, M., Schaefer, U. F., Klotz, U., Lehr, C. M.; The influence of chitosan content in cationic chitosan/PLGA nanoparticles on the delivery efficiency of antisense 2'-O-methyl-RNA directed against telomerase in lung cancer cells. (2008) *Eur. J. Pharm. Biopharm.*, in press

Taetz, S., Bochot, A., Surace, C., Arpicco, S., Schaefer, U.F., Marsaud, V., Kerdine-Roemer, S., Lehr, C.-M., Fattal, E.
Hyaluronic acid- modified DOTAP/DOPE liposomes for the targeted delivery of anti-telomerase siRNA to CD44 expressing lung cancer cells. (2009) *Oligonucleotides*, accepted

Nafee, N., Taetz, S., Schneider, M., Schaefer, U. F., Lehr, C. M.; Chitosan-coated PLGA nanoparticles for DNA/RNA delivery: effect of the formulation parameters on complexation and transfection of antisense oligonucleotides (2007) *Nanomedicine*, **3** (3), 173-183

Piotrowska, K., Kleideiter, E., Mürdter, T. E., Taetz, S., Baldes, C., Schaefer, U. F., Lehr, C. M., Klotz, U.; Optimization of the TRAP assay to

evaluate specificity of telomerase inhibitors. (2005) *Lab. Invest.*, **85** (12), 1565-1569

Beisner, J., Dong, D., Taetz, S., Piotrowska, K., Kleideiter, E., Friedel, G., Schaefer, U. F., Lehr, C. M., Klotz, U., Mürdter, T. E.; Efficient Telomerase Inhibition in Human Non-Small Cell Lung Cancer Cells by Liposomal Delivery of 2'-O-methyl-RNA (2008) *J. Pharm. Sci.*, in press

Poster Presentations

S. Taetz, C. Baldes, U.F. Schaefer, C.M. Lehr; „Inhibition of telomerase activity in human lung cancer cells by BRACO19“; Jahrestagung der Deutschen Pharmazeutischen Gesellschaft, 6. – 9. October 2004, Regensburg, Germany

S. Taetz, C. Baldes, E. Kleideiter, K. Piotrowska, T. E. Mürdter, U.F. Schaefer, U. Klotz, C.-M. Lehr; „Transport of BRACO19 across lung epithelium“; Jahrestagung der Deutschen Pharmazeutischen Gesellschaft, 5. – 8. Oktober 2005, Mainz, Germany

S. Taetz, C. Baldes, E. Kleideiter, K. Piotrowska, T. E. Mürdter, U.F. Schaefer, U. Klotz, C.-M. Lehr; “Transport of BRACO19 in cell culture models of the lung epithelium”; 6th International Conference and Workshop on Cell Culture and In-Vitro Models for Drug Absorption and Delivery, 1. – 10. March 2006, Saarbrücken, Germany

S. Taetz, N. Nafee, C. Baldes, K. Piotrowska, M. Schneider, T. E. Mürdter, U. F. Schaefer, U. Klotz, C.- M. Lehr; “Transfection of 2'-O-Methyl-RNA into A549 cells with chitosan coated PLGA nanoparticles“; 33rd Annual Meeting & Exposition of the Controlled Release Society, 22. – 26. July 2006, Vienna, Austria

S. Taetz, N. Nafee, J. Beisner, K. Piotrowska, C. Baldes, T. E. Mürdter, U.F. Schaefer, U. Klotz, C.-M. Lehr; “Cationic chitosan/PLGA nanoparticles effectively deliver antisense 2'-O-Methyl-RNA into A549 cells to inhibit

telomerase activity”; 3rd Pharmaceutical Sciences World Congress, 22. - 25. April 2007, Amsterdam, The Netherlands

S. Taetz, N. Nafee, C. Baldes, M. Schneider, J. Beisner, T. E. Mürdter, U. F. Schaefer, U. Klotz, C.-M. Lehr; “Chitosan coated PLGA nanoparticles as carriers for antisense 2'-O-Methyl-RNA: evaluation of nanoplex stability and uptake into A549 lung cancer cells”; 34th Annual Meeting & Exposition of the Controlled Release Society, 7. – 11. Juli 2007, Long Beach, California, USA

S. Taetz, A. Bochot, U.F. Schaefer, C.-M. Lehr, E. Fattal; “Hyaluronic acid-modified DOTAP/DOPE liposomes for the targeted delivery of siRNA to CD44 expressing lung cancer cells”; 22th Annual Meeting of the G.T.R.V., 17. – 19. December, Strasbourg, France

S. Taetz, A. Bochot, U.F. Schaefer, C.-M. Lehr, E. Fattal; “Targeting of Hyaluronic Acid modified Liposomes to CD44 expressing Lung Cancer Cells for the Delivery of siRNA”; 7th International Conference and Workshop on Cell Culture and In-Vitro Models for Drug Absorption and Delivery, 20. – 29. February 2008, Saarbrücken, Germany

Oral Presentations

S. Taetz, N. Nafee, C. Baldes, K. Piotrowska, J. Beisner, T. E. Mürdter, U. F. Schaefer, U. Klotz, C.-M. Lehr; „Cationic chitosan/PLGA nanoparticles enhance the uptake of the antisense telomerase inhibitor 2'-O-Methyl-RNA into A549 lung cancer cells”; DPhG Doktorandentagung, 6. – 8. September 2006, Nürnberg-Heroldsberg, Germany

S. Taetz, N. Nafee, J. Beisner, K. Piotrowska, C. Baldes, T. E. Mürdter, U.F. Schaefer, U. Klotz, C.-M. Lehr; “Cationic chitosan/PLGA nanoparticles effectively deliver antisense 2'-O-Methyl-RNA into A549 cells to inhibit telomerase activity”; Pre-Satellite Meeting of the 33rd Pharmaceutical Sciences World Congress, 20. – 21. April 2007, Amsterdam, The Netherlands

S. Taetz, A. Bochot, U.F. Schaefer, C.-M. Lehr, E. Fattal; “Hyaluronan-modified cationic liposomes for the targeted delivery of siRNA to CD44 expressing cancer cells”; 4th International Intensive course and workshop “Nanomedicines- Nanoparticulates for Drug Delivery” & Galenos Thematic Workshop; 11. – 22. September 2008, Patras, Greece

Curriculum Vitae

Personal Data

Name: Sebastian Tätz
Born: 03.09.1977 in Hanover, Germany

Current position

since June 2008 Assistant to the Head of Production for Sterile
Liquid Dosage forms at Ursapharm Arzneimittel
GmbH & Co. KG, Saarbrücken, Germany

Dissertation

Feb. 2004 – March 2007 Thesis in the group of Prof. Dr. ClausMichael Lehr,
Biopharmacy and Pharmaceutical Technology,
Saarland University, Saarbrücken, Germany
Topic: “New Therapeutic Options for the Treatment
of Lung Cancer by Telomerase Inhibition”
April 2007 – March 2008 Year abroad as a fellow of the GALENOS
Network in the group of Prof. Dr. Elias Fattal,
Faculté de Pharmacie, Université Paris Sud 11,
Châtenay-Malabry, France

Undergraduate Studies

January 2004 Approbation as pharmacist
Oct. 1998 – Sept. 2002 Pharmacy at Philipps-University in Marburg an der
Lahn, Germany
Sept. 2001 – Feb. 2002 Erasmus/Sokrates student exchange with the
Faculté de Pharmacie, Université Paris Sud 11,
Châtenay-Malabry, France
Dec. 2002 – June 2003 Postgraduate Certificate in Pharmacy at the School
of Pharmacy of University of Otago, Dunedin, New
Zealand
Topic: “Competitive Inhibition of Lactate
Dehydrogenase by Erythrosine” supervised by
Dr. Robin Ledger

Internships

| | |
|-----------------------|--|
| March 2000 | Aventis Pharma Deutschland GmbH, Department of Quality Assurance Drug Products |
| February – March 2001 | Working Student at Aventis Pharma Deutschland GmbH, Department of Biological Resources, Natural Products |
| July – December 2003 | Sonnen-Apotheke Wunstorf |

School

| | |
|----------------------------|---------------------------------|
| August 1990 – June 1997 | Hölty- Gymnasium Wunstorf |
| August 1988 – July 1990 | Orientierungsstufe Süd Wunstorf |
| September 1984 – July 1988 | Grundschule Kolenfeld |